

ไนโตรแอมโรมาติกเซ็นเซอร์ชนิดใหม่จากแนพทาซีนเบนซิมิดาโซล



นางสาวมนัสชนก บุญศรี

จุฬาลงกรณ์มหาวิทยาลัย

CHULALONGKORN UNIVERSITY

วิทยานิพนธ์นี้เป็นส่วนหนึ่งของการศึกษาตามหลักสูตรปริญญาวิทยาศาสตรมหาบัณฑิต

สาขาวิชาปิโตรเคมีและวิทยาศาสตร์พอลิเมอร์

คณะวิทยาศาสตร์ จุฬาลงกรณ์มหาวิทยาลัย

บทคัดย่อและแฟ้มข้อมูลฉบับเต็มของวิทยานิพนธ์ตั้งแต่ปีการศึกษา 2554 ที่ให้บริการในคลังปัญญาจุฬาฯ (CUIR)
ปีการศึกษา 2556

เป็นแฟ้มข้อมูลของนิสิตเจ้าของวิทยานิพนธ์ ที่ส่งผ่านทางบัณฑิตวิทยาลัย
ลิขสิทธิ์ของจุฬาลงกรณ์มหาวิทยาลัย

The abstract and full text of theses from the academic year 2011 in Chulalongkorn University Intellectual Repository (CUIR) are the thesis authors' files submitted through the University Graduate School.

NOVEL NITROAROMATIC SENSORS FROM NAPHTHALENE BENZIMIDAZOLE

Miss Manutchanok Boonsri



A Thesis Submitted in Partial Fulfillment of the Requirements
for the Degree of Master of Science Program in Petrochemistry and Polymer

Science

Faculty of Science

Chulalongkorn University

Academic Year 2013

Copyright of Chulalongkorn University

Thesis Title	NOVEL NITROAROMATIC SENSORS FROM NAPHTHALENE BENZIMIDAZOLE
By	Miss Manutchanok Boonsri
Field of Study	Petrochemistry and Polymer Science
Thesis Advisor	Associate Professor Paitoon Rashatasakhon, Ph.D.
Thesis Co-Advisor	Associate Professor mongkol Sukwattanasinitt, Ph.D.

Accepted by the Faculty of Science, Chulalongkorn University in Partial
Fulfillment of the Requirements for the Master's Degree

.....Dean of the Faculty of Science
(Professor Supot Hannongbua, Dr.rer.nat.)

THESIS COMMITTEE

.....Chairman
(Assistant Professor Warinthorn Chavasiri, Ph.D.)

.....Thesis Advisor
(Associate Professor Paitoon Rashatasakhon, Ph.D.)

.....Thesis Co-Advisor
(Associate Professor mongkol Sukwattanasinitt, Ph.D.)

.....Examiner
(Assistant Professor Varawut Tangpasuthadol, Ph.D.)

.....External Examiner
(Nakorn Niamnont, Ph.D.)

มนัสชนก บุญศรี : ไนโตรแอรอมาติกเซ็นเซอร์ชนิดใหม่จากแนพทาไลน์เบนซิมิดาโซล.
(NOVEL NITROAROMATIC SENSORS FROM NAPHTHALENE BENZIMIDAZOLE)
อ.ที่ปรึกษาวิทยานิพนธ์หลัก: รศ. ดร.ไพฑูรย์ รัชตะสาคร, อ.ที่ปรึกษาวิทยานิพนธ์ร่วม:
รศ. ดร.มงคล สุขวัฒนาสินธิ์, 67 หน้า.

สารเรืองแสงชนิดใหม่ที่ประกอบด้วยแนพทาไลน์เบนซิมิดาโซลและไพรีนได้ออกแบบและสังเคราะห์ด้วยปฏิกิริยาควบคู่ชูซูกิ สารซึ่งมีความแตกต่างกันที่ตำแหน่งการแทนที่ของหมู่ไพรีนได้ถูกพิสูจน์ทราบโครงสร้างด้วยนิวเคลียร์แมกเนติกเรโซแนนซ์สเปกโตรสโกปี และแมสสเปกโตรเมตรี จากสมบัติเชิงแสงพบว่าสารเหล่านี้มีสโตกส์ชิฟท์ที่กว้างกว่า 100 นาโนเมตรซึ่งบ่งชี้ให้เห็นถึงความแตกต่างอย่างมากของจีโอเมตรีระหว่างสถานะพื้นและสถานะกระตุ้น พิคการคายพลังงานแสงสูงสุดอยู่ระหว่าง 580-585 นาโนเมตรและมีค่าประสิทธิภาพการคายพลังงานระหว่าง 0.006-0.17 ประเด็นที่น่าสนใจที่สุดคือการที่สารที่มีโครงสร้างใกล้เคียงกันนี้มีพฤติกรรมที่แตกต่างกันเมื่ออยู่ในสารละลายที่เป็นน้ำและเตตระไฮโดรฟิวแรนสาร 3 แสดงการจับตัวและตกตะกอนเมื่อมีปริมาณน้ำในตัวทำละลายมากขึ้น แต่สารอีกสองตัวซึ่งมีประสิทธิภาพเชิงแสงที่ต่ำในเตตระไฮโดรฟิวแรนกลับแสดงการเพิ่มพลังงานแสงที่ถูกเหนี่ยวนำด้วยการจับตัวเมื่อมีปริมาณน้ำมากขึ้น สารเหล่านี้ยังสามารถถูกระงับสัญญาณการเรืองแสงได้ด้วยไตรไนโตรโทลีอินด้วยกลไกการถ่ายเทอิเล็กตรอนที่ถูกเหนี่ยวนำโดยแสง และมีประสิทธิภาพในการระงับสัญญาณที่สูง (ค่าคงที่สเทิร์น-โวลเมอร์ เท่ากับ 96,300 และ 60,000 M^{-1}) และพบว่าสาร 2 และ 4 มีขอบเขตของการตรวจวัดที่ไตรไนโตรโทลูอิน 127 และ 252 ส่วนในพันล้านส่วนตามลำดับ



จุฬาลงกรณ์มหาวิทยาลัย
CHULALONGKORN UNIVERSITY

สาขาวิชา ปีโตรเคมีและวิทยาศาสตร์พอลิเมอร์ ลายมือชื่อนิสิต

ปีการศึกษา 2556 ลายมือชื่อ อ.ที่ปรึกษาวิทยานิพนธ์หลัก

ลายมือชื่อ อ.ที่ปรึกษาวิทยานิพนธ์ร่วม

5472242123 : MAJOR PETROCHEMISTRY AND POLYMER SCIENCE

KEYWORDS: PYRENE NAPHTHALENEBENZIMIDAZOLE FLUORESCENT SENSOR
NITROAROMATIC AIEE

MANUTCHANOK BOONSRI: NOVEL NITROAROMATIC SENSORS FROM NAPHTHALENE BENZIMIDAZOLE. ADVISOR: ASSOC. PROF. PAITON RASHATASAKHON, Ph.D., CO-ADVISOR: ASSOC. PROF. MONGKOL SUKWATTANASINITT, Ph.D., 67 pp.

New fluorescent compounds based on naphthalenebenzimidazole and pyrenes were designed and synthesized in via Suzuki-coupling. These compounds, which are different in the substitution positions of the pyrene unit, are fully characterized by NMR spectroscopy and MALDI-TOF mass spectrometry. For the photophysical properties, these compounds exhibit large Stokes shift (>100 nm) indicating significant geometry differences between ground and excited states. The maximum emission peaks are ranging between 580-585 nm with fluorescence quantum efficiencies (Φ_f) of 0.006-0.17. Most interestingly, these structurally related compounds show difference photophysical behaviors in aqueous/THF solution. The compound 3 exhibits simple aggregation and precipitation in high aqueous-content media. Meanwhile, the compounds 2 and 4, which show very low quantum yields in pure THF, exhibit interesting Aggregation-Induced Emission Enhancement (AIEE) when aqueous content is increased. These compounds also exhibit selective fluorescent quenching by photo-induced electron transfer mechanism towards trinitrotoluene (TNT) with high quenching efficiencies ($K_{sv} = 96,300$ and $60,000 \text{ M}^{-1}$) and detection limits of 127 and 252 ppb, respectively.

จุฬาลงกรณ์มหาวิทยาลัย
CHULALONGKORN UNIVERSITY

Field of Study: Petrochemistry and
Polymer Science

Academic Year: 2013

Student's Signature

Advisor's Signature

Co-Advisor's Signature

ACKNOWLEDGEMENTS

I would like to express my sincere gratitude to my thesis advisor, Associate Professor Dr. Paitoon Rashatasakhon and my co-advisor, Associate Professor Dr. Mongkol Sukwattanasinitt for valuable advice, guidance and kindness throughout this research. Sincere thanks are also extended to Assistant Professor Dr. Warinthorn Chavasiri, Assistant Professor Dr. Varawut Tangpasuthadol and Dr. Nakorn Niamnont attending as the committee members, for their valuable comments and suggestions.

I also would like to thank Assistant Professor Dr. Sumrit Wacharasindhu and Dr. Anawat Ajavakom for their attention and suggestion during our group meeting. My appreciation is also given to many people in our research group; Mr. Sakan Sirilaksanapong and Ms. Kunnigar Vongnam for training; Ms. Kanokthorn Boonkitpatarakul and Ms. Nopparat Thavornsin for their helpful suggestion; Mr. Napatthachai Kongdechawiwat for his helpful of XRD analysis; Ms. Pondchanok Chinapang, Mr. Janewit Khaokeaw and everyone in MAPS group for a greatest friendships and encouragement.

In particular, I thank the financial support from the National Nanotechnology Center (NANOTEC), NSTDA, Ministry of Science and Technology, Thailand, through its program of Center of Excellence Network. This work is part of the Project for Establishment of Comprehensive Center for Innovative Food, Health Products and Agriculture supported by the Thai Government Stimulus Package 2 (TKK2555, SP2) and the Higher Education Research Promotion and National Research University Project of Thailand, Office of the Higher Education Commission (AM1006A-56) and the Ratchadaphiseksomphot Endowment Fund of Chulalongkorn University (RES560530126-AM).

Finally, I would like to express thankfulness to my family for their love, care, encouragement and support throughout my study.

CONTENTS

	Page
THAI ABSTRACT	iv
ENGLISH ABSTRACT	v
ACKNOWLEDGEMENTS	vi
CONTENTS	vii
CHAPTER I Introduction.....	1
1.1 Introduction of nitroaromatic compounds.....	1
1.2 Introduction of fluorescence.....	2
1.2.1 Fluorescent chemosensor	4
1.2.1.1 Fluorescence quenching.....	4
1.2.2 Mechanism of changing fluorescent signals.....	5
1.2.2.1 Photo induced-electron transfer (PET) effect.....	5
1.2.2.2 Internal charge transfer (ICT) effect	6
1.2.2.3 Aggregation induced enhanced emission (AIEE) effect	7
1.4 Introduction of naphthalimide.....	11
1.5 Introduction of Pyrene unit	13
1.6 Objective.....	15
CHAPTER II Experiment.....	17
2.1 Analytical instruments	17
2.2 Materials and chemicals.....	17
2.3 Synthesis and characterization.....	18
2.3.1 Compound 1.....	18
2.3.2 Bromo Naphthalene benzimidazole 2a, 3a.....	18
2.3.3 Compound 2.....	19
2.3.4 Compound 3.....	20
2.3.5 <i>N,N'</i> -(1,2-phenylene)bis(4-methylbenzenesulfonamide).....	20
2.3.6 <i>N,N'</i> -(4,5-Dibromo-1,2-phenylene)bis(4 methylbenzenesulfonamide).....	21
2.3.7 4,5-Dibromobenzene-1,2-diamine	21

	Page
2.3.8 Dibromo Naphthalene benzimidazole	22
2.3.9 Compound 4.....	22
2.4 Photophysical property study.....	23
2.4.1 UV-visible spectroscopy	23
2.4.1.1 Molar extinction coefficient (ϵ)	23
2.4.2 Fluorescence spectroscopy.....	23
2.4.2.1 Fluorescence quantum yield (Φ_F).....	23
2.4.2.2 Effect of water content	24
2.4.2.3 Time-dependent effect	24
2.5 Electronic test.....	24
2.6 Nitroaromatic sensor's studies.....	25
2.6.1 Fluorescent nitroaromatic sensors.....	25
2.6.2 Stern-Volmer constant.....	25
2.6.3 Paper test	25
2.6.4 ^1H NMR experiment.....	25
2.7 Particle size	26
2.8 ^1H -NMR titration	26
CHAPTER III Results and discussion	27
3.1 Synthesis.....	27
3.2 Photophysical property	32
3.3 Effect of water content on photophysical properties	33
3.3.1 Fluorophore 1.....	33
3.3.2 Fluorophore 2.....	34
3.3.3 Fluorophore 3.....	36
3.3.4 Fluorophore 4.....	37
3.4 X-ray diffraction.....	39
3.5 Electrochemical properties.....	41

	Page
3.6 Sensing studies for nitroaromatic compounds	42
3.6.2 Selectivity	43
3.6.2 Stern-Volmer plots: sensitivity determination	45
3.6.4 ^1H NMR experiment	47
3.6.5 Paper-based sensor for nitroaromatic compound	48
CHAPTER IV Conclusion.....	50
4.1 Conclusion.....	50
REFERENCES	51
APPENDIX.....	56
VITA.....	67

LIST OF FIGURE

Figure 1.1 Structures of all nitroaromatic compounds.....	2
Figure 1.2 Typical fluorescent substances.	3
Figure 1.3 Jablonski Energy Diagram explaining fluorescence processes.....	4
Figure 1.4 Orbital energy diagrams for fluorescent “turn-off” PET sensors before and after binding cation and (a) fluorescence emission; (b) forward electron transfer; (c) backward electron transfer processes	5
Figure 1.5 Potential energy surfaces of the ground state (S_0) is excited to and S_1 or ..	6
Figure 1.6 Planar compounds such as pyrene tend to aggregate just as discs pile up due to strong π - π stacking interactions, which commonly turn “off” light emission, whereas nonplanar propeller-shaped luminogens such as hexaphenylsilole (HPS) behave oppositely, with their light emissions turned “on” by aggregate formation, due to the restricted intramolecular rotation in the aggregates.....	8
Figure 1.7 Chemical structure of pentacenequinone derivative and its selectivity toward Cu^{2+} ion [23].....	9
Figure 1.8 Hetero-oligophenylene carbazole derivatives and Change in fluorescence of hetero-oligophenylene carbazole derivatives (1 μM in 8:2 $\text{H}_2\text{O}/\text{THF}$) on exposing to the vapors of solid 2,4,6-trinitrotoluene [24].....	9
Figure 1.9 Hexaphenylbenzene-based derivative [5].....	10
Figure 1.10 Hexa-peri-hexabenzocoronene-Based derivatives and fluorescence spectrum of this compound (1 μM) on addition of PA in 4:6 $\text{H}_2\text{O}:\text{THF}$. Inset shows the quenching in fluorescence of the compound after addition of PA [25].....	11
Figure 1.11 Structure of copolymer and π - π interaction between copolymer and 2,5- dinitrobenzonitrile. [35]	13
Figure 1.12 Structure of dipyrenylamidocalix[4]arene-[15]crown-5 (L) and selectivity with aromatic compounds [36].....	14
Figure 1.13 The structure of copolymer and the quenching process of film by TNT [37].....	14

Figure 1.14 Structure of Calix[2]pyreno[2]pyrrole [38].	15
Figure 1.15 The structure of TAP and Emission spectra of TAP in the presence of TNT at various concentrations [39].	15
Figure 1.16 Target molecule 1-4 .	16
Figure 3.1 ^1H NMR (400 MHz, CDCl_3) of 1 .	27
Figure 3.2 Systematic positions in 1,8-naphthalimide-benzimidazole structure.	28
Figure 3.3 ^1H NMR (400 MHz, CDCl_3) of compounds 2a, 2 .	29
Figure 3.4 ^1H NMR (400 MHz) of compounds 3a, 3 (CDCl_3).	29
Figure 3.5 ^1H NMR (400 MHz) of compounds 4a, 4 (CDCl_3).	31
Figure 3.6 Proposed structures of two diastereomeric conformers of 4 .	31
Figure 3.7 Normalized absorption and emission spectra of 1-4 in THF.	32
Figure 3.8 Fluorescent spectra of fluorophore 1 in THF with various water contents.	34
Figure 3.9 Fluorescent spectra of fluorophore 2 in THF and various water contents, inset is the photographs of solutions of 2 (100 μM) in THF, 50% water in THF, and 90% water in THF, respectively.	35
Figure 3.10 Absorption spectra of fluorophore 2 in THF and various water contents.	35
Figure 3.11 Fluorescent intensities of 3 (30 μM) at various times after dilution of stock THF solution with Milli Q water ($\text{H}_2\text{O} : \text{THF} = 9:1$) in the presence (blue) and absence (orange) of Tween-20.	36
Figure 3.12 Fluorescent spectra of fluorophore 3 in THF and various water contents.	37
Figure 3.13 Absorption spectra of fluorophore 3 in THF and various water contents.	37
Figure 3.14 Fluorescent spectra of fluorophore 3 in THF and various water contents.	38
Figure 3.15 Fluorescent emission response under blacklight of 4 in THF with various water content.	39
Figure 3.16 Particle size of fluorophore 4 .	39

Figure 3.17 Fluorescent intensities of 4 (30 μM) at various times after dilution of stock THF solution with Milli Q water ($\text{H}_2\text{O} : \text{THF} = 9:1$)	39
Figure 3.18 XRD of 1	40
Figure 3.19 XRD of 2	40
Figure 3.20 XRD of 3	41
Figure 3.21 XRD of 4	41
Figure 3.22 Energy level of all fluorophores and 3 nitroaromatic compounds	42
Figure 3.23 Structures of all tested nitroaromatic compounds	43
Figure 3.24 Selectivity of 4 (30 μM), after addition of each nitroaromatic compound (10 eq) in THF (blue), and in aqueous media (20% THF (orange)), (3% THF (gray)) ($\lambda_{\text{ex}} = 350 \text{ nm}$).....	44
Figure 3.25 Selectivity of 2 (30 μM), after addition of each nitroaromatic compound (10 eq) in aqueous media (3% THF) ($\lambda_{\text{ex}} = 344$)	44
Figure 3.26 Selectivity of 1 (5 μM), after addition of each nitroaromatic compound (20 eq) in THF (orange) and $\text{H}_2\text{O} : \text{THF}$ (40 : 60) ($\lambda_{\text{ex}} = 380 \text{ nm}$).....	45
Figure 3.27 The fluorescence intensity of compound 2 (30 μM) with TNT titration (0-100 μM) in aqueous media (3% THF and tween-20 100 μM)	46
Figure 3.28 The fluorescence intensity of compound 4 (30 μM) with TNT titration (0-100 μM) in aqueous media (3% THF).....	46
Figure 3.29 The Stern-Volmer plot of 4 (30 μM) vs TNT in aqueous media (3% THF).	47
Figure 3.30 The Stern-Volmer plot of 2 (30 μM) vs TNT in aqueous media (3% THF, Tween-20 100 μM).....	47
Figure 3.31 ^1H -NMR of 2 with various amounts of TNT	48
Figure 3.32 Photographic images for paper-based detection of TNT under 20W black light (365 nm).	49
Figure A.1 The ^1H NMR of compound 1 in CDCl_3	56
Figure A.2 The ^1H NMR of 2a in CDCl_3	56

Figure A.3 The ^1H NMR of 2 in CDCl_3	57
Figure A.4 The ^{13}C NMR of 2 in CDCl_3	57
Figure A.5 The ^1H NMR of 3a in CDCl_3	58
Figure A.6 The ^1H NMR of 3 in CDCl_3	58
Figure A.7 The ^{13}C NMR of 3 in CDCl_3	59
Figure A.8 The ^1H NMR of 4a in CDCl_3	59
Figure A.9 The ^1H NMR of 4b in CDCl_3	60
Figure A.10 The ^1H NMR of 4c in CDCl_3	60
Figure A.11 The ^1H NMR of 4d in CDCl_3	61
Figure A.12 The ^1H NMR of 4 in CDCl_3	61
Figure A.13 The ^{13}C NMR of 4 in CDCl_3	62
Figure A.14 The IR spectra of 1	62
Figure A.15 The IR spectra of 2	63
Figure A.16 The IR spectra of 3	63
Figure A.17 The IR spectra of 4	63
Figure A.18 MS spectra of 2	64
Figure A.19 MS spectra of 3	64
Figure A.20 MS spectra of 4	65
Figure A.21 Molar absorptivity of 1-4	65
Figure A.22 Quantum yield of 1-4	66
Figure A.23 Absorption spectra of TNT.....	6

LIST OF TABLE

Table 1.1 Naphthalene benzimidazole derivatives.....	13
Table 3.1 Photophysical properties of fluorophore 1-4.....	33
Table 3.2 Energy level of 1-4.....	42



LIST OF SCHEME

Scheme 3.1 Synthesis of 1	27
Scheme 3.2 Synthesis of fluorophore 2 and 3	28
Scheme 3.3 Synthesis of 4	30



จุฬาลงกรณ์มหาวิทยาลัย
CHULALONGKORN UNIVERSITY

LIST OF ABBREVIATIONS

Ar	Aromatic
calcd	Calculated
^{13}C NMR	Carbon-13 nuclear magnetic resonance
CDCl_3	Deuterated chloroform
CH_3COOH	Acetic acid
$\text{DMSO-}d_6$	Deuterated dimethyl sulfoxide
DMSO	Dimethylsulfoxide
d	Doublet (NMR)
dd	Doublet of doublet (NMR)
equiv	Equivalent (s)
EtOAc	Ethyl acetate
FT-IR	Fourier transform infrared spectroscopy
g	Gram (s)
^1H NMR	Proton nuclear magnetic resonance
Hz	Hertz
h	Hour (s)
IR	Infrared
J	Coupling constant
mg	Milligram (s)
min	Minute (s)
mL	Milliliter (s)
mmol	Millimole (s)
m/z	Mass per charge
m	Multiplet (NMR)
M.W.	Molecular weight
M	Molar
MHz	Megahertz

Na_2SO_4	Sodium sulfate
$\text{Pd}(\text{dppf})\text{Cl}_2$	[1,1'-Bis(diphenylphosphino)ferrocene]dichloropalladium(II)
PhMe	Toluene
PPb	Parts per billion
K_2CO_3	Potassium carbonate
rt	Room temperature
s	Singlet (NMR)
THF	Tetrahydrofuran
TLC	Thin layer chromatography
UV	Ultraviolet
δ	Chemical shift
ϵ	Molar absorptivity
λ	Wavelength
$^\circ\text{C}$	Degree Celsius
μL	Microliter (s)
μM	Micromolar (s)
Φ	Quantum yield
% yield	Percentage yield

CHAPTER I

Introduction

1.1 Introduction of nitroaromatic compounds

Nitroaromatic compounds are important groups of industrial chemicals used in polyurethane foams, herbicides, insecticides, pharmaceuticals, and dyes industry [1-3] and some of them are often used as explosives. Examples of nitroaromatic compounds are shown in **Figure 1.1**. The best-known nitroaromatic compound is the most common bulk explosive TNT (2,4,6-trinitrotoluene). It is used in military munitions and in civilian mining and quarrying activities. TNT has been used on large scales since the World War I. The residual amount of TNT contaminating in environment is hazardous to human and animal healths. Its toxic manifestation to human includes skin sensitization, immunotoxicity, and methaemoglobinemia [4]. Moreover, high concentration of TNT can be caused toxic to liver, kidney and spleen toxic. Development of high-efficiency and easy-to-use TNT sensors are also very important in combating terrorism, for maintaining national security, and for providing environmental safety [5]. There are a lot of detection methods for TNT. Some techniques are highly sensitive, but require expensive instrument and skillful operators. In addition, the application of these techniques for on-site field tests are not practical. such as gas chromatography coupled with mass spectrometry, energy dispersive X-ray diffraction, neutron activation analysis, electron capture detection, and cyclic voltammetry [2, 6]. Fluorescence technique has also been used for detecting TNT due to its high sensitivity and selectivity. However, fluorogenic chemosensors for TNT detection is still less selective between TNT and DNT since their LUMO states are at nearly similar energy level, and the detection limits of these sensors need to be further improved.

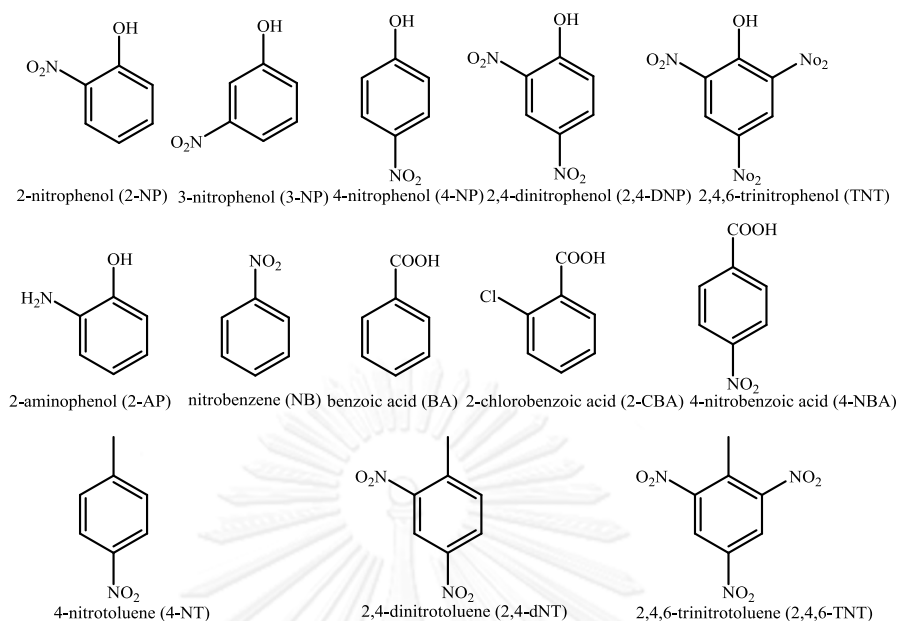
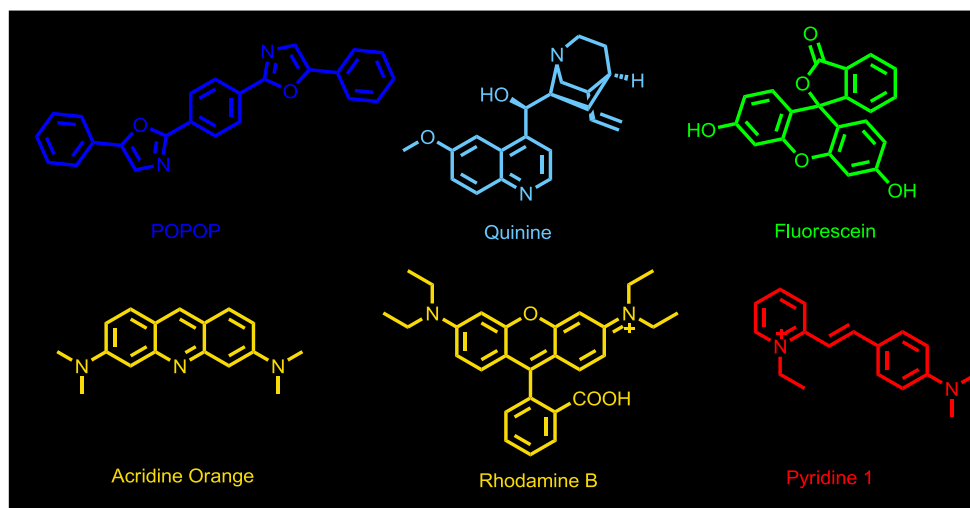


Figure 1.1 Structures of all nitroaromatic compounds.

1.2 Introduction of fluorescence

Fluorescence phenomenon is one of the processes that has been applied in the field of chemistry and biological sciences because it is high selectivity, sensitivity and rapid detection. With the made of portable devices, it can be applied easily for real-time and on-site detection. Highly fluorescent molecule should possess long π -conjugation systems which generally are planar molecules so that electrons can delocalize through the molecule. Molecules with multiple aromatic rings usually have high rigidity that prevents C-C bond rotation. As the result, these molecules will exhibit fluorescence light in high efficiencies.



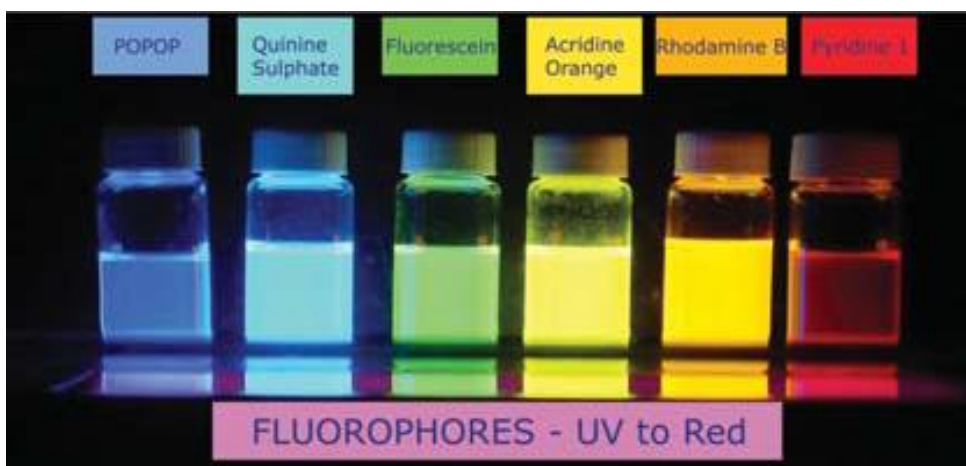


Figure 1.2 Typical fluorescent substances.

The fluorescence process occurs when the molecules exhibit absorption and emission of light energy and this process is usually illustrated by the Jablonski diagram (Figure 1.3). When a fluorescent molecule is irradiated by a sufficient amount of energy, it will become an unstable molecule or as well-known as molecule in excited state. In order to return to the stable state, the molecule will first release some energy in the forms of molecular rotation and vibration, or thermal energy until the molecule reaches a semi-stable or locally excited state (LE) which is usually the lowest electronic excited state. Then the remaining portion of energy will be released in the form of fluorescent light as the molecule completely return to the ground state (S_0). Applications of fluorescence technique towards the development of chemosensors usually rely on the disturbance of the fluorescent process by analytes, and fluorescent signal comparison in the absence and presence of analytes.

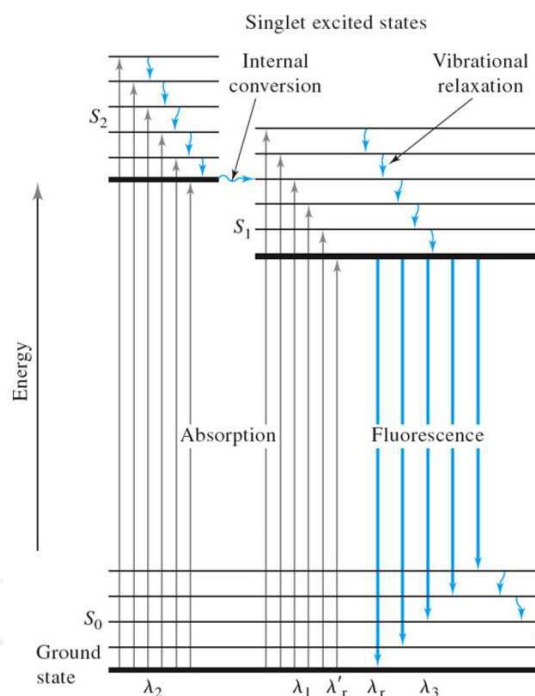


Figure 1.3 Jablonski Energy Diagram explaining fluorescence processes

1.2.1 Fluorescent chemosensor

Generally, a fluorescent sensor contains two major components; a receptor and a fluorophore. The receptor should have the ability to discriminate and bind a specific target substance known as the analyte. A successful and selective receptor-analyte complex formation depends on the size, shape and binding energy of the receptor and analyte molecules[7]. Fluorophore provides the part responsible of reporting the binding event, whether by fluorescence quenching or enhancement [8].

1.2.1.1 Fluorescence quenching

The intensity of fluorescence can be decreased by several quenching processes. The fluorescence quenching usually was characterized by Stern–Volmer equation [8].

$$\frac{I_0}{I} = 1 + k_q \tau_0 [Q] = 1 + K_{SV} [Q]$$

In this equation I_0 and I are the fluorescence intensities in the absence and presence of quencher, respectively; k_q is the bimolecular quenching constant; τ_0 is the lifetime of the fluorophore in the absence of quencher; and $[Q]$ is the concentration of quencher. The Stern-Volmer quenching constant is given by $K_D = k_q \tau_0$. If the quenching is known to be dynamic, the Stern-Volmer constant will be

represented by K_D . Otherwise, this constant will be described as K_{SV} . Quenching data are usually presented as plots of I_0/I versus $[Q]$. This is because I_0/I is expected to be linearly dependent upon the concentration of quencher. A plot of I_0/I versus $[Q]$ yields an intercept of one on the y-axis and a slope equal to K_{SV} .

1.2.2 Mechanism of changing fluorescent signals

From the Jablonski's diagram, it is apparent that the increase in molecular rigidity can offer fluorescent signal with higher intensity or emission at the shorter wavelength due to the lower degree of geometrical relaxation. On the other hands, the decrease in rigidity would allow excited molecule to vibrate and rotate more vigorously; therefore, most energy should be lost prior to the returning to the ground state. In this case, the emission wavelength should be longer and the intensity might be lower. Apart from the rigidity, there are several processes which can also alter the fluorescent signals.

1.2.2.1 Photo induced-electron transfer (PET) effect.

Photo-induced electron transfer (PET) often results in signal quenching [8]. The phenomenon of PET has been widely used in fluorescent sensor development [7, 9]. The PET-based sensors can be categorized into two modes: fluorescence "turn-off" or fluorescence "turn-on". For the "turn-off" sensor, the receptor takes part only indirectly in the photophysical process. If the LUMO state of analyte is between the energy levels of the fluorophore HOMO and LUMO, the binding of the analyte by the receptor provides a non-radiative path to dissipate the excitation energy, resulting in a quenching of the fluorescence of the chemosensor (**Figure 1.4**) [10].

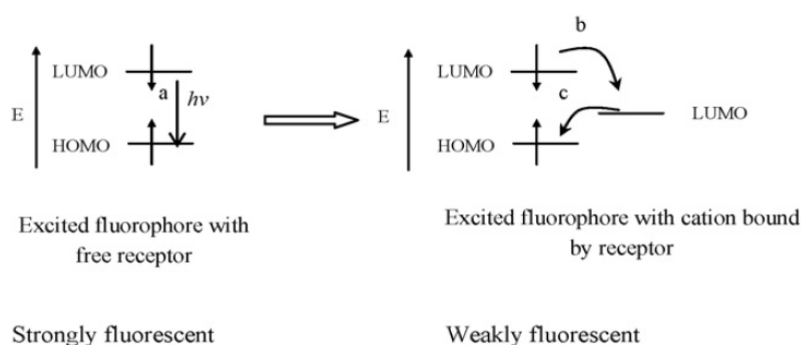


Figure 1.4 Orbital energy diagrams for fluorescent "turn-off" PET sensors before and after binding cation and (a) fluorescence emission; (b) forward electron transfer; (c) backward electron transfer processes

For the “turn-on” sensor, the overall process is opposite. The fluorescent sensors often contain the PET donor and receptor which cause relatively low emission efficiencies. If the binding of the sensor with analytes can diminish the PET process, thus the fluorescent signal will be greatly enhanced.

1.2.1.2 Internal charge transfer (ICT) effect

Internal charge transfer (ICT) is an important and common process that changes fluorescent intensity [11]. In a typical fluorescence process, the molecule will emit fluorescent signal when it returns from the locally excited state (LE) to the ground state. For molecules containing both electron-donating and electron-withdrawing groups, the excited molecules at LE state can adapt into a more stable state called “ICT” state following the Frank-Condon principle (**Figure 1.5**). Then, the emission energy will be lower and the molecules show a large Stoke shift - emission wavelength will be red shift. Sometimes, fluorescent signals disappear if the emitted energy is out of the UV-visible range [9].

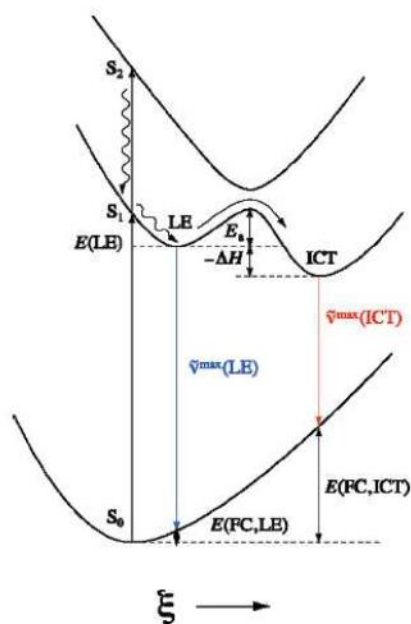


Figure 1.5 Potential energy surfaces of the ground state (S_0) is excited to and S_1 or S_2 and then relaxed to LE, and ICT (FC = Franck-Condon).

1.2.1.3 Aggregation induced enhanced emission (AIEE) effect

[12] Most of fluorescent organic compounds of which structures are disc-like, are highly emissive in dilute solution or good solvent, but they become weakly fluorescent in solid state or aggregate-form in poor solvent. This signal decrease results from the strong π - π stacking interactions between molecules. The aggregation is side-by-side which promotes the formation of H-aggregates with ordered or random structures [13]. The excited states of the aggregates often decay via non-radiative pathways, which is notoriously known as aggregation-caused quenching (ACQ) [12, 14] of light emission in the condensed phase (**Figure 1.6**) ACQ phenomena has been problems in applications of light-emitting organic molecules [14-16].

In some cases, the applications of light-emitting organic molecules need to be formed into solid state which reduces their fluorescent efficiencies. As unusual phenomena, aggregation-induced emission (AIE) and aggregation-induced emission enhancement (AIEE) [17] have recently been much interested [18] because their aggregations or solid states are strongly luminescent. AIEE is a unique photoluminescence property that was first discovered in 2001. This property always happen in Propeller-shaped molecule. Propeller-shaped fluorophores are non-emissive when have been dissolved in good solvent or in dilute solution because the intramolecular rotation converts photonic energy to heat and deactivates the excited states non-radiatively [19]. The restriction of intramolecular rotations (RIR) [20] in J-aggregated formation have been predicated as a main cause for the AIEE effect [21]. To date, a variety of compounds with AIE characteristics have been developed for applications in chemical sensors, biological imaging, and optoelectronic devices [22].

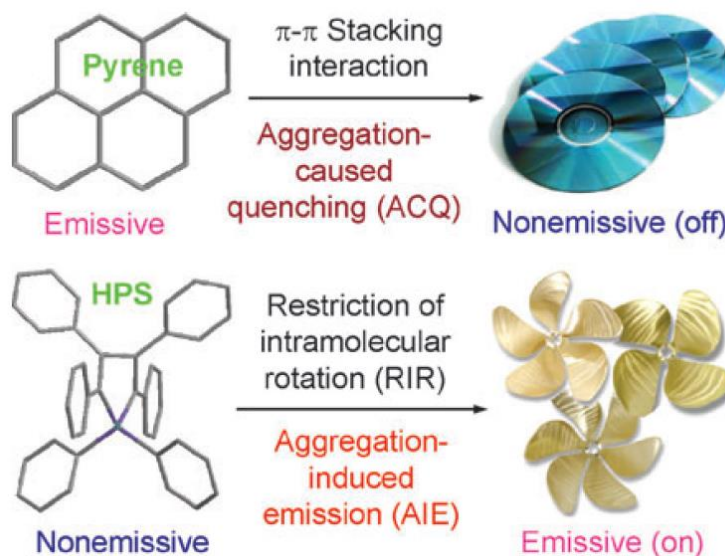


Figure 1.6 Planar compounds such as pyrene tend to aggregate just as discs pile up due to strong π - π stacking interactions, which commonly turn “off” light emission, whereas nonplanar propeller-shaped luminogens such as hexaphenylsilole (HPS) behave oppositely, with their light emissions turned “on” by aggregate formation, due to the restricted intramolecular rotation in the aggregates.

AIEE makes the fluorescent signal to have higher intensity when it is in the solid state or poor solvent. Therefore, AIEE is widely applied for sensing nitroaromatic explosive compounds in environment which they are dissolved in water. AIEE will make the sensor which has higher sensitivity as the example in the literature reviews below:

In 2012, V. Bhalla et al. designed and synthesized AIEE-active pentacenequinone derivative (**Figure 1.7**) using the Suzuki-Miyaura coupling. This compound exhibits weak emission at 460 nm ($\Phi_F = 0.2$) in THF. Upon addition of 90% volume fraction of water, the emission band is red-shifted to 560 nm and nearly a 2-fold enhancement ($\Phi_F=0.4$) in emission intensity due to its aggregation-induced emission enhancement which results in restriction of the intramolecular rotation and works as efficient and selective fluorescent sensor for nanomolar detection of picric acid in solution with a detection limit of 500 ppb ($K_{sv}=4.3 \times 10^3 \text{ M}^{-1}$) as well as in solid state.

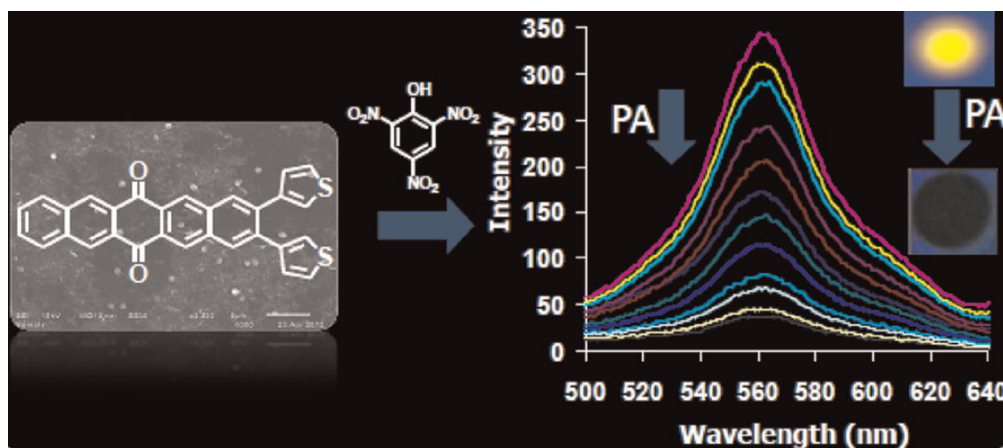


Figure 1.7 Chemical structure of pentacenequinone derivative and its selectivity toward Cu^{2+} ion [23].

New AIEE-active hetero-oligophenylene carbazole derivatives (**Figure 1.8**) has been synthesized and served as fluorescent probes for the selective detection of 2,4,6-trinitrotoluene (TNT) in the vapor phase, the solid phase, and aqueous media. In addition, paper strips prepared by dip-coating a solution of aggregates of this compound can provide a simple, portable, sensitive, selective, low-cost method for the detection of TNT on the picogram level. The detection limits of this compound as fluorescent sensors for TNT are found to be $30 \times 10^{-9} \text{ mol L}^{-1}$. The Stern–Volmer plots of aggregates compound is linear and give quenching constants (K_{SV}) of 13.3×10^5 and M^{-1}

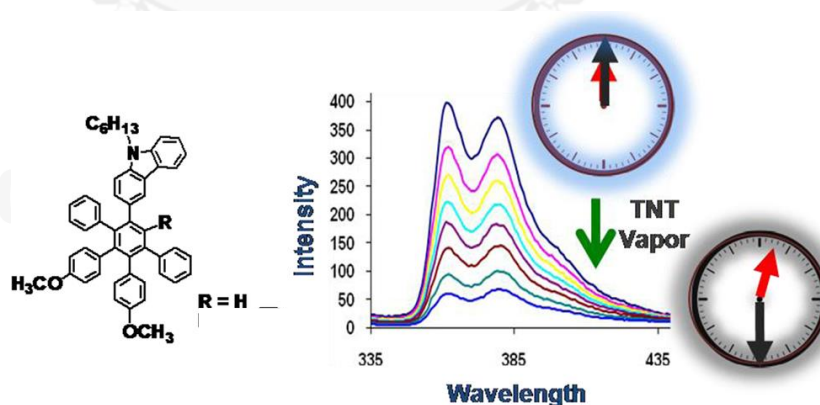


Figure 1.8 Hetero-oligophenylene carbazole derivatives and Change in fluorescence of hetero-oligophenylene carbazole derivatives ($1 \mu\text{M}$ in $8:2 \text{ H}_2\text{O}/\text{THF}$) on exposing to the vapors of solid 2,4,6-trinitrotoluene [24].

In 2013, hexaphenylbenzene derivative has been developed as a fluorescent chemosensor for selective detection of TNP [5]. V. Bhalla et al. designed and synthesized hexaphenylbenzene-based derivative having AIEE characteristics. In the fluorescence spectrum, this compound exhibits a weak fluorescence emission at 460 nm ($\Phi = 0.03$) when excited at $\lambda_{\text{ex}} = 380$ nm. However, a subsequent increase of the volume fraction of water up to 60% leads to enhancement of the emission intensity ($\Phi = 0.48$). The aggregates of this derivative undergo modulation in the presence of Hg^{2+} ions to form nanorods. Interestingly, supramolecular assemblies of this ensemble work as an efficient and sensitive fluorescent chemosensor for PA at the ppb level. In addition, the present study demonstrates the utility of solution-coated dip strips of the ensemble for the trace detection of PA with a detection limit of 6.87 ppb ($\text{KSV} = 1.92 \times 10^5 \text{ M}^{-1}$).

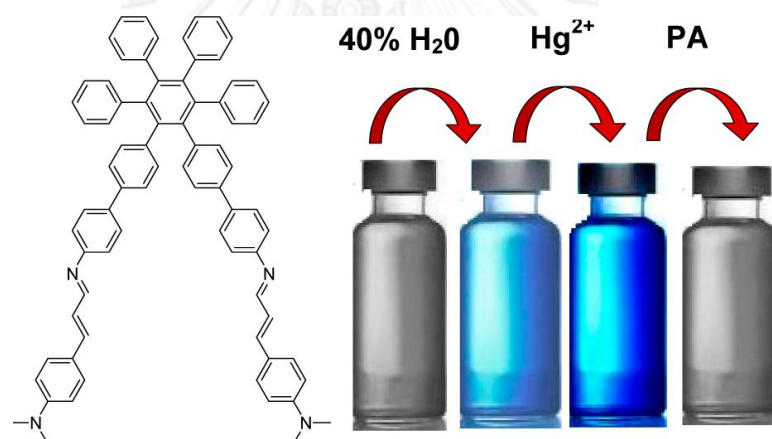


Figure 1.9 Hexaphenylbenzene-based derivative [5].

Hexa-peri-hexabenzocoronene (HBC) based molecules [25] has been designed and synthesized. This planar structure is appended with rotors to invoke aggregation induced emission enhancement (AIEE) phenomenon by controlling the ratio of H_2O in solutions of aggregates. This aggregates of HBC derivative serves as highly selective chemosensors for picric acid (PA) in mixed aqueous solution. This aggregates are also able to detect PA in vapor phase. In addition, fluorescent test strips have been prepared by dip-coating the Whatman paper with aggregates of both compounds for trace detection of PA in contact mode with detection limits in attograms. The aggregates of this compound possesses detection limits of 4 nM. The Stern–Volmer plot of aggregates of the compound is linear with high quenching constant K_{SV} of $3.2 \times 10^6 \text{ M}^{-1}$.

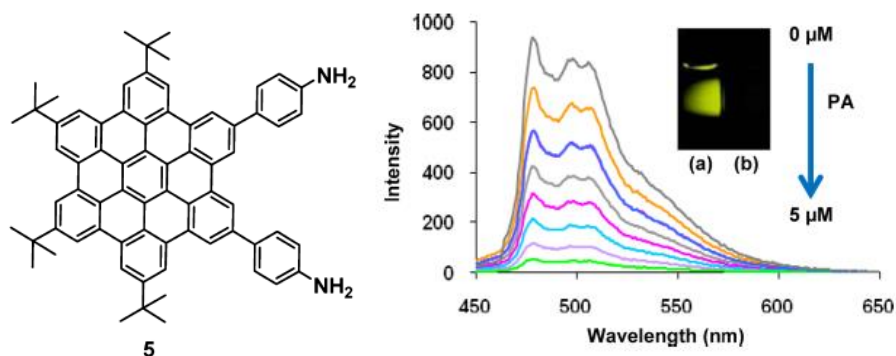
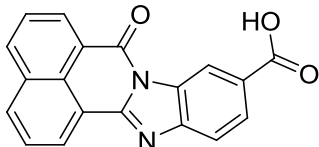


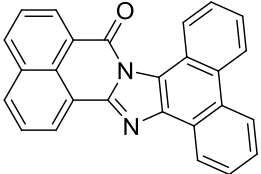
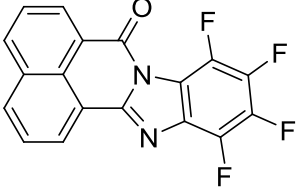
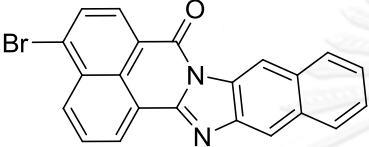
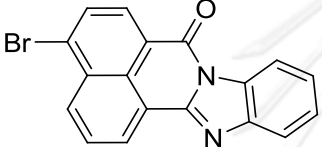
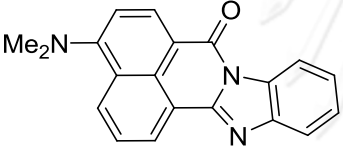
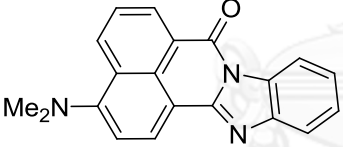
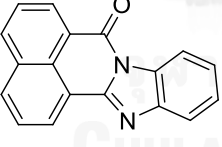
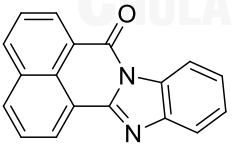
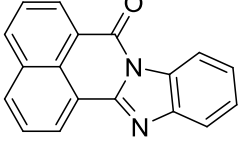
Figure 1.10 Hexa-peri-hexabenzocoronene-Based derivatives and fluorescence spectrum of this compound ($1 \mu\text{M}$) on addition of PA in 4:6 H_2O : THF. Inset shows the quenching in fluorescence of the compound after addition of PA [25].

1.4 Introduction of naphthalimide

Naphthalimide derivatives are a special class of environmentally sensitive fluorophores. Naphthalimide derivatives have been used as pigments, dyes, optical brighteners, fluorescent markers in biology, anticancer agents in medicine [26, 27] and materials for organic electronics such as light-emitting devices (OLED) [28]. As some naphthalimide derivatives do not exhibit noticeable fluorescence. However, naphthalic anhydride is condensed with ortho-phenylene diamine giving naphthalene benzimidazole causes the fluorescence to be switched on [29]. It is known to have high quantum yields, high thermal stability and photostability. Recently, it has become more popular in the field of molecular sensors [30] because of its chemical and thermal stabilities as well as its excellent photophysical characters. A breakthrough of Naphthalene benzimidazole is widely applied to use as an efficient fluorophore. The structure of naphthalene benzimidazole can be functionalized the substitution on the part of naphthalene side or benzimidazole side which exhibits different photophysical properties. These research are shown in this table. [29, 31-34].

Table 1.1 Naphthalene benzimidazole derivatives.

compound	Solvent	$\lambda_{\text{abs}}(\text{nm})$	$\lambda_{\text{em}}(\text{nm})$	Φ_{F}
	Solid state	400	500	-

	CH ₂ Cl ₂	436	589	0.15
	CH ₂ Cl ₂	382	466	0.82
	o-xylene	341/398/440	536	0.28
	o-xylene	349,392	500	0.82
	Toluene	425	490	0.50
	Toluene	435	575	0.40
	Toluene	386	484	0.55
	CH ₂ Cl ₂	384	499	0.71
	CH ₃ CN	331,379	492	0.36

1.5 Introduction of Pyrene unit

The development of artificial receptors for the sensing and recognition of environmentally and biologically important species has been actively investigated in recent years. Pyrene group is used to be a receptor unit for detecting of nitroaromatic explosive compounds in many reports.

In 2009, Burattini S. and et al. have synthesized pyrene-functionalised copolymer in a single step via imidisation of poly(maleic anhydride-alt-1-octadecene) with 1-pyrenemethylamine. The new copolymer forms complexes in solution with NACs such as 2,5-dinitrobenzonitrile. The Stern–Volmer plot of copolymer is linear with high quenching constant K_{SV} of 660 M^{-1} during one minute. Moreover, thin films of this copolymer, cast from THF solution, undergo almost instantaneous fluorescence quenching when exposed to the vapour of 2,5-dinitrobenzonitrile (a model for TNT) at ambient temperatures and pressures.

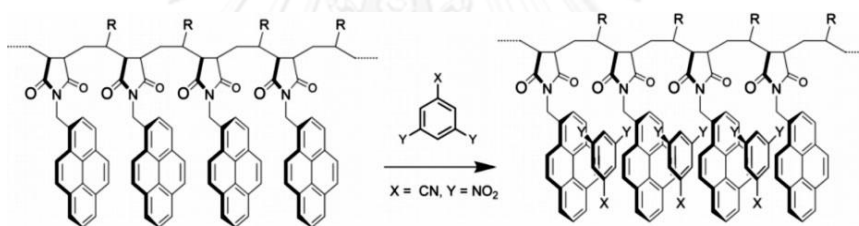


Figure 1.11 Structure of copolymer and π - π interaction between copolymer and 2,5-dinitrobenzonitrile. [35]

In 2010, dipyrenylamidocalix[4]arene-[15]crown-5 (L) have been developed a new and effective fluorescent chemosensor for the detection of trinitroaromatics species in CH_3CN . When DNT, TNT and TNB are added to solutions of L in CH_3CN , the fluorescent emission is quenched. This is considered to a charge-transfer complexes between the electron donor (pyrene) and the electron acceptor (quencher).

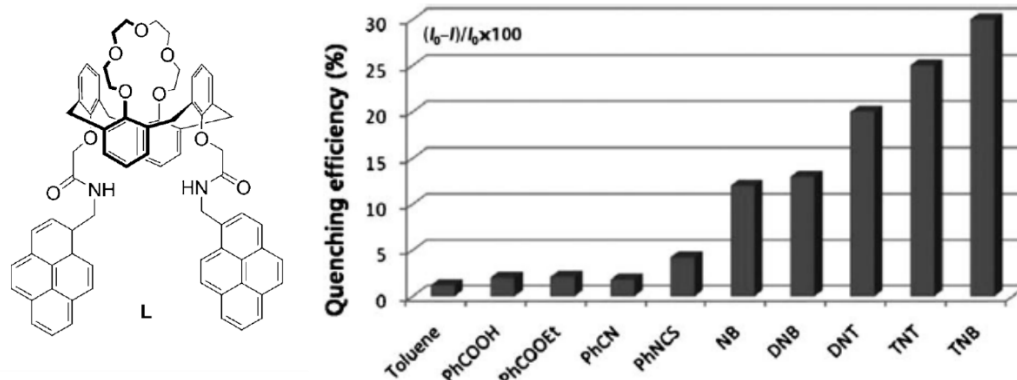


Figure 1.12 Structure of dipyrenylamidocalix[4]arene-[15]crown-5 (L) and selectivity with aromatic compounds [36].

In 2011, He, G. and et al. have synthesized poly(pyrene-co-phenyleneethynylene) and characterized. The polymer had been casted, separately, onto glass plate surfaces to fabricate film for sensing performance studies. The fluorescence emission of polymer is sensitive to the presence of TNT in aqueous phase via specific π - π interaction and the match of the LUMO of the copolymers to that of the quencher. It can be seen that nearly 70% of the emission is quenched when TNT reaches 60 $\mu\text{mol/L}$. A linear Stern-Volmer relationship was obtained in all the cases with highest quenching constant ($K_{SV} = 3.26 \times 10^4 \text{ M}^{-1}$) for TNT. The film is clear that the responsibility with TNT is fully reversible. Furthermore, the film is stable for 6 months at least provided it is properly preserved.

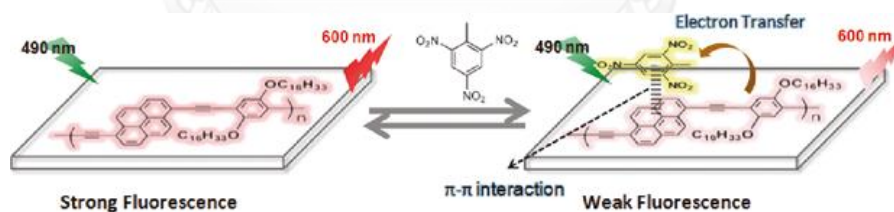


Figure 1.13 The structure of copolymer and the quenching process of film by TNT [37]

Calix[2]pyreno[2]pyrrole was synthesized and well characterized to be fluorescence molecular probe which can detect polynitroaromatic compounds with high affinity. In addition, this highly fluorescent neutral molecular receptor also exhibits enhanced binding affinity towards TNT which is associated with the formation of a π -complex. The fluorescence quenching titration was performed with increasing amounts of TNT concentration. The value of stern-volmer constant is $1.1 \times 10^6 \text{ M}^{-1}$. The complex

formation between the compound and nitroaromatics is 1:1. The detection limit was found to approach up to nanomolar range.

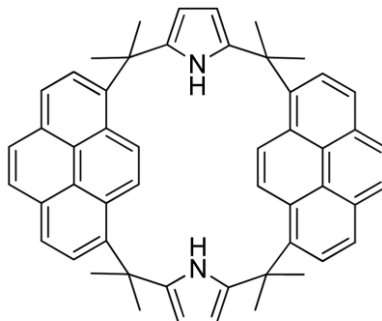


Figure 1.14 Structure of Calix[2]pyreno[2]pyrrole [38].

Triphenylamine-based fluorophores containing pyrene (TAP) has been synthesized and characterized. It shows the fluorescence quenching sensitivity toward nitro explosives. TAP showed the highest sensitivity toward TNT ($K_{SV} = 1.7 \times 10^4 \text{ M}^{-1}$). When the temperature is increased from 0°C to 45°C , the value of stern-volmer constants are $1.4 \times 10^4 \text{ M}^{-1}$ and $2.0 \times 10^4 \text{ M}^{-1}$, respectively that prove the fluorescence quenching between TAP and TNT likely occurs through a dynamic process.

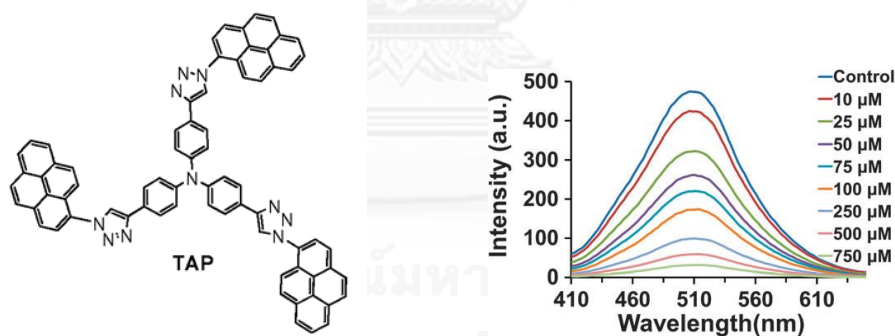


Figure 1.15 The structure of TAP and Emission spectra of TAP in the presence of TNT at various concentrations [39].

1.6 Objective

From the literature reviewed above, they show a problem about selectivity between DNT and DNT due to nearly LUMO of them. Moreover, many sensors present blue emission that do not clearly distinguish in naked-eyes. The objectives of this

research are design and synthesize novel fluorescent sensors which have the fluorophore is naphthalene benzimidazole. It is derivative of 1,8-Naphthalimide which has excellent photophysical properties such as high quantum yield, chemical resistance, high photostability. Furthermore, the naphthalene benzimidazole is more π - π conjugations and rigidity than 1,8-Naphthalimide so it may show the higher quantum yield and the emission wavelength will shift to lower energy due to high stability of molecule. As the applying of sensor, the fluorophore will emit light energy to long wavelength that is easy detection in naked-eyes. Pyrene unit is considered to be the receptor for the interaction of π - π stacking between pyrene and nitro aromatic compound. The application of these new fluorophores as nitroaromatic sensors in aqueous media will also be investigated.

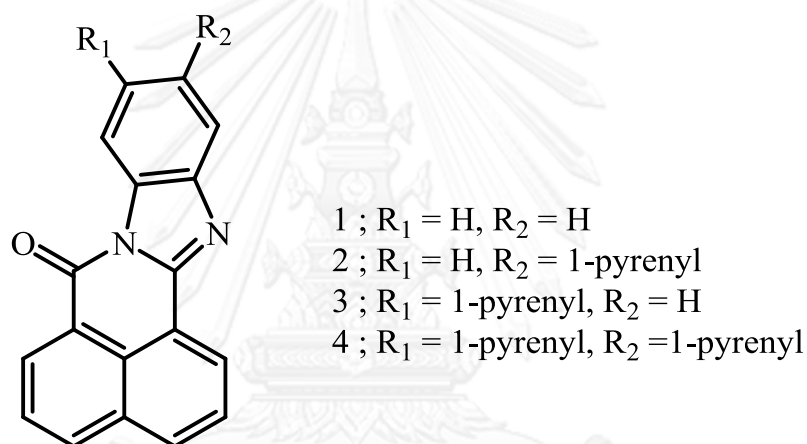


Figure 1.16 Target molecule 1-4

CHAPTER II

Experiment

2.1 Analytical instruments

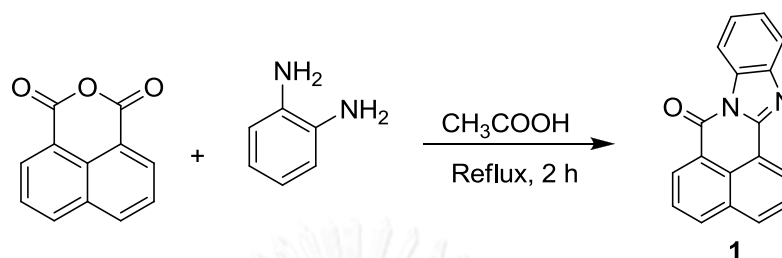
All ^1H - and ^{13}C -NMR spectra were recorded on a Varian Mercury NMR spectrometer, which operated at 400 MHz for ^1H and 100 MHz for ^{13}C (Varian Company, CA, USA) using CDCl_3 or $d_6\text{-DMSO}$ as the solvents. Mass spectra were recorded on a Microflex MALDI-TOF mass spectrometer (Bruker Daltonics) using doubly recrystallized 2-cyano-4-hydroxy cinnamic acid (CCA) or dithranol as a matrix. Melting points were uncorrected and determined by a melting point apparatus (Electrothermal 9100, Fisher Scientific, USA). Absorption spectra were measured by a UV-2550 UV-Vis spectrophotometer (SHIMADZU, Japan). Fluorescence spectra were obtained from a Carry Eclipse Fluorescence Spectrophotometer (Agilent Technologies) using a mixture of water and THF as solvents. Cyclic voltammograms were conducted on cyclic voltammetry instrument (Autolab). Particle size of all fluorophores were measured by Zetatract Dynamic Light Scattering (DLS) particle size analyzer with zeta potential capability.

2.2 Materials and chemicals

All reagent grade chemicals were obtained from Merck® (Germany), Sigma-Aldrich (USA), or Fluka®, (Switzerland). For general reactions, solvents such as methylene chloride (CH_2Cl_2) and acetonitrile (CH_3CN) were reagent grade and stored over molecular sieves for at least 24 h prior uses. In anhydrous reactions, solvents such as tetrahydrofuran (THF) and toluene (PhCH_3) were dried and distilled before use according to the standard procedures. All column chromatography were operated using silica gel 60 (70-230 mesh) purchased from Merck. Thin layer chromatography (TLC) was performed on silica gel plates (Merck F245). Solvents used for extraction and chromatography were commercial grade and distilled before use. Diethyl ether (Et_2O) and chloroform (CHCl_3) used for extraction was reagent grade. De-ionized water was used in all fluorescence experiments unless specified otherwise. All reactions were carried out under positive pressure of N_2 filled in rubberballoons.

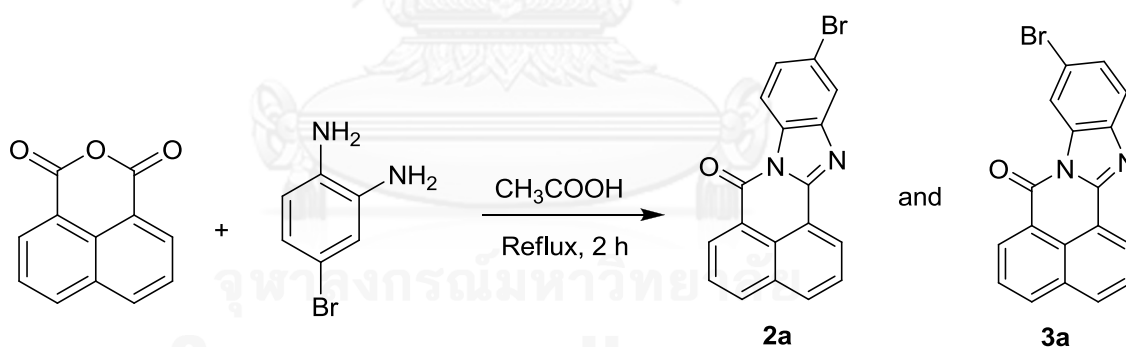
2.3 Synthesis and characterization

2.3.1 Compound 1



A mixture of 1,8-naphthalic anhydride (1 g, 5.05 mmol) and benzene-1,2-diamine (0.82 g, 7.57 mmol) was refluxed in acetic acid (20 mL) for 2 hours, then a mixture was poured to ice-water and stirred for 15 minutes. Precipitate formed was filtrated by vacuum filtration. The crude was crystallized in ethyl acetate to afford **1** as green crystal (1.2 g, 78%) ^1H NMR (400 MHz, CDCl_3) δ 8.84 (d, $J = 7.3$ Hz, 1H), 8.78 (d, $J = 7.4$ Hz, 1H), 8.56 (t, 1H), 8.27 (d, $J = 8.2$ Hz, 1H), 8.13 (d, $J = 8.2$ Hz, 1H), 7.88 (d, $J = 4.8$ Hz, 1H), 7.83 – 7.77 (m, 2H), 7.55 – 7.42 (m, 2H). This data agreed with the literature report [40].

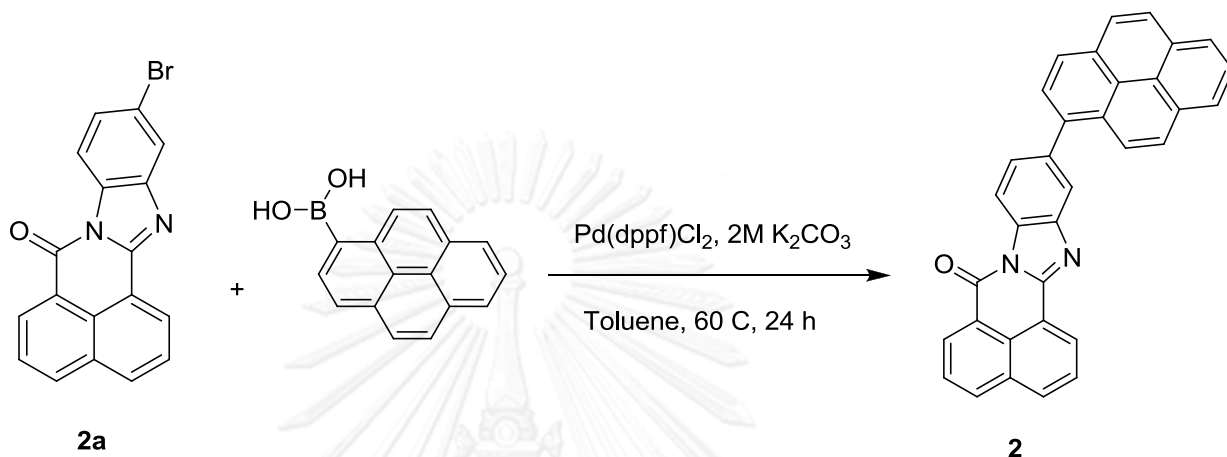
2.3.2 Bromo Naphthalene benzimidazole **2a**, **3a**



A mixture of 1,8-naphthalic anhydride (2 g, 7.22 mmol) and benzene-4-Bromo-1,2-diamine (1.48 g, 7.94 mmol) was refluxed in acetic acid (20 mL) for 2 hours, then a mixture was poured to ice-water and stirred for 15 minutes. Precipitate formed was filtrated by vacuum filtration. The mixture of compounds was separated by column chromatography using hexane/dichloromethane (4:1, v/v) as the eluent. The first compound that was obtained from the chromatographic column was **2a** ^1H NMR (400 MHz, CDCl_3) δ 8.84 (d, $J = 6.7$, 1H), 8.68 (d, $J = 7.1$, 1H), 8.40 (d, $J = 8.5$, 1H), 8.29 (d, $J = 7.8$, 1H), 8.17 (d, $J = 8.1$ Hz, 1H), 8.00 (s, 1H), 7.85 – 7.79 (m, 2H), 7.56 (d, $J = 8.5$ Hz, 1H). The second compound was **3a** ^1H NMR (400 MHz, CDCl_3) δ 8.85 – 8.80 (m, 2H),

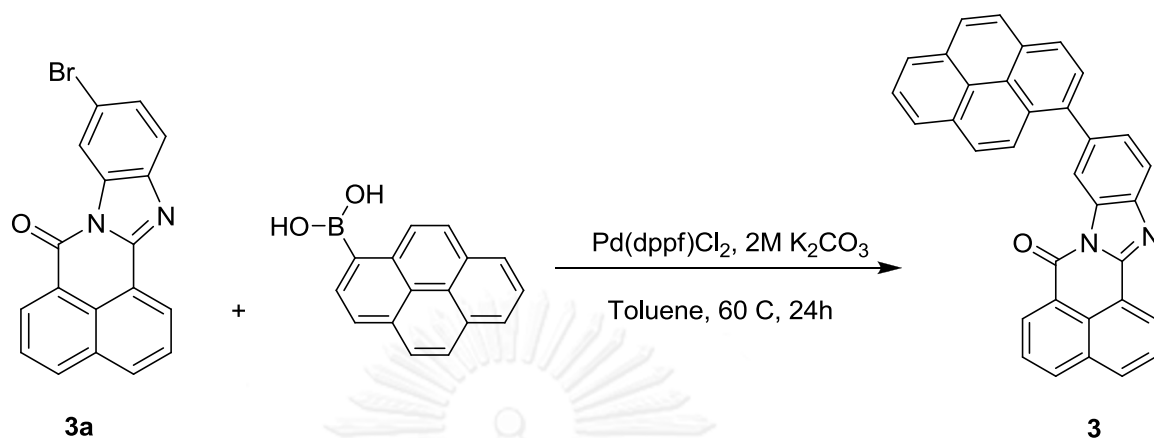
8.75 (s, 1H), 8.31 (d, $J = 8.0$ Hz, 1H), 8.18 (d, $J = 8.4$ Hz, 1H), 7.87 – 7.82 (m, 2H), 7.73 (d, $J = 8.5$ Hz, 1H), 7.59 (d, $J = 8.4$ Hz, 1H). Both **2a** and **3a** were yellow crystalline solid which was obtained in the overall yield of 89 %.

2.3.3 Compound 2

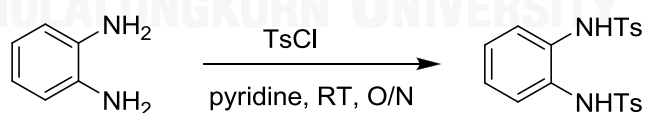


A mixture of **2a** (0.3 g, 0.86 mmol), pyren-1-ylboronic acid (0.32 g, 1.29 mmol), Pd(dppf)Cl_2 (0.031 g, 0.043 mmol), $2\text{M K}_2\text{CO}_3$ (2 mL) in toluene (5 mL) was stirred at 70°C for 24 h under nitrogen. After cooled reaction mixture, dichloromethane (50 mL) was added and the organic solution was extracted with DI water. After that organic phase was dried over Na_2SO_4 and concentrated under reduced pressure. The residue was purified by column chromatography using gradient solvent from a mixture of hexane/dichloromethane (8:1, v/v) to hexane/ dichloromethane (4:1, v/v) to give **2** as a yellow solid (0.38 g, 85%). The melting point of **2** is 210°C . $^1\text{H NMR}$ (400 MHz, CDCl_3) δ 8.94 (d, $J = 7.2$ Hz, 1H), 8.84 (d, $J = 6.4$ Hz, 1H), 8.73 (d, $J = 8.3$ Hz, 1H), 8.32 (d, $J = 7.8$ Hz, 1H), 8.27 – 7.97 (m, 11H), 7.85 (m, 7.8 Hz, 2H), 7.77 (dd, $J = 8.3, 1.5$ Hz, 1H). $^{13}\text{C NMR}$ (100 MHz, CDCl_3) δ 160.7, 150.0, 143.5, 139.2, 137.3, 135.5, 132.4, 132.32, 132.29, 132.0, 131.5, 131.0, 131.0, 130.8, 128.7, 128.5, 127.8, 127.7, 127.7, 127.5, 127.4, 127.2, 127.0, 126.0, 125.21, 125.16, 125.04, 125.01, 124.91, 124.7, 123.1, 121.6, 120.3, 115.7. MS (MALDI-TOF) Calculated for $\text{C}_{34}\text{H}_{18}\text{N}_2\text{O}$: 470.1 Found: 469.4

2.3.4 Compound 3



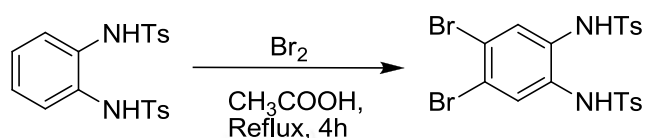
The mixture of **3a** (0.2 g, 0.057 mmol), pyren-1-ylboronic acid (0.21 g, 0.86 mmol), Pd(dppf)Cl₂ (0.021 g, 0.069 mmol), 2M K₂CO₃ (2 mL) in toluene (4 mL) was stirred at 70°C for 24 h under nitrogen. After cooled reaction mixture, dichloromethane (50mL) was added and the organic solution was extracted with DI water. After that organic phase was dried over Na₂SO₄ and concentrated under reduced pressure. The residue was purified by column chromatography using gradient solvent from a mixture of hexane/ dichloromethane (8:1, v/v) to hexane/ dichloromethane (4:1, v/v) to give **3** as a yellow solid (0.23 g, 93%). ¹H NMR (400 MHz, CDCl₃) δ 9.03 (d, *J* = 7.5 Hz, 1H), 8.91 (s, 1H), 8.73 (d, *J* = 7.3 Hz, 1H), 8.30 – 7.97 (m, 12H), 7.80 (t, *J* = 7.6 Hz, 3H). ¹³C NMR (100 MHz, CDCl₃) δ 160.4, 149.4, 139.3, 137.2, 135.6, 132.6, 132.24, 132.18, 131.8, 131.4, 131.0, 130.7, 129.2, 128.7, 128.3, 128.2, 128.0, 127.7, 127.6, 127.6, 127.5, 127.4, 127.1, 127.0, 126.0, 125.2, 125.1, 124.9, 124.8, 124.6, 122.9, 122.8, 119.0, 117.9. MS (MALDI-TOF) Calculated for C₃₄H₁₈N₂O: 470.1 Found: 469.4.

2.3.5 *N,N'*-(1,2-phenylene)bis(4-methylbenzenesulfonamide)

The solution of 4-toluenesulfonyl chloride (21 g, 110 mmol) in pyridine (50 ml) was stirred at temperature lower than 0°C for 20 minute. Benzene-1,2-diamine (54.1 mmol, 5.85 g) was slowly added to the solution, and then the mixture was stirred at room temperature for 4 h in a NaCl-ice bath. The resulting mixture was stirred at room temperature for 18 h after that the mixture was acidified to pH 4 by 15% aqueous HCl, precipitate was formed. The product was refluxed in ethyl acetate (150ml) for 1h, the solution stored in room temperature overnight for crystallization. After filtration, the

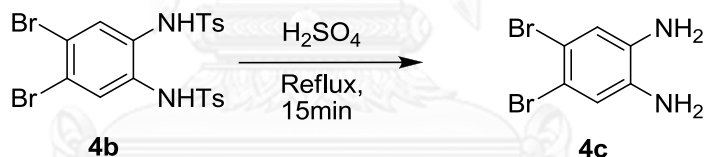
produce was obtained as a pale solid (15.4 g, 69%) ^1H NMR (400 MHz, CDCl_3) δ 7.56 (d, $J = 8.3$ Hz, 1H), 7.22 (d, $J = 8.0$ Hz, 1H), 7.04 (dd, $J = 5.9, 3.6$ Hz, 1H), 6.95 (dd, $J = 5.8, 3.6$ Hz, 1H), 6.80 (s, 1H), 2.39 (s, 2H).

2.3.6 *N,N'*-(4,5-Dibromo-1,2-phenylene)bis(4-methylbenzenesulfonamide)



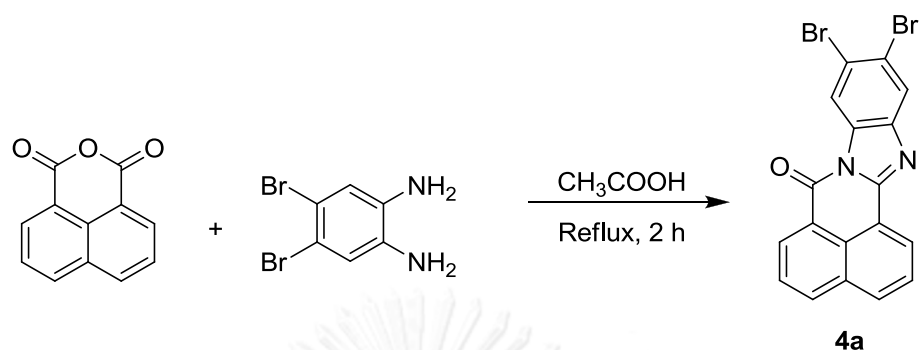
Bromine (1.92 g, 18.0 mmol) was slowly added to an ice-cooled and stirred suspension of *N,N'*-(1,2-phenylene)bis(4-methylbenzenesulfonamide) (3.75 g, 9.0 mmol) and anhydrous NaOAc (1.5 g, 18.0 mmol) in glacial acetic acid (15 ml). The yellow suspension was stirred reflux for 3 h. Then, poured into ice water (40 ml) and stirred for 1 h, and ethanol (20 ml) was added. Finally, the precipitate was filtered. The product was obtained as a fine colorless powder of *N,N'*-(4,5-dibromo-1,2-phenylene)bis(4-methylbenzenesulfonamide) (1.1g, 98%). ^1H NMR (400 MHz, CDCl_3) δ 7.59 (d, $J = 8.3$ Hz, 1H), 7.31 – 7.23 (m, 2H), 6.76 (s, 1H), 2.42 (s, 2H).

2.3.7 4,5-Dibromobenzene-1,2-diamine



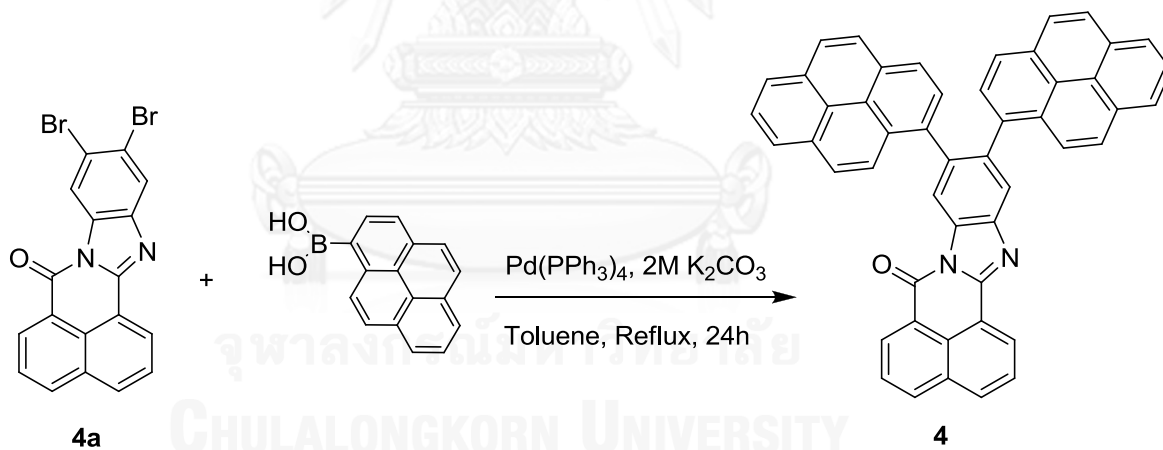
The compound *N,N'*-(4,5-Dibromo-1,2-phenylene) bis (4-methylbenzenesulfonamide) (3.4 g, 5.9 mmol) was heated in concentrated Sulphuric acid (20 ml) at 110 °C for 15 min. After cooling to room temperature, the solution was poured into ice-water and neutralized with 50% NaOH solution until pH 7, precipitate was formed. After filtration, the precipitate gave beige powder of 4,5-Dibromobenzene-1,2-diamine (3.3 g, 96%). ^1H NMR (400 MHz, CDCl_3) δ 6.93 (s, 1H), 3.50 – 3.29 (m, 2H).

2.3.8 Dibromo Naphthalene benzimidazole



A mixture of 1,8-naphthalic anhydride (1.03 g, 3.7 mmol) and 4,5-Dibromobenzene-1,2-diamine (2 g, 4.1 mmol) was refluxed in acetic acid (25 mL) for 2 h, then a mixture was poured to ice-water and stirred for 15 minute. Precipitate formed was filtrated by vacuum filtration to give green powder (1.5 g, quantitative yield) ^1H NMR (400 MHz, CDCl_3) δ 8.88 (s, 1H), 8.86 – 8.79 (m, 2H), 8.34 (d, $J = 8.7$ Hz, 1H), 8.21 (d, $J = 8.4$ Hz, 1H), 8.14 (s, 1H), 7.89 - 7.82 (m, 2H).

2.3.9 Compound 4



The mixture of **4a** (0.47 mmol, 0.2 g), pyren-1-ylboronic acid (1.2 mmol, 0.3 g), $\text{Pd}(\text{dppf})\text{Cl}_2$ (0.021 g, 0.069 mmol), 2M K_2CO_3 (2 mL) in toluene (4 mL) was stirred at 70°C for 24 h under nitrogen. After cooled reaction mixture, dichloromethane (50mL) was added and the organic solution was extracted with DI water. After that organic phase was dried over Na_2SO_4 and concentrated under reduced pressure. The residue was purified by column chromatography using gradient solvent from a mixture of hexane/ dichloromethane (8:1, v/v) to hexane/ dichloromethane (4:1, v/v) to give **4** as a yellow solid (0.09 g, 30%). ^1H NMR (400 MHz, CDCl_3) δ 8.93 (d, $J = 7.3$ Hz, 1H), 8.90

(s, 1H), 8.71-8.67 (m, 1H), 8.24 – 7.64 (m, 21H), 7.49 – 7.41 (m, 2H). ¹³C NMR (100 MHz, CDCl₃) δ 160.6, 150.3, 139.4, 139.1, 136.7, 136.6, 135.5, 132.4, 132.3, 132.1, 131.3, 131.25, 131.15, 131.1, 131.0, 131.0, 130.7, 130.2, 130.1, 130.1, 129.5, 129.5, 129.1, 129.1, 128.0, 127.9, 127.6, 127.5, 127.3, 127.2, 127.1, 127.1, 127.0, 127.0, 125.9, 125.7, 125.6, 125.4, 125.0, 124.9, 124.8, 124.75, 124.69, 124.0, 124.0, 123.7, 123.1, 123.0, 119.5, 119.4. MS (MALDI-TOF) Calculated for C₅₀H₂₆N₂O: 670.2 Found: 669.6

2.4 Photophysical property study

The stock solution of **1** that concentration is 1 mM was prepared by dissolving in THF 10 mL. The stock solutions of other fluorophore are prepared by the same condition.

2.4.1 UV-visible spectroscopy

The each of stock solutions are diluted to 30 μ M in THF. The UV-visible absorption spectra were recorded from 200 nm to 500 nm at room temperature.

2.4.1.1 Molar extinction coefficient (ϵ)

The molar extinction coefficient (ϵ) of **1-4** were calculated from the UV-Visible absorption spectra in THF analytical samples at various concentrations. The maximum intensity of all samples had better not be more than value of 1. The absorption intensity of maximum wavelengths (λ) of each compound was plotted versus the concentrations (C) at the respective excitation wavelengths. Each plot should be a straight go through origin-point. The molar extinction coefficient (ϵ) represented into the following equation:

$$A = \epsilon bC$$

2.4.2 Fluorescence spectroscopy

The emission spectra of fluorophores which were diluted to 30 μ M in THF were recorded from 400 nm to 750 nm at room temperature using an excitation wavelength at 380 nm (**1**), 344 nm (**2, 3**), 350 nm (**4**).

2.4.2.1 Fluorescence quantum yield (Φ_F)

The fluorescence quantum yield of fluorophores were performed in THF by using quinine sulphate ($\Phi_F = 0.54$) in 0.1 M H₂SO₄ as a reference. The UV-visible absorption spectra of fluorophores that maximum intensity should never be above 0.1 were recorded at varied concentrations. The fluorescent emission spectra of the same

concentration using appropriate excitation wavelengths selected were recorded based on the absorption maximum wavelength (λ_{\max}) of each compound. The integrated fluorescent intensities were plotted versus the absorbance at the respective excitation wavelengths. Each plot should be a straight with 1 interception. η_x^2 , In addition, the fluorescent quantum yield (Φ_F) was obtained from graph of integrated fluorescence intensity vs absorbance represented into the following equation:

$$\Phi_X = \Phi_{ST} \left(\frac{Grad_X}{Grad_{ST}} \right) \left(\frac{\eta_x^2}{\eta_{st}^2} \right)$$

The subscripts Φ_{ST} is the fluorescence quantum yield of a standard reference which is quinine sulfate ($\Phi=0.54$) and Φ_X is the fluorescence quantum yield of sample and η is the refractive index of that solvent.

2.4.2.2 Effect of water content

The stock solutions are diluted into 30 μM by varied water content between 10% - 90% water in THF. The UV-Visible absorption spectra were recorded from 200 nm to 500 nm at room temperature and the emission spectra of fluorophores were recorded from 400 nm to 750 nm at room temperature using an excitation wavelength at 380 nm (1), 344 nm (2,3), 350 nm (4).

2.4.2.3 Time-dependent effect

The emission intensity of fluorophore 2 and 4 that concentrations were 30 μM at 90% water in THF had been monitored for 30 minutes. After that, non-ionic surfactant (tween-30) was added into the new solutions in the same conditions that had been monitored for 30 minutes.

2.5 Electronic test

HOMO and LUMO energy level of fluorophores were detected by cyclic voltammogram technique with Ag/ 0.01 M AgNO₃ as reference electrode, glassy carbon as working electrode and Pt wire electrode as counter electrode under nitrogen atmosphere. For the sample preparation step, all fluorophores and ferrocene (external standard) were mixed with 0.1 M of TBAFF, then dissolved in acetonitrile and adjusted their concentration to 1 mM for 5 mL. A determinations of cyclic voltammogram were managed at 50 mV per second scan rate

$$E_{HOMO}(eV) = - \left(E_{\text{onset oxidation at cathode}} - E_{\frac{1}{2} \text{ ferrocene}} + 4.8 \right)$$

$$E_{HOMO} (eV) = -4.8 - E_{onset\ oxidation\ at\ cathode} - E_{\frac{1}{2}ferrocene}$$

$$E_{LUMO} = E_{HOMO} + E_{gap}$$

$$E_{gap} = \frac{hc}{onset\ wavelength}$$

$$h = \text{plank's constant} = 6.626 \times 10^{-34} J.s$$

$$c = 3 \times 10^8 m/s$$

Onset wavelength is the first longest absorption wavelength that molecule can absorb

2.6 Nitroaromatic sensor's studies

2.6.1 Fluorescent nitroaromatic sensors

The fluorophores **1**, **2**, **4** were dissolved by THF that concentrations were 1 mM. The nitroaromatic compounds were dissolved by water that concentrations were 0.5 mM. The non-ionic surfactant (tween-20) was dissolved by water to concentrate 1 mM. Concentration of each of fluorophores, all nitroaromatic compounds and tween-20 were adjusted to 0.03 mM, 0.3 mM and 0.1 mM, respectively.

2.6.2 Stern-Volmer constant

Compound **3** and compound **4** were dissolved in THF and adjusted their concentration to 1,000 μ M. TNT stock was dissolved in water and were evaluated for ϵ to find certain concentration of TNT. The non-ionic surfactant (tween-20) was dissolved in water and adjusted its concentration to 1,000 μ M. According to the experiment, concentration of fluorophore and surfactant were 30 μ M and 100 μ M respectively, by using mixed solvent between water and THF with ratio 97:3 and varied concentration of TNT from 0 to 50 μ M.

2.6.3 Paper test

The solution of **4** (200 μ M) in THF was dropped into filter paper (2 μ L). After that, the paper was dipped in to different concentration of TNT. The paper was observed under an ordinary 20W black light lamp.

2.6.4 1H NMR experiment

Fluorophore **3** (4.9 mg, 10 μ mol) was dissolved in $CDCl_3$ (1.04 mL). 1H NMR experiment was then conducted immediately with a NMR spectrometer (Bruker, 400 MHz). The solution of TNT (11.35 mg, 50 μ mol) in $CDCl_3$ (1 mL) was added into NMR

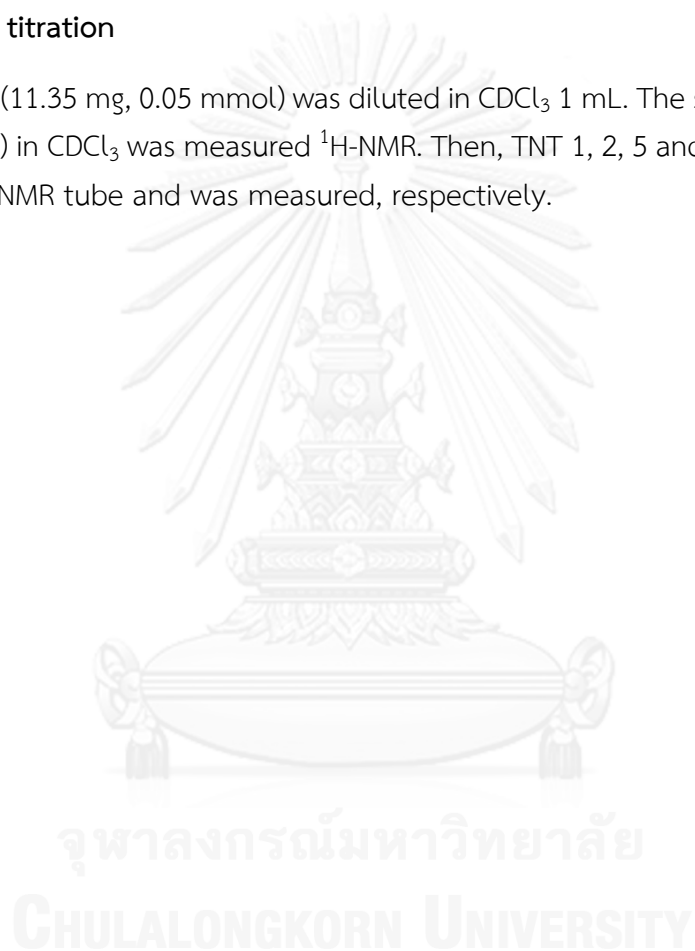
tube and shaken thoroughly. ^1H NMR experiment was measured. The spectra of these experiments were compared.

2.7 Particle size

Fluorophore **4** (1.34 mg, 0.002 mmol) was dissolved by varied water content between 10% - 90% water in THF. All particle sizes were measured by Dynamic Light Scattering (DLS) particle size analyzer.

2.8 ^1H -NMR titration

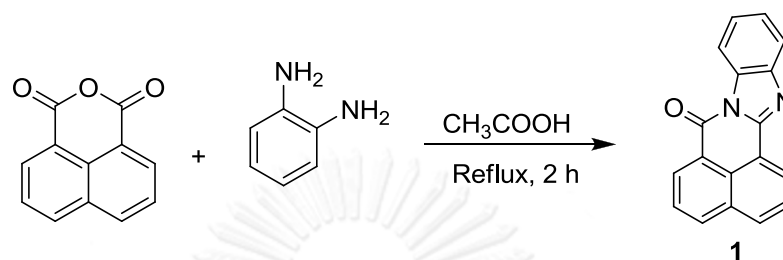
TNT (11.35 mg, 0.05 mmol) was diluted in CDCl_3 1 mL. The solution of **2** (1.2mg, 0.003 mmol) in CDCl_3 was measured ^1H -NMR. Then, TNT 1, 2, 5 and 10 eq solution was added into NMR tube and was measured, respectively.



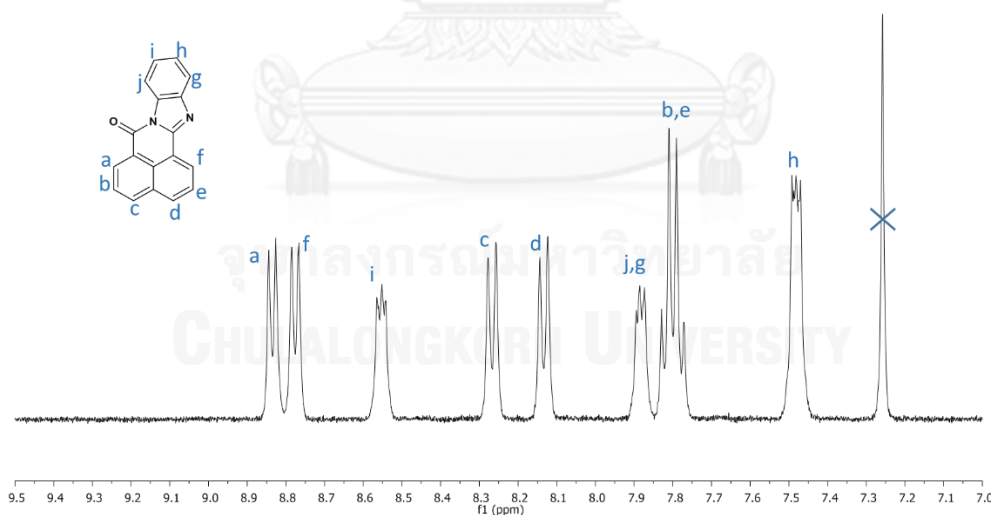
CHAPTER III

Results and discussion

3.1 Synthesis

Scheme 3.1 Synthesis of **1**

Fluorophore **1** was synthesized and used as a reference for three other fluorophores which have pyrene unit(s) on the benzimidazole pendant. A treatment of the commercially available 1,8-naphthalic anhydride with *o*-phenylenediamine in glacial acetic acid under reflux produced **1** in good yield of 82 %. The fluorophore **1** was characterized by ^1H NMR spectroscopy in CDCl_3 as shown in **Figure 3.1**. This synthetic method and NMR data are similar to that reported in literature [40].

Figure 3.1 ^1H NMR (400 MHz, CDCl_3) of **1**

Fluorophore **2** and **3** are basically the fluorophore **1** with 1-pyrenyl group substituted at the 10- and 11-position (**Figure 3.1b**), respectively.

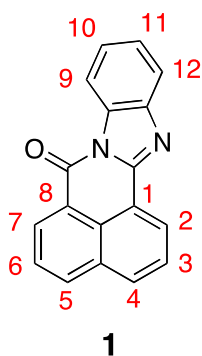
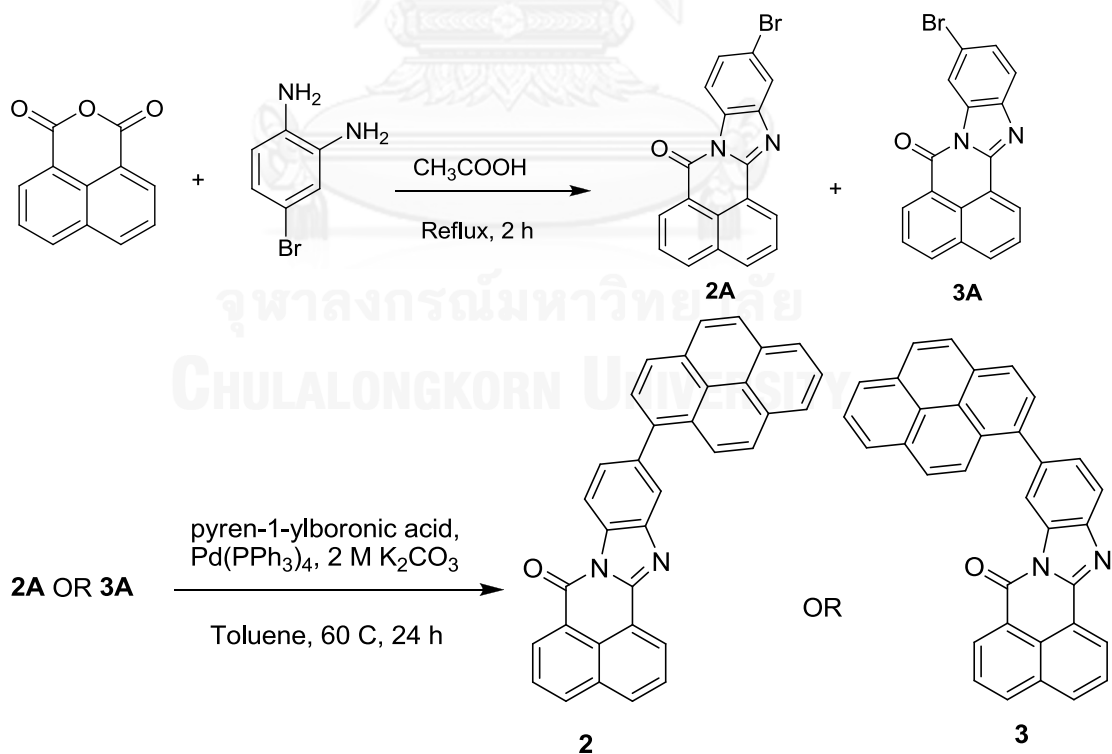


Figure 3.2 Systematic positions in 1,8-naphthalimide-benzimidazole structure.

Synthetic routes of fluorophore **2** and **3** are shown in **Scheme 3.2**. The synthesis started from a reaction of naphthalic anhydride and 4-bromo-1,2-diamine which afforded a mixture of compounds with a bromine at the 10- and 11-positions (**2a** and **3a**, respectively). When the products were purified by column chromatography using solvent from the mixture of hexane/CH₂Cl₂ (4:1, v/v), compound **2a** was eluted out first, followed by compound **3a**. Then, a Suzuki coupling reaction between the compound **2a** or **3a** and pyren-1-boronic acid in toluene catalyzed by tetrakis (triphenylphosphine) palladium(0) gave rise to **2** and **3**. The final products were characterized by MALDI-TOF MS, ¹H NMR spectroscopy and ¹³C NMR spectroscopy.



Scheme 3.2 Synthesis of fluorophore **2** and **3**

The ^1H NMR spectra of **2a** and **2** in CDCl_3 are shown in **Figure 3.3**. The appearance of naphthalimide (a-f) and pyrenyl protons (k-s) in the spectrum of **2** suggested that the coupling reaction was successful. In addition, the signal for proton i, j, and g shifted towards downfield indicating a replacement of bromine by a weaker electron-donating pyrenyl group.

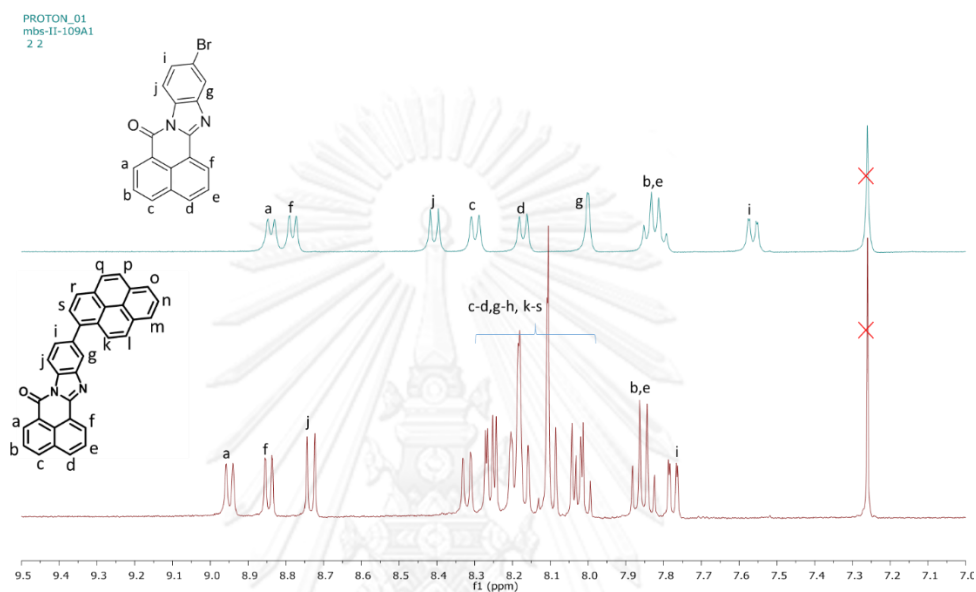


Figure 3.3 ^1H NMR (400 MHz, CDCl_3) of compounds **2a**, **2**

^1H NMR spectra of **3a** and **3** in CDCl_3 are shown in **Figure 3.4**. All signals are assigned to protons in each corresponding structure. The assignments, which are shown by alphabetical symbols, were conducted using the same analogy as compound **2**.

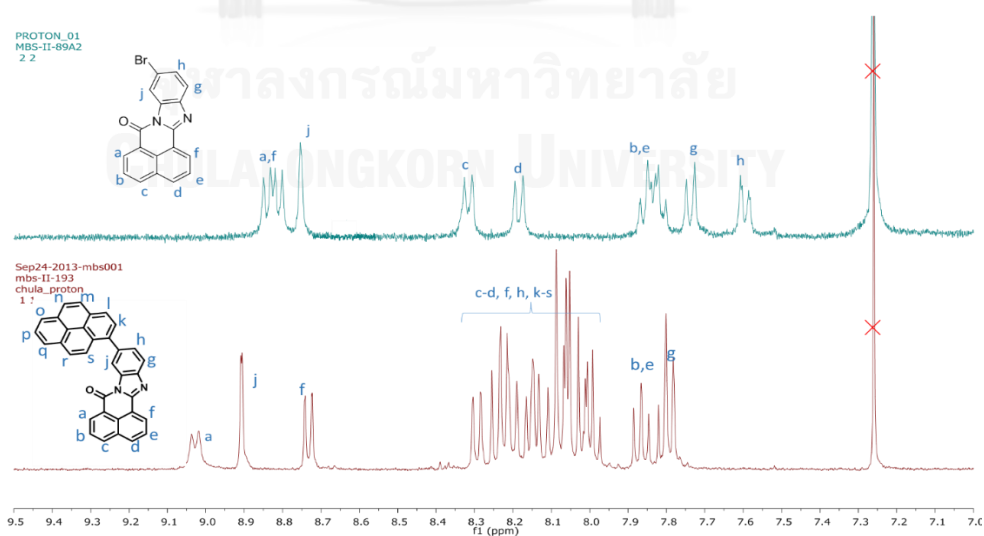
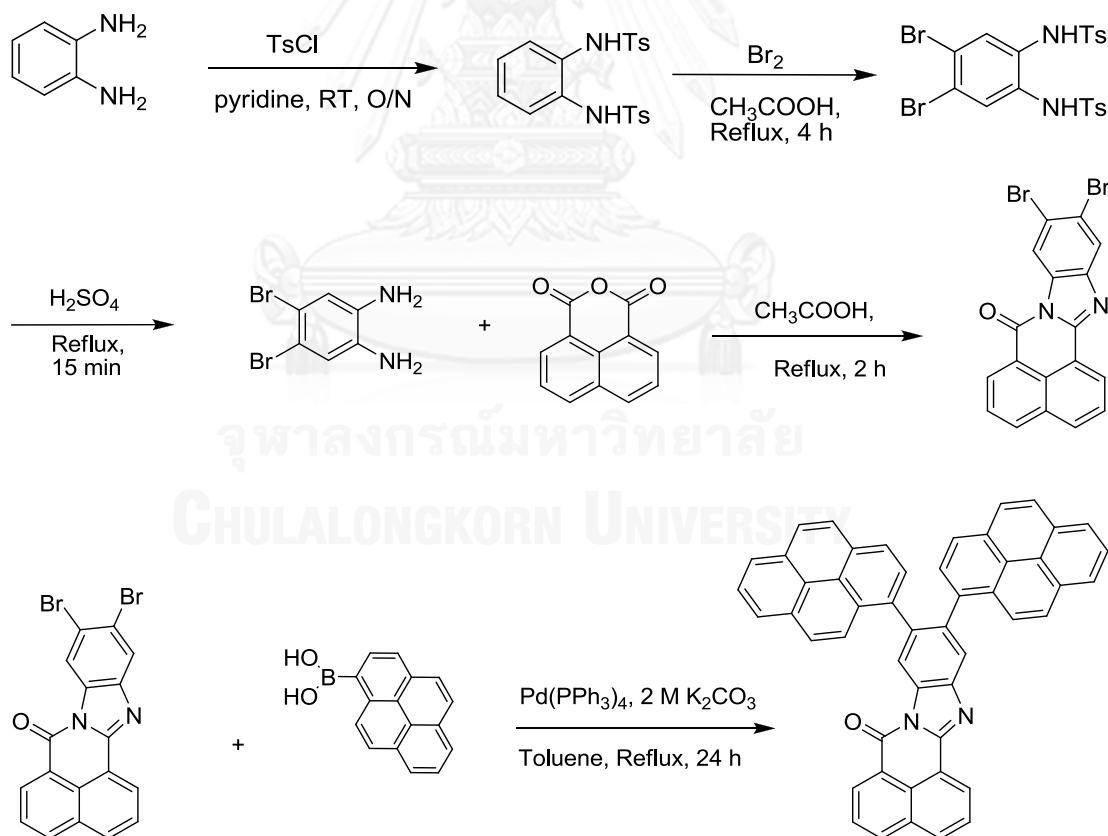


Figure 3.4 ^1H NMR (400 MHz) of compounds **3a**, **3** (CDCl_3)

The synthesis of **4** was started by a known preparation of 3,5-dibromo-1,2-phenylenediamine [42] (**Scheme 3.3**). Protection of the amino groups of o-phenylenediamine using p-toluenesulfonyl chloride (TsCl) afforded the disulfonamide in good yield of 69%. Bromination in refluxing acetic acid produced dibromo compound regioselectively. Acid-catalyzed hydrolysis of the sulfonamide gave rise to 3,5-dibromo-1,2-phenylenediamine in 96% yield. Upon treatment of this diamine with 1,8-naphthalic anhydride, the expected **4a** was produced in quantitative yield. Since the ¹H-NMR and TLC suggested a reasonable purity of the crude compound, the crude product **4a** was used in the Suzuki coupling without purification. The coupling reaction produced the desired compound **4** in 30% yield along with the mono-substitution and debromination products. The low efficiency of this reaction might result from the steric hindrance between the two adjacent reacting centers prohibiting the formation of the desired compound. The product **4** was characterized by NMR spectroscopy, MALDI-TOF MS and IR spectroscopy



Scheme 3.3 Synthesis of **4**

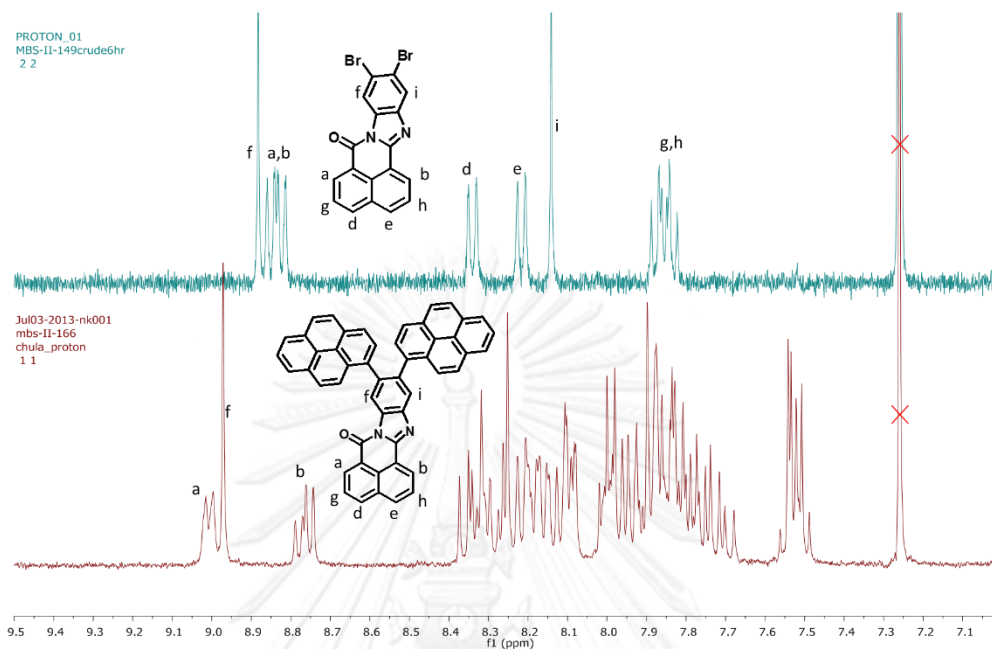


Figure 3.5 ^1H NMR (400 MHz) of compounds **4a**, **4** (CDCl_3)

Compared to the ^1H NMR spectra of **4a**, the spectrum of **4** appeared more complicated due to the presence of two different pyrene groups (Figure 3.5). The signals for naphthalimide fragment in **4** (a,b, g, and h) also became multiplet. This may result from the existence of this compound in two different rotational constraint diastereomers (Figure 3.6)

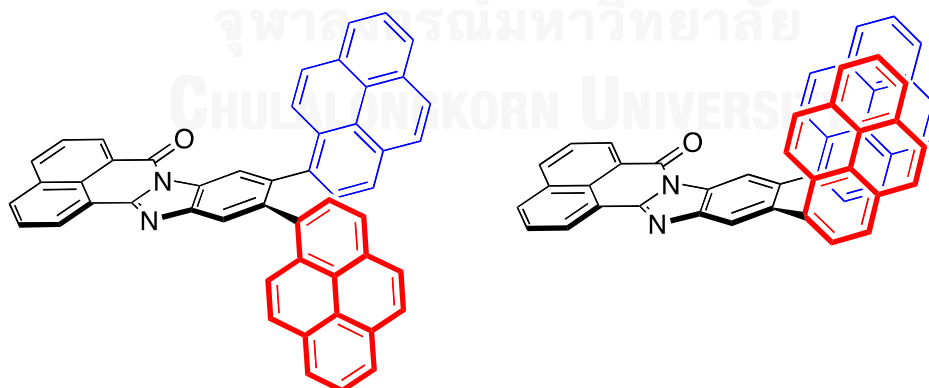


Figure 3.6 Proposed structures of two diastereomeric conformers of **4**

3.2 Photophysical property

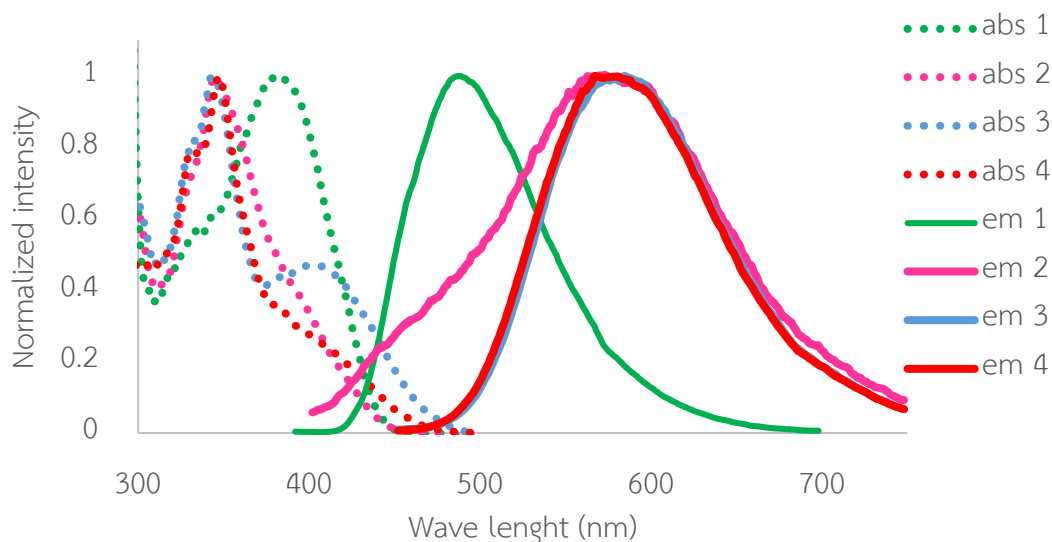


Figure 3.7 Normalized absorption and emission spectra of **1-4** in THF

The photophysical properties of all fluorophores in THF are summarized as shown in **Figure 3.7** and **Table 3.1**. Fluorophore **1** shows maximum wavelength of absorption at 380 nm and maximum wavelength of emission at 487 nm. This fluorophore shows high quantum yield and small stoke shift due to its planar and very rigid structure. For the molar extinction coefficient, fluorophore **1** has the lowest value of all compounds in this study because it has shortest π conjugation system. On the other hands, fluorophore **4** has the highest molar extinction coefficients because it has two highly absorptive pyrene units in the molecule.

In theory, the longer conjugation usually leads to a narrower HOMO-LUMO gap, which results in the red-shifting of the absorption band when the conjugation was extended. In our study, however, the absorption of fluorophores with pyrene unit(s) (**2-4**) shifted to higher energy (blue-shift) compared to compound **1**. This may result from the much higher molar extinction coefficient of pyrene ($54,000 \text{ M}^{-1}$ at 335 nm, [43]) which is the dominating pendant. Nevertheless, the broadening of the absorption bands in **2-4** indicated that there is a conjugated connection between pyrene and the less absorptive naphthalimide unit.

For the emission property, these compounds showed maximum wavelengths around 580-585 nm, presumably due to a similar conjugated system and HOMO-LUMO

energy gap. These compounds exhibit a large Stoke shift (>100 nm), indicating a significant geometry difference between ground and excited states.

The quantum yields (Φ) were determined by using a comparative method with well-characterized standard sample which their quantum yield value was well-known and their emission range was covered in emission of compound. Fluorophore **2**, **3** and **4** exhibited lower quantum yields than **1** because their excited molecules may lost some energy via geometrical relaxation involving rotation and vibration of the pyrene units.

A solution of quinine sulphate in 0.1 M H₂SO₄ ($\Phi = 0.54$) was used as a standard solution because its emission range overlaps with those of **1-4**. However, the quantum yields of **3** and **4** are over 10-fold higher than that of **2**.

Table 3.1 Photophysical properties of fluorophore **1-4**

Compound	Absorption (nm)	Epsilon (M ⁻¹ cm ⁻¹)	Emission (nm)	Quantum yield ^a
1	380	11,700	487	0.64
2	344	26,900	580	0.006
3	344	28,400	585	0.09
	400	13,500	585	0.17
4	350	60,000	582	0.07

^a Quinine sulphate in 0.1 M H₂SO₄ ($\Phi = 0.54$) was used as references.

3.3 Effect of water content on photophysical properties

3.3.1 Fluorophore 1

According to fluorescent signals of fluorophore **1** in solvent of different water contents (**Figure 3.8**), the ACQ effect was a dominating process. Polarizability of solvent inversely affects with solubility of fluorophore **1** which causes H-aggregation, side-by-side aggregation, and self fluorescent quenching. Moreover, high polarizability of solvent will stabilize the excited state, and therefore the releasing energy will be decreased as the fluorescent signal will be red-shifted as shown in **Figure 3.8**.

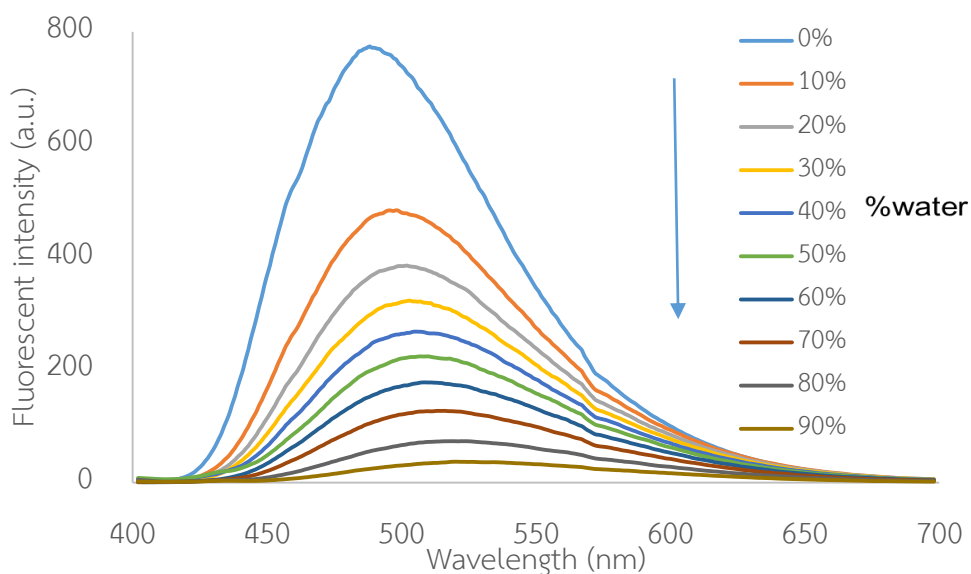


Figure 3.8 Fluorescent spectra of fluorophore **1** in THF with various water contents

3.3.2 Fluorophore 2

Data from the experiment of **2** in THF with various water contents are shown in **Figure 3.9**. Addition of water 10 – 80 % w/v to the process could turn off the fluorescence signal, presumably via ACQ effect. However, addition of water up to 90 % could cause restore the fluorescent the signal back with higher intensity (**Figure 3.9**). This might be due to the Aggregation-Induced Emission Enhancement (AIEE) effect which was preliminarily proven by the decreasing of absorption band shown in **Figure 3.10**. This enhancement was not permanent as the fluorescence intensity was continuously decreased. Addition of surfactant (Tween-20) could prolong the enhanced intensity for approximately 10 minutes (**Figure 3.11**).

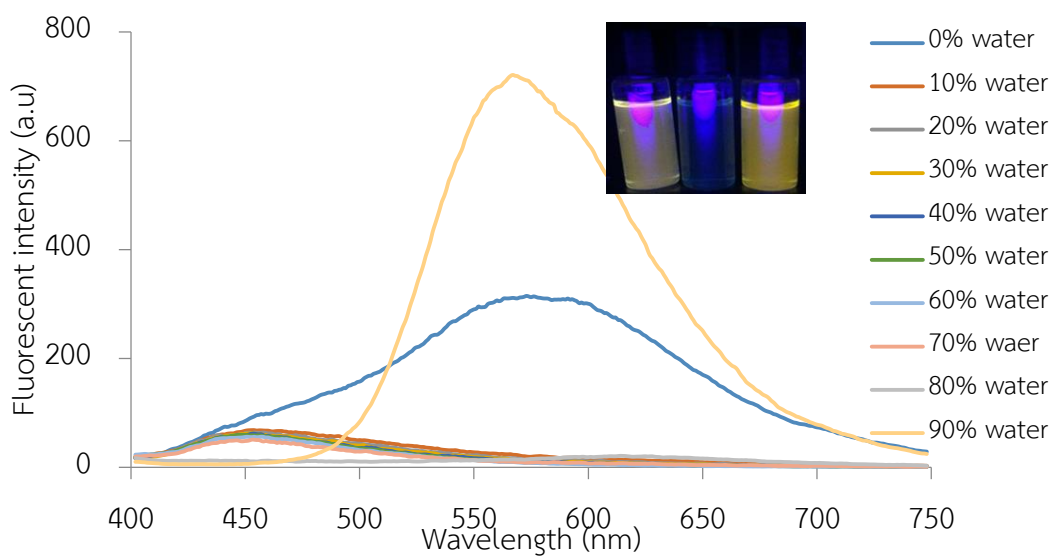


Figure 3.9 Fluorescent spectra of fluorophore 2 in THF and various water contents, inset is the photographs of solutions of 2 (100 μ M) in THF, 50% water in THF, and 90% water in THF, respectively.

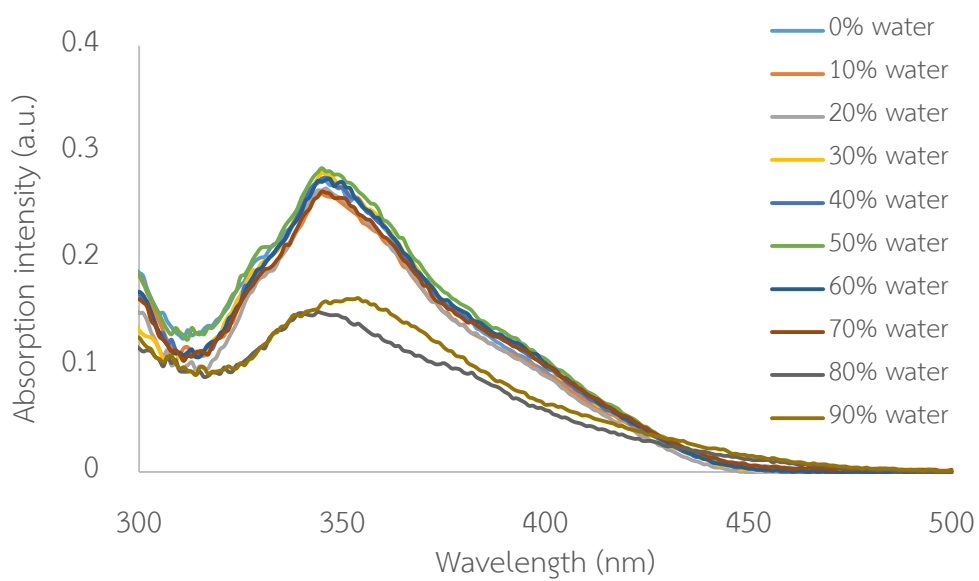


Figure 3.10 Absorption spectra of fluorophore 2 in THF and various water contents

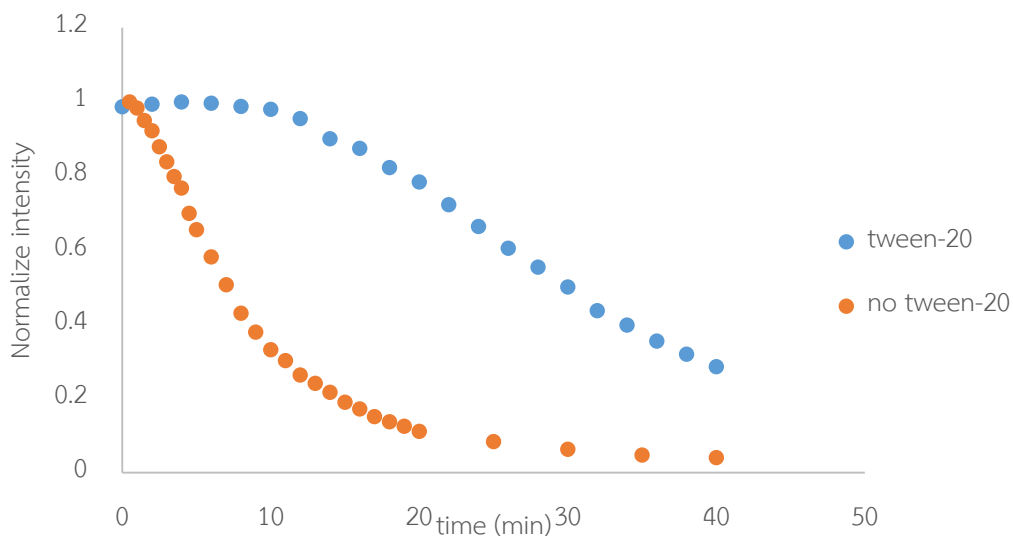


Figure 3.11 Fluorescent intensities of **3** (30 μM) at various times after dilution of stock THF solution with Milli Q water ($\text{H}_2\text{O} : \text{THF} = 9:1$) in the presence (blue) and absence (orange) of Tween-20.

3.3.3 Fluorophore 3

Under the same experimental conditions, fluorophore **3** exhibits different fluorescent property compared to **2**. The increase of water content could not enhance the fluorescent intensity. In fact, the intensity was sharply diminished when 10% of water in THF was used as the solvent (**Figure 3.12**). However, the solutions of **3** in 90% water in THF could emit orange light upon radiation by a black-light bulb. This might cause by the eximer formation of the pyrene units. Absorption spectra from various THF-water ratios also confirmed the aggregation of this compound (**Figure 3.13**). Thus, it was believe that only ACQ was the major behavior of this compound under this experimental condition.

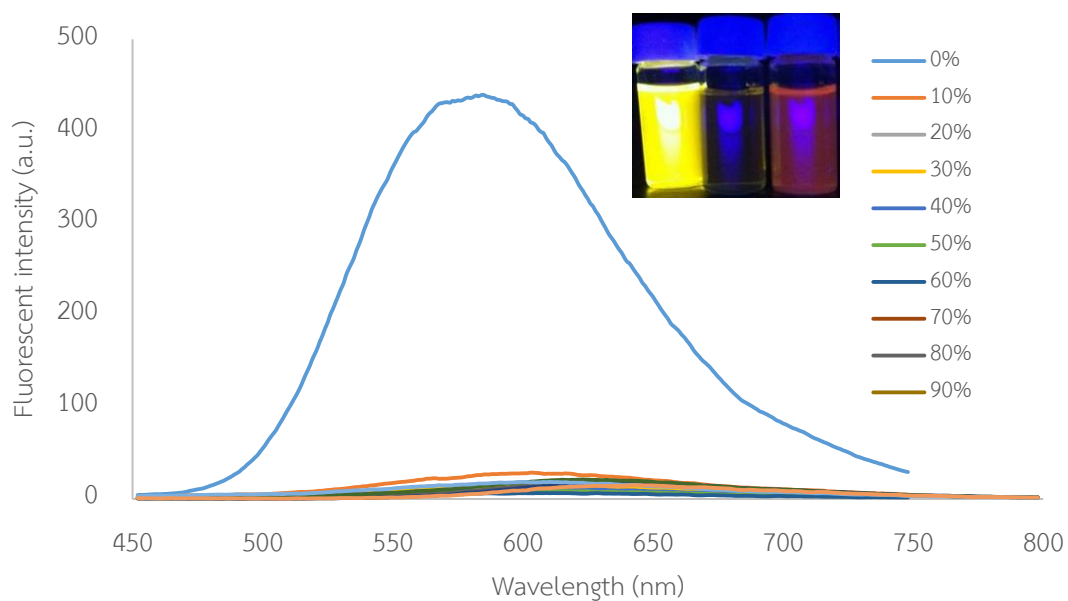


Figure 3.12 Fluorescent spectra of fluorophore 3 in THF and various water contents

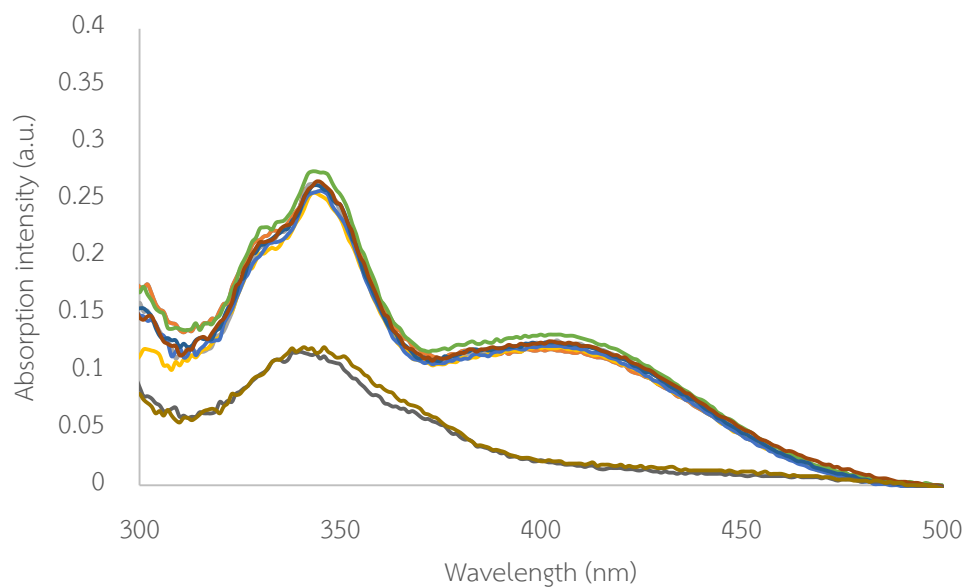


Figure 3.13 Absorption spectra of fluorophore 3 in THF and various water contents

3.3.4 Fluorophore 4

By varying the water content in THF used as solvent for **4**, it was found that this compound possesses similar property as **2**. Upon addition of 10% water, the fluorescent signal was dramatically quenched, but the signal was enhanced as the

water content reached 70-90% **Figure 3.14**. Interestingly, this enhancement could last for more than 40 minutes – a suitable period of time for further sensing property studies.

The particle size determination data was shown in **Figure 3.16**. It was found that particle size was enlarged in poor solvent in which the compound could aggregate. However, addition of water about 70 – 90 % v/v to the process refluorescented the signal back which can be observed by naked eyes under black light (**Figure 3.15**) as well as the Tyndall effect which is detectable under laser lighting. As **Figure 3.17** shows fluorophore **4** which dissolved in mixture solvent between 1:9 of THF and water and give fluorescent signal which still their stability without forming any sediment although 40 minutes have passed so adding surfactant is unnecessary.

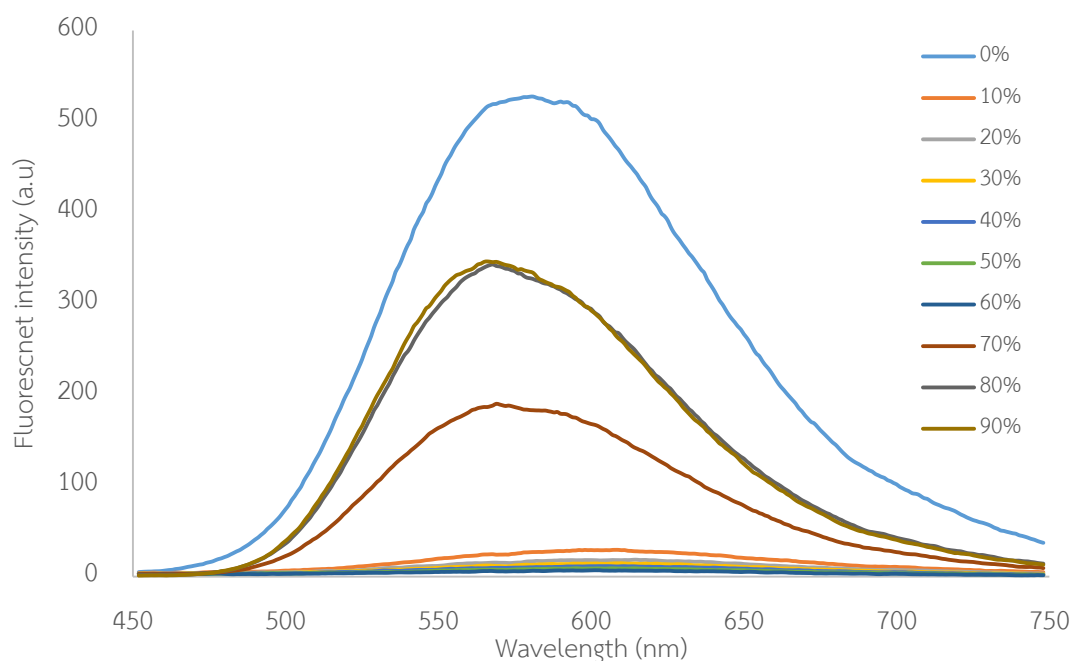


Figure 3.14 Fluorescent spectra of fluorophore **3** in THF and various water contents

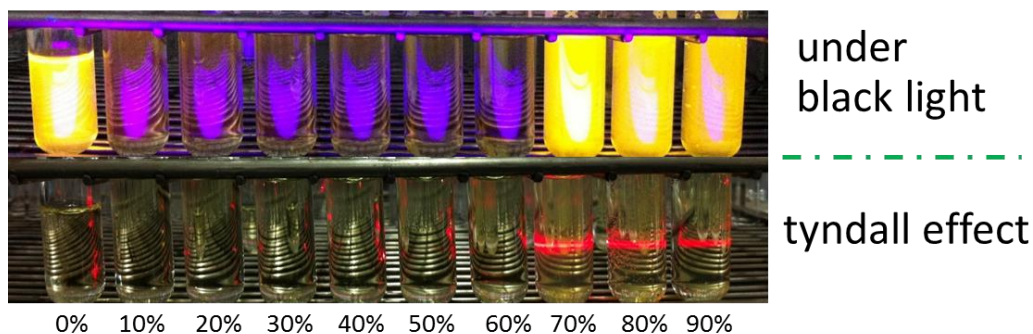


Figure 3.15 Fluorescent emission response under blacklight of **4** in THF with various water content

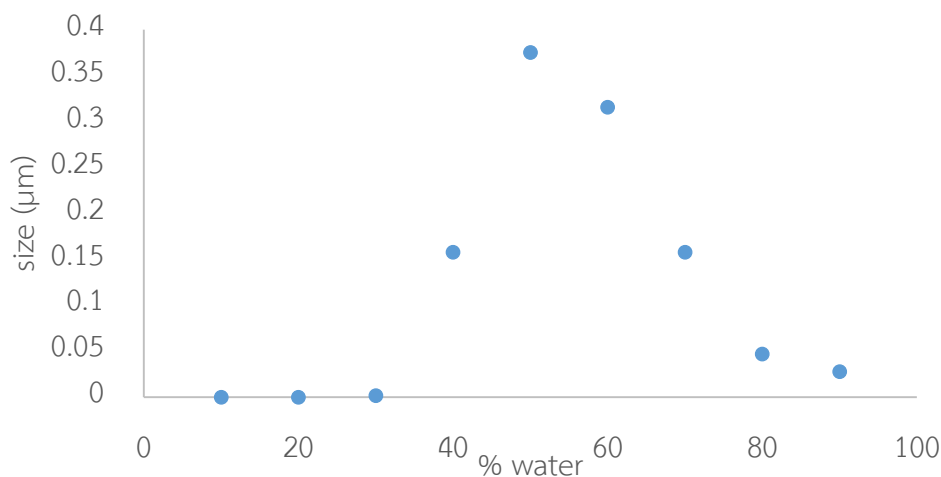


Figure 3.16 Particle size of fluorophore **4**

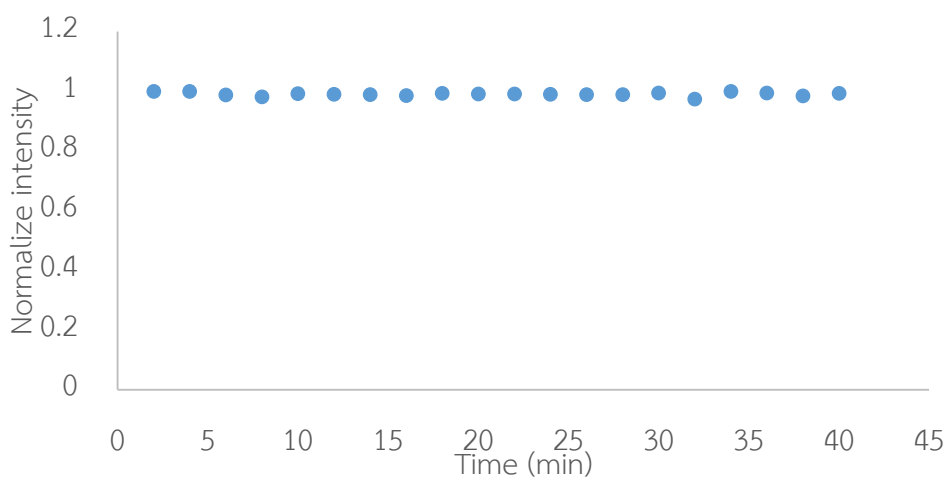


Figure 3.17 Fluorescent intensities of **4** (30 μM) at various times after dilution of stock THF solution with Milli Q water ($\text{H}_2\text{O} : \text{THF} = 9:1$)

3.4 X-ray diffraction

Fluorophore **1**, **2**, **3** and **4** were characterized by XRD techniques. As **figure 3.18**, XRD spectrum of fluorophore **1** shows sharp and strong peak which indicates high crystallinity because molecules is rigid and planar. From **figure 3.19** and **3.20** show XRD spectra of fluorophore **2** and **3** respectively, which are broad peak and indicate fluorophore **2** and **3** lose their crytallinity properties and illustrated as amorphous

properties because of addition pyrene unit to the structure. Fluorophore **3** which has a pyrene unit at the 11 position shows a reflection peak at 5° and 10° peaks which refer to larger unit cells. For fluorophore **4**, sharp peaks at 5° and 10° were observed which indicates higher crystallinity due to the presence of 2 pyrenes in the structure prohibit the rotation of pyrene as shown in **Figure 3.21**.

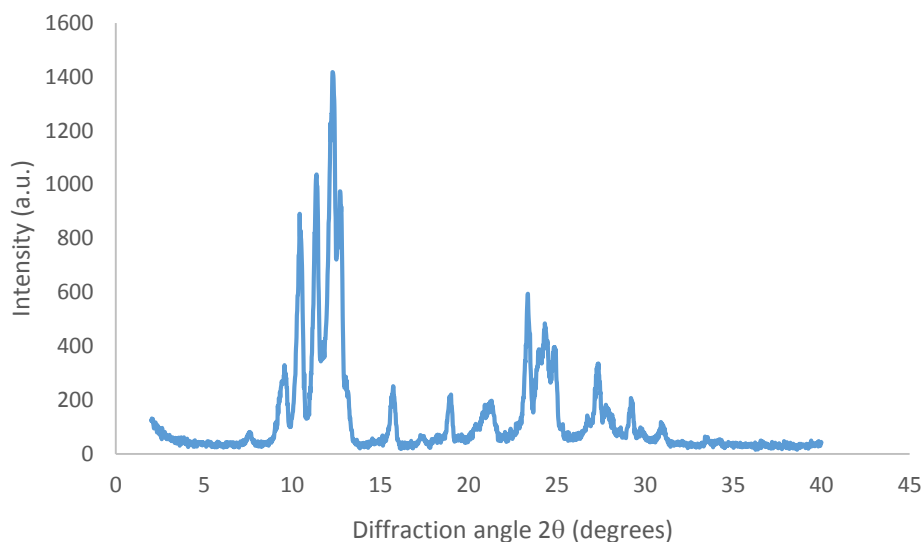


Figure 3.18 XRD of 1

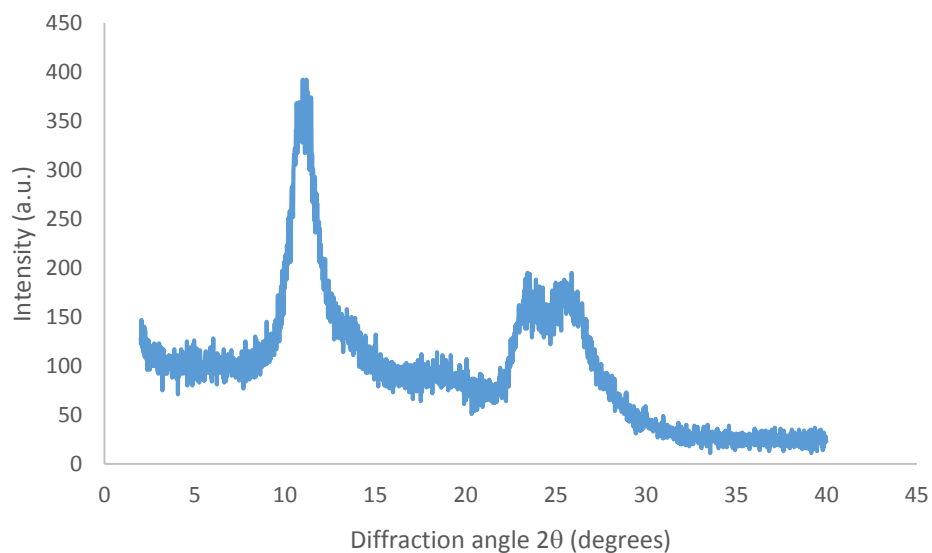


Figure 3.19 XRD of 2

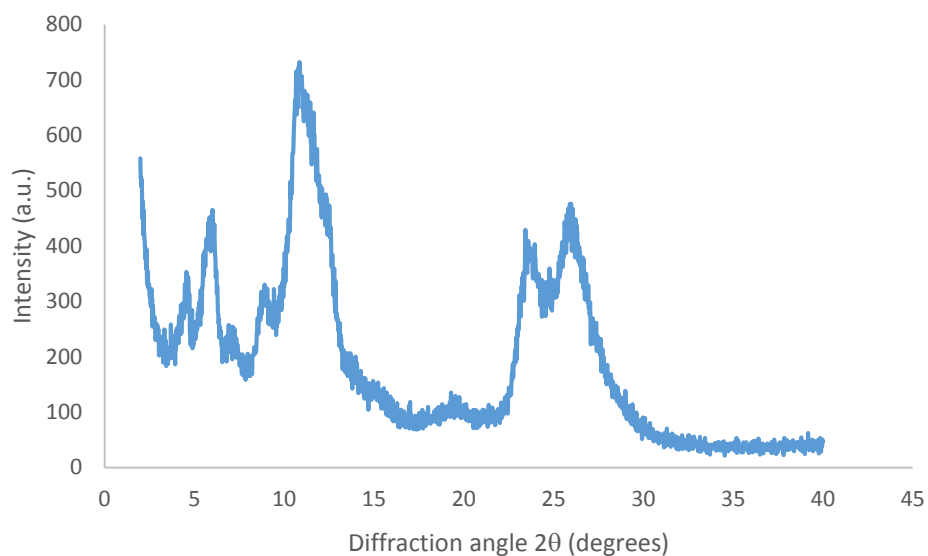


Figure 3.20 XRD of 3

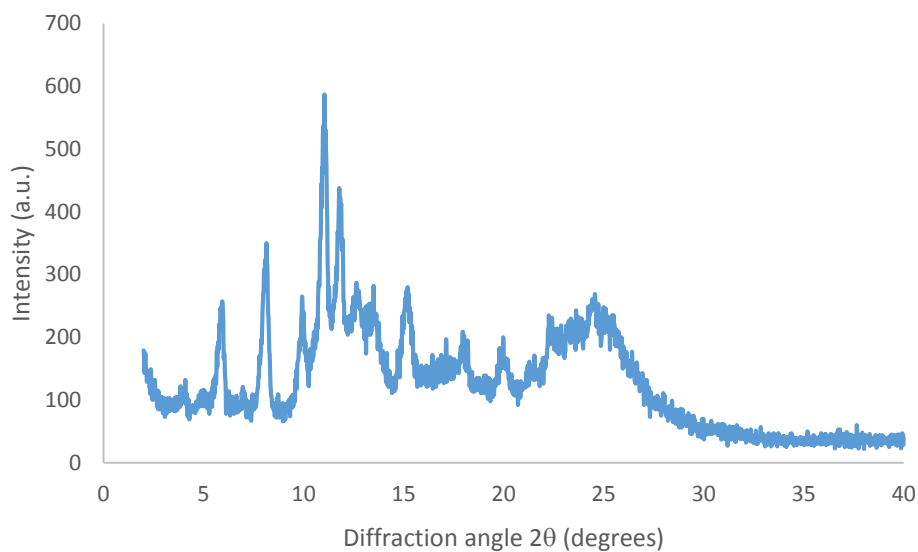


Figure 3.21 XRD of 4

3.5 Electrochemical properties

From the cyclic voltammetry and UV-visible techniques, the HOMO and LUMO energy levels of all fluorophores were determined and shown in **Figure 3.22**. Fluorophore **1** has the lowest energy level of HOMO and LUMO. Addition of pyrene functional groups raised the HOMO and LUMO energy levels. A comparison of energy levels of these fluorophores and three nitroaromatic compounds - DNT, TNT and TNP - indicated that all of these analytes have a LUMO energy level between the HOMO

and LUMO levels of the synthesized fluorophores. Therefore, these compounds can be further studied for their uses as sensor for nitroaromatic compounds via a fluorescent turn-off mechanism.

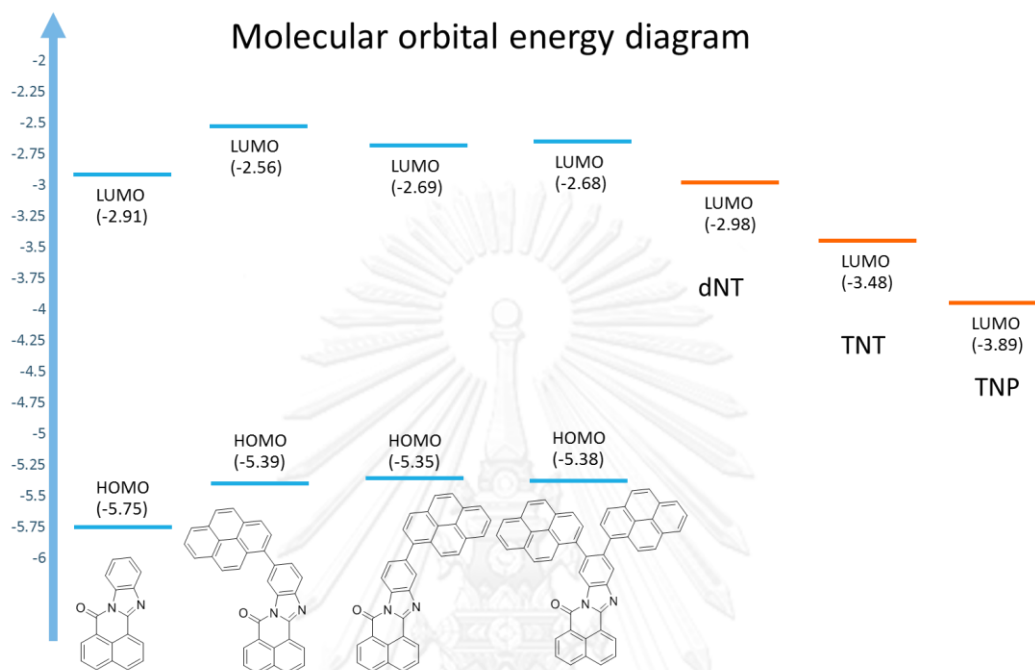


Figure 3.22 Energy level of all fluorophores and 3 nitroaromatic compounds

Table 3.2 Energy level of 1-4

Compound	HOMO	LUMO	E_{gap}
1	-5.75	-2.91	2.84
2	-5.39	-2.56	2.83
3	-5.35	-2.69	2.66
4	-5.38	-2.68	2.70

3.6 Sensing studies for nitroaromatic compounds

3.6.1. Tested analytes

In order to screen the selectivity of **1,2** and **4** towards nitroaromatic compounds, the solutions of each compound were mixed with thirteen nitroaromatic compounds such as 2NP, 3NP, 4NP, DNP, TNP, 2AP, BA, NBA, 2CBA, NB, 4NT, DNT, and TNT. The emission spectra were then observed and compared to the original intensity.

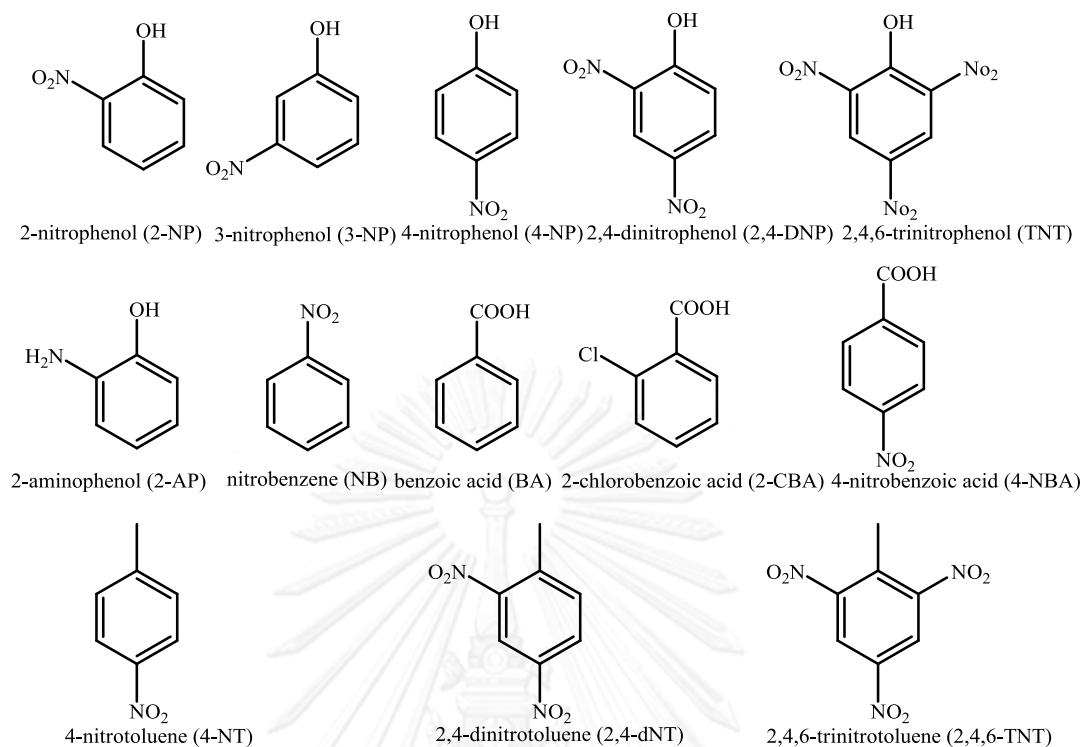


Figure 3.23 Structures of all tested nitroaromatic compounds

3.6.2 Selectivity

Compound **4** was chosen first in this selectivity screening due to its high and stable enhanced fluorescent signal in aqueous THF media. However, the effect of solvent polarity towards selectivity was also examined. **Figure 3.24** summarized the screening data using solutions of **4** (30 μ M) in pure THF, 80% water in THF, and 97% water in THF with all of the tested analytes. In 100% THF, there was no significant selectivity which might result from high solubilities of both **4** and the analytes preventing interaction between them. This was proven when a change to a more polar solvent could reveal some selectivity of **4** towards dNP, tNP, and TNT. As the polarity increases, it was expected that the hydrophobic interaction between **4** and analytes should be stronger, thus the photo-induced electron transfer would be more feasible. The optimum conditions occurred when the water content was increased to 97%, as the sensitivity towards the three analytes was maximized.

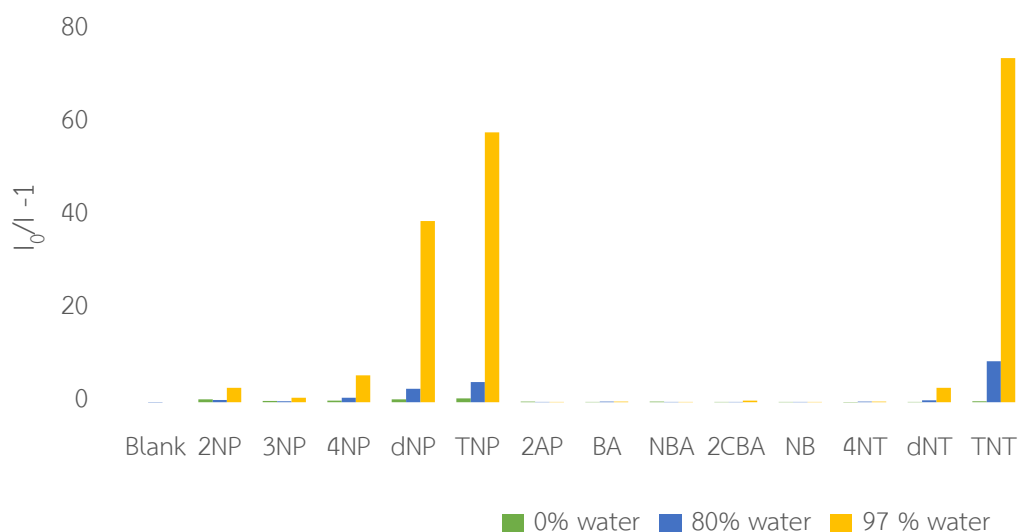


Figure 3.24 Selectivity of **4** (30 μM), after addition of each nitroaromatic compound (10 eq) in THF (blue), and in aqueous media (20% THF (orange)), (3% THF (gray)) ($\lambda_{\text{ex}} = 350 \text{ nm}$).

For the selectivity of **2**, the water content in THF of 97% was chosen and the data was shown in **Figure 3.25**. Tween-20 (0.1 μM) was added in order to delay the decrease of enhanced signal. The selectivity of this compound was similar to that of **4**, but the sensitivities were much higher. This might be due to the micellar effect that force a closer proximity between **2** and analytes.

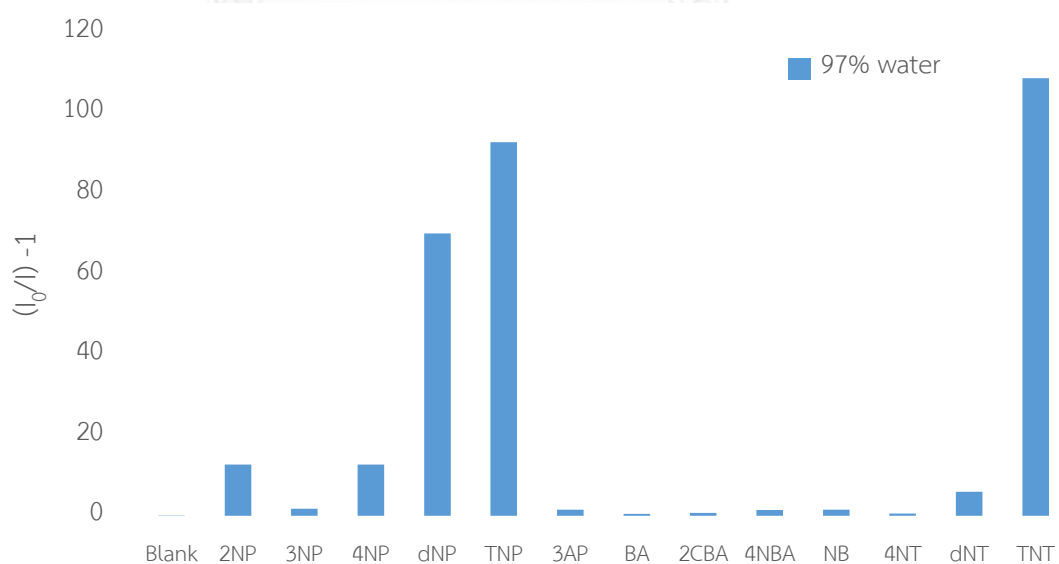


Figure 3.25 Selectivity of **2** (30 μM), after addition of each nitroaromatic compound (10 eq) in aqueous media (3% THF) ($\lambda_{\text{ex}} = 344$)

In order to prove whether the selectivity was caused by filtering effect or competitive absorption by the analytes, we thus performed a screening using fluorophore without pyrene group (**1**). The data in **Figure 3.26** showed that the fluorescent signal of **1** could also be quenched by dNP and tNP. Detailed analysis found that these two analytes possess absorption bands near the excitation wavelength of **1**, **2** and **4** (380 nm, 12,900 M⁻¹ and 350 nm, 13,900 M⁻¹ for TNP). Therefore, it is possible that the selectivity of **2** and **4** towards DNP and TNP might as well be a result of this competitive absorption.

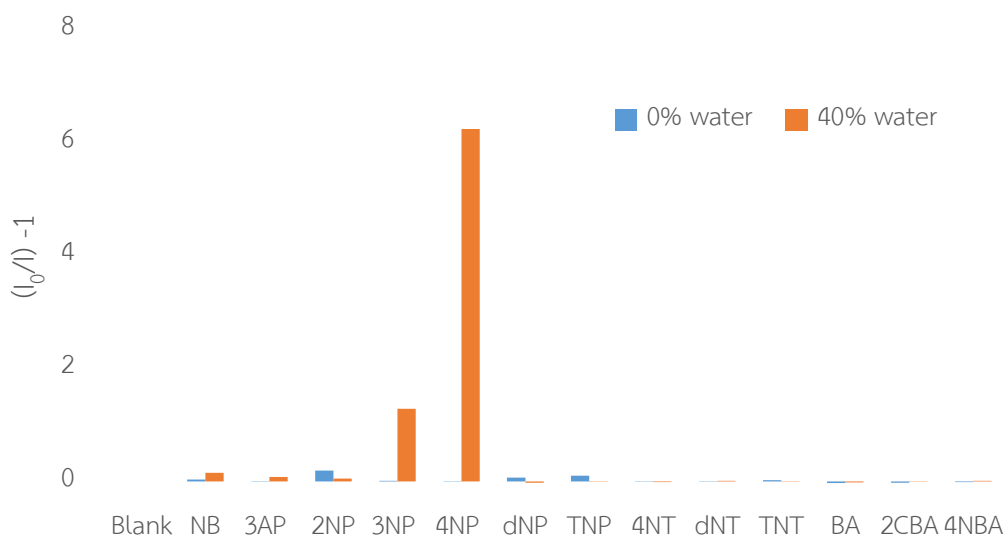


Figure 3.26 Selectivity of **1** (5 μM), after addition of each nitroaromatic compound (20 eq) in THF (orange) and H₂O : THF (40 : 60) ($\lambda_{\text{ex}} = 380 \text{ nm}$).

3.6.2 Stern-Volmer plots: sensitivity determination

In order to determine the sensitivity of **2** and **4** for TNT detection, the fluorescent signals of solutions with varying concentrations of TNT were observed (**Figure 3.27** and **3.28**). Then the plot between $(I_0/I)-1$ and the concentration of TNT were constructed (**Figure 3.29** and **3.30**). Slope of these plots corresponded to the Stern-Volmer constants (K_{sv}) as equation:

$$\frac{I_0}{I} = 1 + K_{\text{sv}}[\text{TNT}]$$

The K_{sv} value reflects the efficiency of fluorescent quenching on **2** and **4** by TNT. From the plots in **Figure 3.29** and **3.30**, the K_{sv} for fluorophore **2** and **4** are 9.63 $\times 10^4 \text{ M}^{-1}$ and 6.00 $\times 10^4 \text{ M}^{-1}$, respectively.

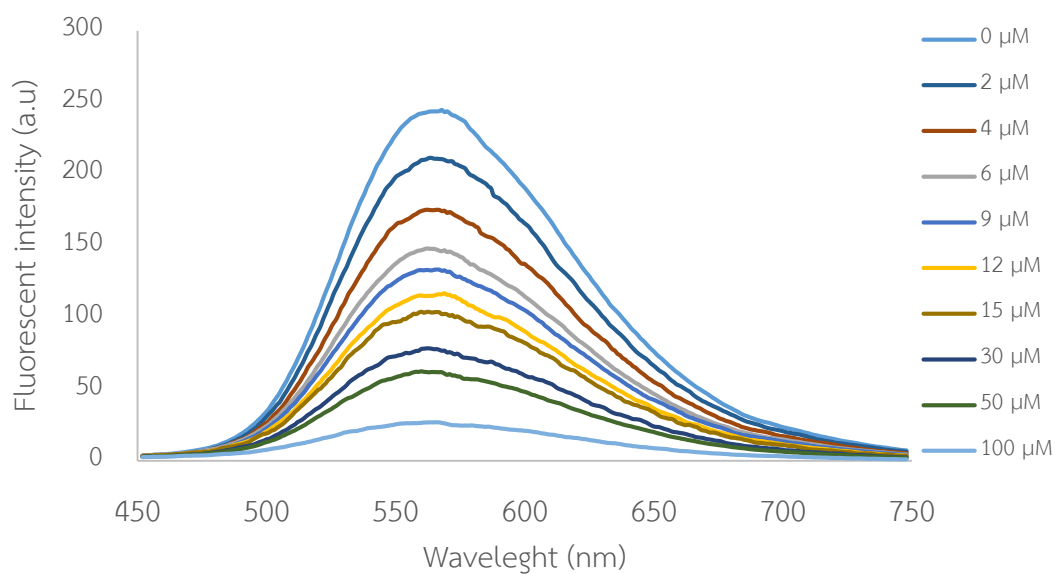


Figure 3.27 The fluorescence intensity of compound 2 (30 μM) with TNT titration (0-100 μM) in aqueous media (3% THF and tween-20 100 μM).

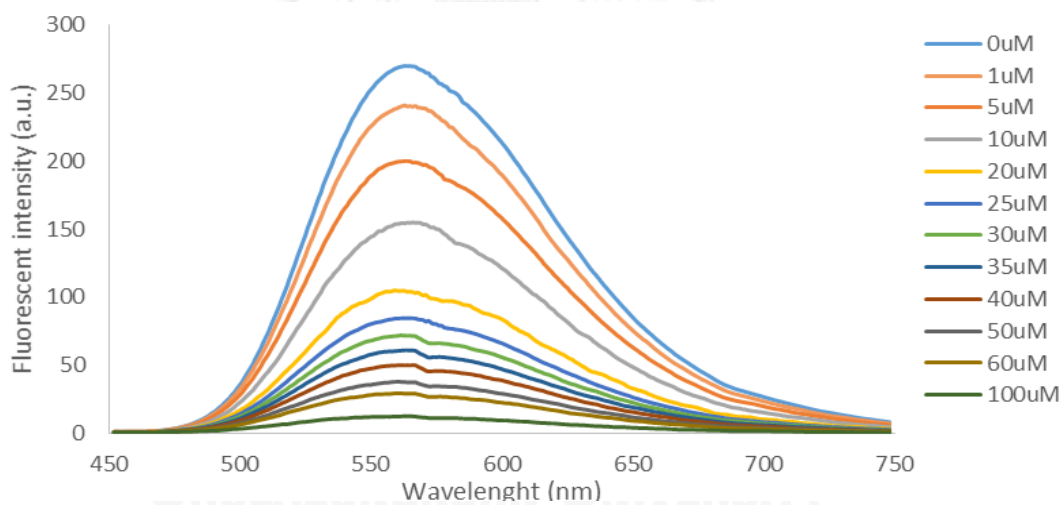


Figure 3.28 The fluorescence intensity of compound 4 (30 μM) with TNT titration (0-100 μM) in aqueous media (3% THF).

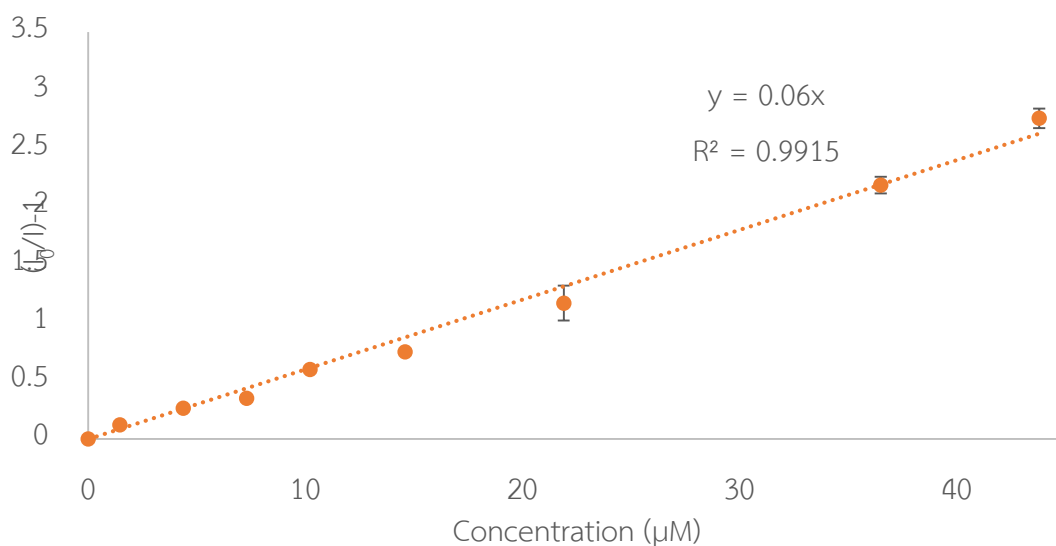


Figure 3.29 The Stern-Volmer plot of **4** (30 μM) vs TNT in aqueous media (3% THF).

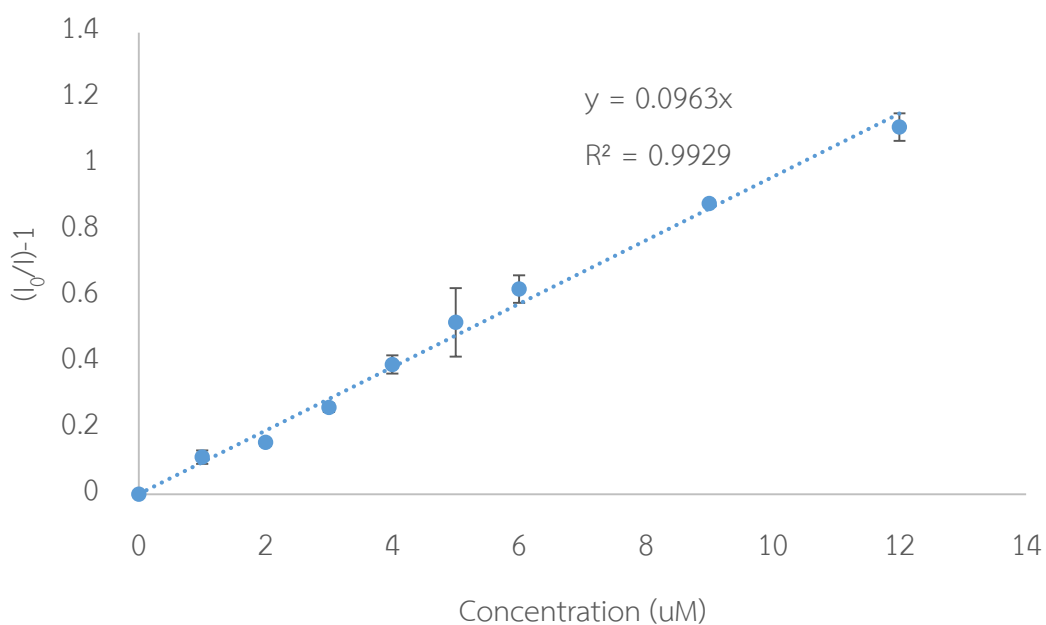


Figure 3.30 The Stern-Volmer plot of **2** (30 μM) vs TNT in aqueous media (3% THF, Tween-20 100 μM).

3.6.4 ^1H NMR experiment

In an attempt to monitor the interaction of fluorophore **2** and TNT, a series of NMR spectra were recorded at ambient temperature using a 10mM solution of **2** and varying amount of TNT (**Figure 3.31**). As the concentration of TNT increases, no

significant change was observed for the signals of **2**. Therefore, it is not likely that there is a static interaction between **2** and TNT. This observation supports a proposed quenching mechanism via photo-induced electron transfer, which is a dynamic process that cannot be observed by NMR technique.

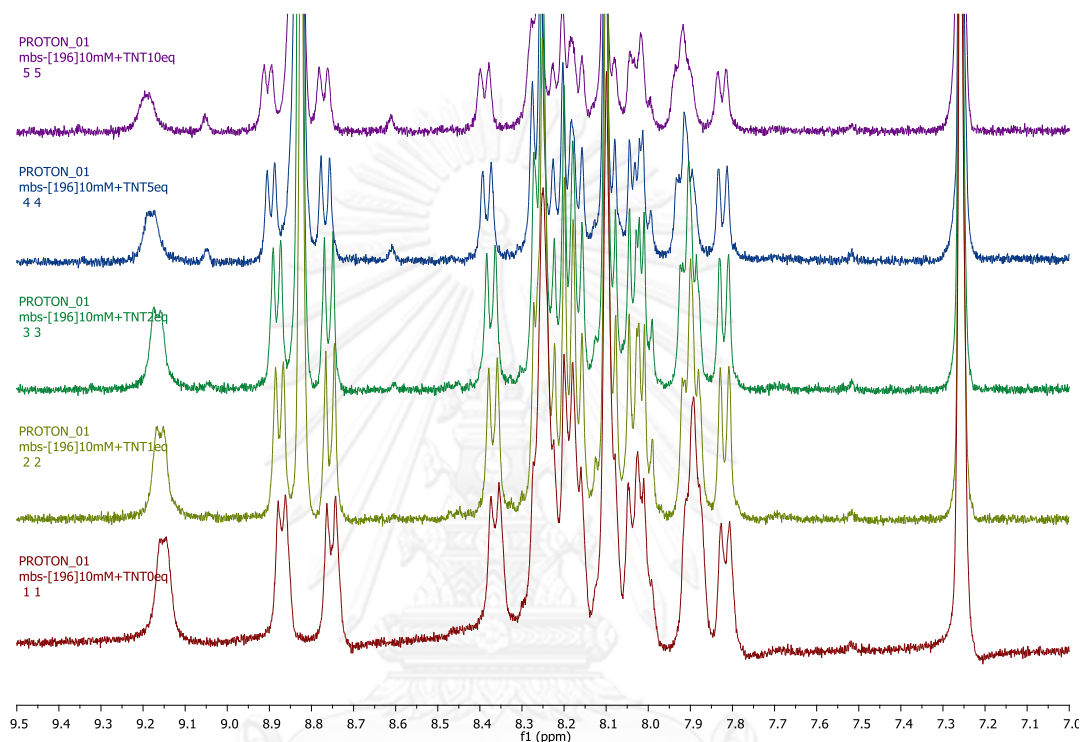


Figure 3.31 $^1\text{H-NMR}$ of **2** with various amounts of TNT

3.6.5 Paper-based sensor for nitroaromatic compound.

For a preliminary demonstration of solid state sensor fabrication, solutions of fluorophore **4** in THF with concentration between 50-500 μM were dropped on to a clean piece of filter paper (2 μL each). The volatile solvent was allowed to evaporate at room temperature and the original fluorescent signals were observed under a black light radiation (**Figure 3.32**, top row). The concentration of 200 μM appears to be the most suitable concentration as it is the lowest concentration that gave vivid and evenly dispersed fluorescent spots.

When the prepared paper-based sensors were immersed into TNT solutions of various concentrations (up to 300 μM) for 5 min and allowed to dry completely, the fluorescent dots faded away. From the **Figure 3.31**, bottom row, the noticeable

change in fluorescent color dot was observed when the paper-base sensor was treated with 100 μM . These preliminary results suggested a potential application of these new fluorophores as solid state sensors for TNT.

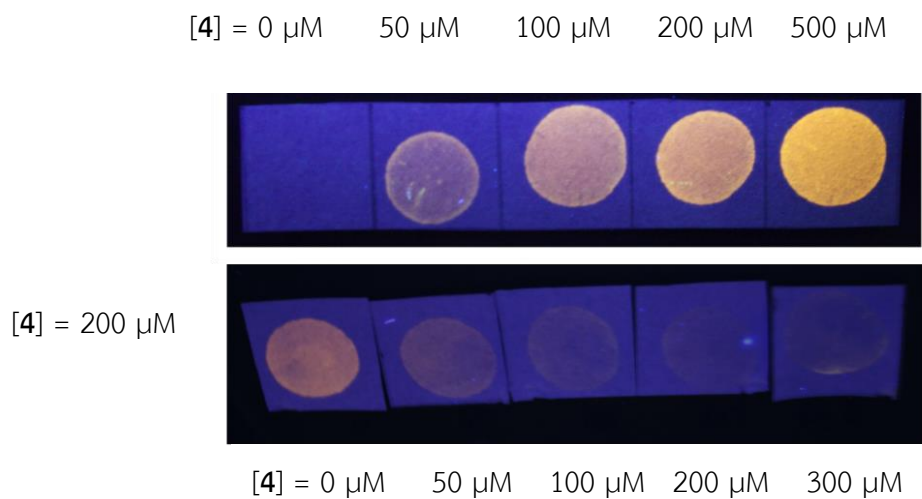


Figure 3.32 Photographic images for paper-based detection of TNT under 20W black light (365 nm).

CHAPTER IV

Conclusion

4.1 Conclusion

Three new fluorophores composed of pyrenes and naphthalene benzimidazoles were successfully synthesized by Suzuki coupling reaction. They were characterized by NMR spectroscopy, UV-Vis and fluorescence spectrophotometry and mass spectrometry. The photophysical properties of all fluorophores were determined using their solutions in THF. The maximum absorption wavelengths were in the range of 344-350 nm and the emission maxima were around 580-585 nm. The large Stoke shifts (>100 nm) indicated a significant geometry difference between ground and excited states. The quantum yields were measured in THF, using quinine sulfate solution as a standard. The fluorophores **2** and **4** that have low fluorescent quantum yields in THF exhibit an interesting AIEE behavior upon dissolving in 90% water in THF. In the selectivity screening toward explosive nitroaromatic compounds, the fluorophore **2** and **4** exhibited a selective fluorescence turn-off in the presence of DNP, TNP, and TNT. However, it was proven that the selectivities towards dNP and TNP were caused by a competitive absorption of the analytes. A linear Stern-Volmer relationship of both **2** and **4** with TNT were obtained with quenching constants (K_{sv}) of $9.63 \times 10^4 \text{ M}^{-1}$ and $6.00 \times 10^4 \text{ M}^{-1}$, respectively. The fluorophore **2** provided the lowest detection limit for TNT at 127 ppb.

REFERENCES



จุฬาลงกรณ์มหาวิทยาลัย
CHULALONGKORN UNIVERSITY

REFERENCES

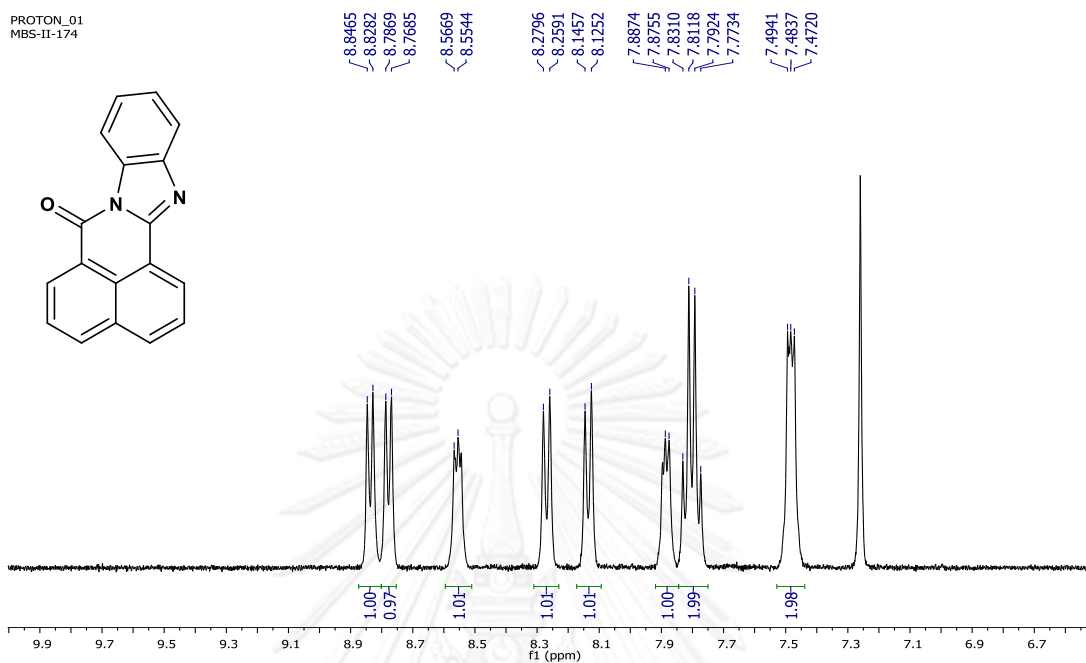
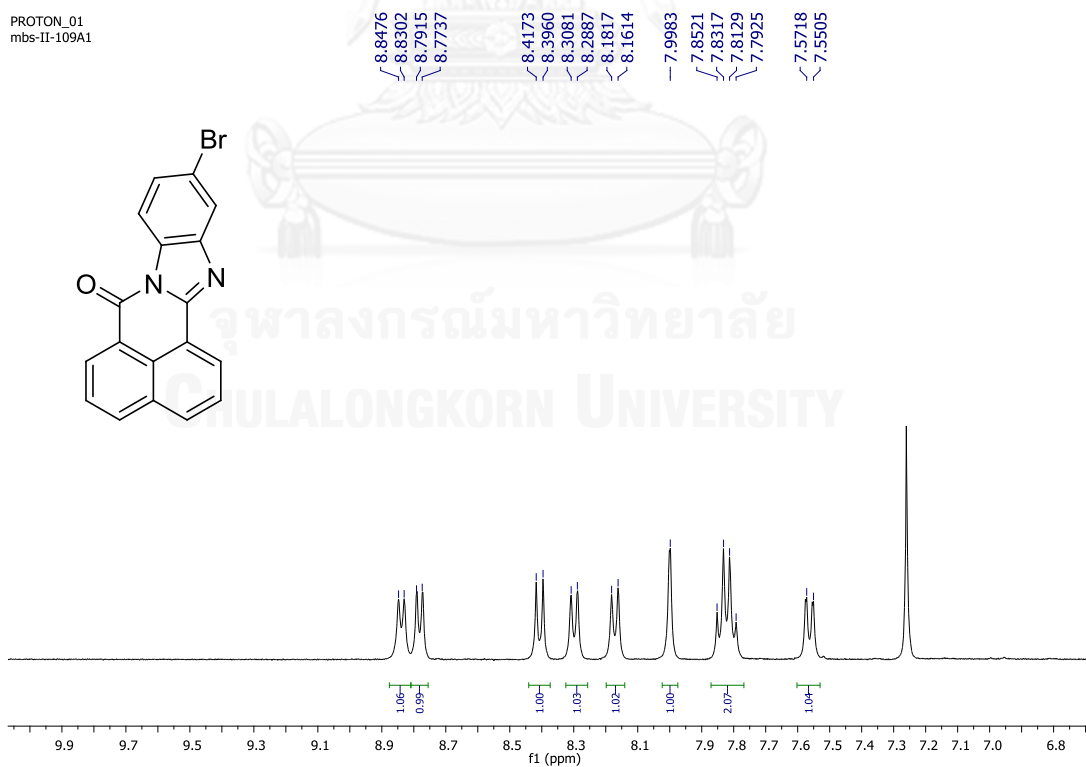
1. Jim, C., biodegradation of nitroaromatic compounds. Annual Review of Microbiology. **49** (1995): p. 523-555.
2. Toal, S.J. and Trogler, W.C., Polymer sensors for nitroaromatic explosives detection. Journal of Materials Chemistry. **16**(28) (2006): p. 2871.
3. Ju, K.S. and Parales, R.E., Nitroaromatic compounds, from synthesis to biodegradation. Microbiology and Molecular Biology Reviews. **74**(2) (2010): p. 250-72.
4. Pouredal, H.R.K.M.H., prediction of toxicity of nitroaromatic compounds through their molecular structures. Journal of the Iranian Chemical Society. **8**(1) (2011): p. 78-89.
5. Bhalla, V., Kaur, S., Vij, V., and Kumar, M., Mercury-modulated supramolecular assembly of a hexaphenylbenzene derivative for selective detection of picric acid. Inorganic Chemistry. **52**(9) (2013): p. 4860-5.
6. Yan, Z.X., Z.; Zhang, W.; Zhao, S.; Xu, Y., A novel electrochemical nitrobenzene sensor based on nicu alloy electrode. International Journal of Electrochemical Science. **7** (2012): p. 2938 - 2946.
7. Fan, L.J.Z., Y.; Murphy, C.B.; Angell, S.E.; Parker, M.; Flynn. B.R.; Jones Jr., W.E., Fluorescent conjugated polymer molecular wire chemosensors for transition metal ion recognition and signaling. Coordination Chemistry Reviews. **253** (2009): p. 410–422.
8. Lakowicz, J.R., *Principles of Fluorescence Spectroscopy*, ed. 3. 2006.
9. Prasanna de Silva, A.G., H. Q.; Gunnlaugsson, T.; Huxley, A.; McCoy, C. P.; Rademacher, J. T.; Rice, T. E., Signaling recognition events with fluorescent sensors and switches. Chemical Reviews. **97** (1997): p. 1515-1566.
10. Vu, A.P., J.; Bühlmann, P.; Stein, A., Quenching performance of surfactant-containing and surfactant-free fluorophore-doped mesoporous silica films for nitroaromatic compound detection. Chemistry of Materials. **25** (2013): p. 711–722.
11. Arimori, S.B., L. I.; Ward, C. J.; James, T. D., Fluorescent internal charge transfer (ICT) saccharide sensor Tetrahedron Letters. **42** (2001): p. 4553–4555.
12. Hong, Y.L., J.; Tang, B. Z., Aggregation-induced emission: phenomenon, mechanism and applications. Chemical Communications. (2009): p. 4332–4353.

13. AN, B.-K.G., J.; PARK, S.Y., π -Conjugated cyanostilbene derivatives: a unique self-assembly motif for molecular nanostructures with enhanced emission and transport. Accounts of Chemical Research. **45**(4) (2012): p. 544–554.
14. Yu, G.Y., S.; Liu, Y.; Chen, J.; Xu, X.; Sun, X.; Ma, D.; Zhan, X.; Peng, Q.; Shuai, Z.; Tang, B.; Zhu, D.; Fang, W.; Luo, Y., Structures, electronic states, photoluminescence, and carrier transport properties of 1,1-disubstituted 2,3,4,5-tetraphenylsiloles. Journal of the American Chemical Society. **127** (2005): p. 6335-6346.
15. Chen, J.L., C.; Lam, J.; Dong, Y.; Lo, S.; Williams, I. D.; Zhu, D.; Tang, B. Z., Synthesis, light emission, nanoaggregation, and restricted intramolecular rotation of 1,1-substituted 2,3,4,5-tetraphenylsiloles. Chemistry of Materials. **15** (2003): p. 1535-1546.
16. Jang, S.K., S. G.; Jung, D.; Kwon, H.; Song, J.; Cho, S.; Ko, Y. C.; Sohn, H., Aggregation-induced emission enhancement of polysilole nanoaggregates. Bulletin of the Korean Chemical Society. **27**(12) (2006): p. 1965-1966.
17. Deans, R.K., J.; Machacek, M. R.; Swager, T. M., A poly(p-phenyleneethynylene) with a highly emissive aggregated phase. Journal of the American Chemical Society. **122** (2000): p. 8565-8566.
18. Wang, W.L., T.; Wang, M.; Liu, T.X.; Ren, L.; Chen, D.; Huang, D., Aggregation emission properties of oligomers based on tetraphenylethylene. The Journal of Physical Chemistry B. **114**(18) (2010): p. 5983–5988.
19. Tang, W.X., Y.; Tong, A., Salicylaldehyde azines as fluorophores of aggregation-induced emission enhancement characteristics. The Journal of Organic Chemistry. **74** (2009): p. 2163–2166.
20. Kubota, Y.T., S.; Funabiki, K.; Matsui, M., Synthesis and fluorescence properties of thiazole boron complexes bearing a β -ketoiminate ligand. Organic Letters. **14**(17) (2012): p. 4682–4685.
21. Liu, J., et al., Hyperbranched conjugated polysiloles: synthesis, structure, aggregation-enhanced emission, multicolor fluorescent photopatterning, and superamplified detection of explosives. Macromolecules. **43**(11) (2010): p. 4921-4936.
22. Shi, H.K., R.; Liu, J.; Xing, B.; Tang, B.Z.; Liu, B., Real-time monitoring of cell apoptosis and drug screening using fluorescent light-up probe with aggregation-induced emission characteristics. Journal of the American Chemical Society. **134** (2012): p. 17972–17981.

23. Bhalla, V.G., , A.; Kumar, M., Fluorescent nanoaggregates of pentacenequinone derivative for selective sensing of picric acid in aqueous media. Organic Letters. **14**(12) (2012): p. 3112–3115.
24. Kumar, M., Vij, V., and Bhalla, V., Vapor-phase detection of trinitrotoluene by AIEE-active hetero-oligophenylene-based carbazole derivatives. Langmuir. **28**(33) (2012): p. 12417-21.
25. Vij, V., Bhalla, V., and Kumar, M., Attogram detection of picric acid by hexa-peri-hexabenzocoronene-based chemosensors by controlled aggregation-induced emission enhancement. ACS Applied Materials & Interfaces. **5**(11) (2013): p. 5373-80.
26. Jin, W.J., J.; Wang, X.; Zhu, X.; Wang, G.; Song, Y.; Bai, C., Continuous intra-arterial blood pH monitoring in rabbits with acid–base disorders. Respiratory Physiology & Neurobiology. **177** (2011): p. 183–188.
27. Xie, J.C., Y.; Yang, W.; Xu, D.; Zhang, K., Water soluble 1,8-naphthalimide fluorescent pH probes and their application to bioimaging. Journal of Photochemistry and Photobiology A: Chemistry. **223** (2011): p. 111– 118.
28. Gan, G.A.S., Q.L.; Hou, X.Y.; Chen, K.; Tian, H., 1,8-Naphthalimides for non-doping OLEDs: the tunable emission color from blue, green to red. Journal of Photochemistry and Photobiology A: Chemistry. **162** (2004): p. 399–406.
29. Galunov, N.Z.K., B.M.; Lyubenko, O.N.; Yermolenko, I.G.; Patsenker, L.D.; Doroshenko, A.O., Spectral properties and applications of the new 7H-benzo[de]pyrazolo[5,1-a]isoquinolin-7-ones. Journal of Luminescence. **102-103** (2003): p. 119–124.
30. Georgiev, N.I.B., V.B., Design, synthesis and sensor activity of a highly photo-stable blue emitting 1,8-naphthalimide. Journal of Luminescence. **132** (2012): p. 2235–2241.
31. Ertena, S.E., E.; Iclib S., Dye sensitized solar cell based on 1,8-naphthalene benzimidazole comprising carboxyl group. The European Physical Journal Applied Physics. **38** (2007): p. 227–230.
32. Lee, J.F.H., S., Green polymer-light-emitting-diodes based on polyfluorenes containing N-aryl-1,8-naphthalimide and 1,8-naphthoiline-arylimidazole derivatives as color tuner. Polymer. **50**((2009): p. 5668–5674.
33. Erten-Ela, S.O., S.; Eren, E., Synthesis and photophysical characterizations of thermal -stable naphthalene benzimidazoles. Journal of Fluorescence. **21** (2011): p. 1565–1573.

34. Masashi, M.C.e., P.B.; Pavel, A. Jr., Green synthesis of polycyclic benzimidazole derivatives and organic semiconductors. Organic Letters. **13** (2011): p. 4882–4885.
35. Burattini, S.C., H.M.; Greenland, B.W.; Hayes, W.; Wade, M., Pyrene-functionalised, alternating copolyimide for sensing nitroaromatic compounds. Macromolecular Rapid Communications. **30** (2009): p. 459–463.
36. Lee, Y.H., et al., Dipyrenylcalix[4]arene--a fluorescence-based chemosensor for trinitroaromatic explosives. Chemistry. **16**(20) (2010): p. 5895-901.
37. He, G.Y., N.; Yang, J.; Wang, H.; Ding, L.; Yin, S.; Fang, Y., Pyrene-containing conjugated polymer-based fluorescent films for highly sensitive and selective sensing of tnt in aqueous medium. Macromolecules. **44** (2011): p. 4759–4766.
38. Park, K.-H., Yoo, J.-D., Ka, J.-W., and Lee, C.-H., Calix[2]pyreno[2]pyrrole as a fluorescence chemical probe for polynitroaromatics. Bulletin of the Korean Chemical Society. **33**(2) (2012): p. 675-677.
39. Niamnont, N.; Kimpitak, N.; Wongravee, K.; Rashatasakhon, P.; Baldrige, K.K.; Siegel, J.S.; Sukwattanasinitt, M., Tunable star-shaped triphenylamine fluorophores for fluorescence quenching detection and identification of nitroaromatic explosives. Chemical Communications. **49** (2013): p. 780-782.
40. Tamuly, C., Barooah, N., Laskar, M., Sarma, R.J., and Baruah, J.B., Fluorescence quenching and enhancement by h-bonding interactions in some nitrogen containing fluorophores. Supramolecular Chemistry. **18**(8) (2006): p. 605-613.
41. Roy, B., Bar, A.K., Gole, B., and Mukherjee, P.S., Fluorescent tris-imidazolium sensors for picric acid explosive. The Journal of Organic Chemistry. **78**(3) (2013): p. 1306-10.
42. Shao, J., Chang, J., and Chi, C., Linear and star-shaped pyrazine-containing acene dicarboximides with high electron-affinity. Organic & Biomolecular Chemistry. **10**(35) (2012): p. 7045-7052.
43. Berlman, I.B., *Handbook of fluorescence spectra of aromatic molecules*. 1971: Academic Press

APPENDIX

Figure A.1 The ^1H NMR of compound **1** in CDCl_3 .Figure A.2 The ^1H NMR of **2a** in CDCl_3 .

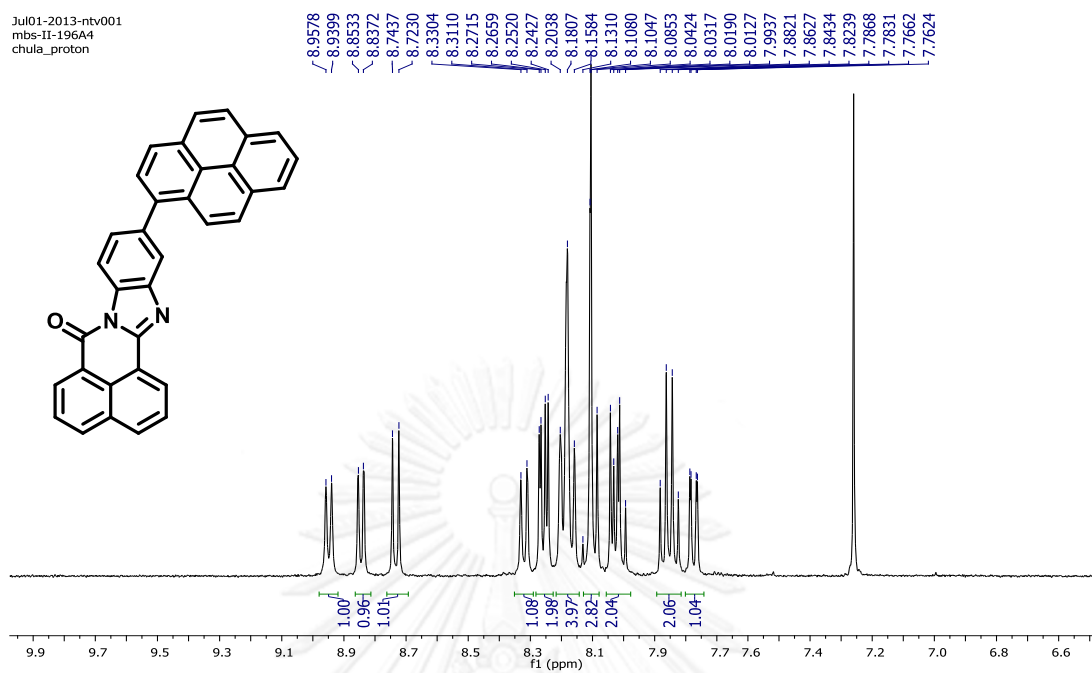


Figure A.3 The ^1H NMR of 2 in CDCl_3 .

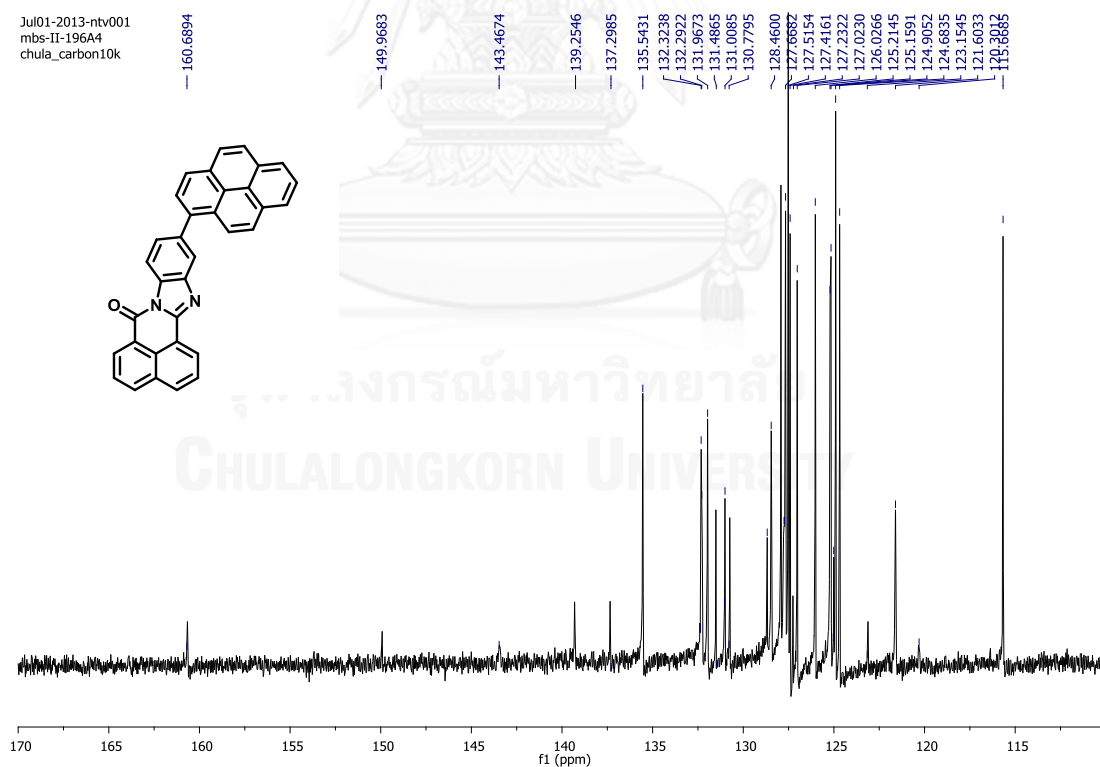


Figure A.4 The ^{13}C NMR of 2 in CDCl_3 .

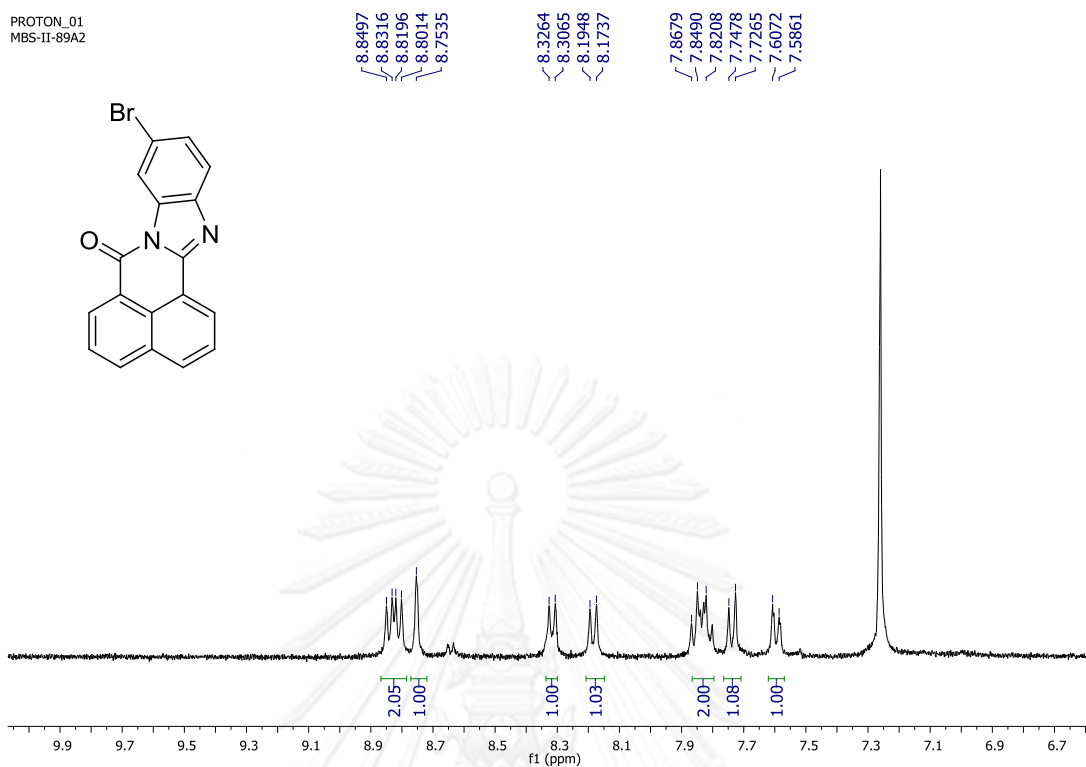


Figure A.5 The ^1H NMR of **3a** in CDCl_3 .

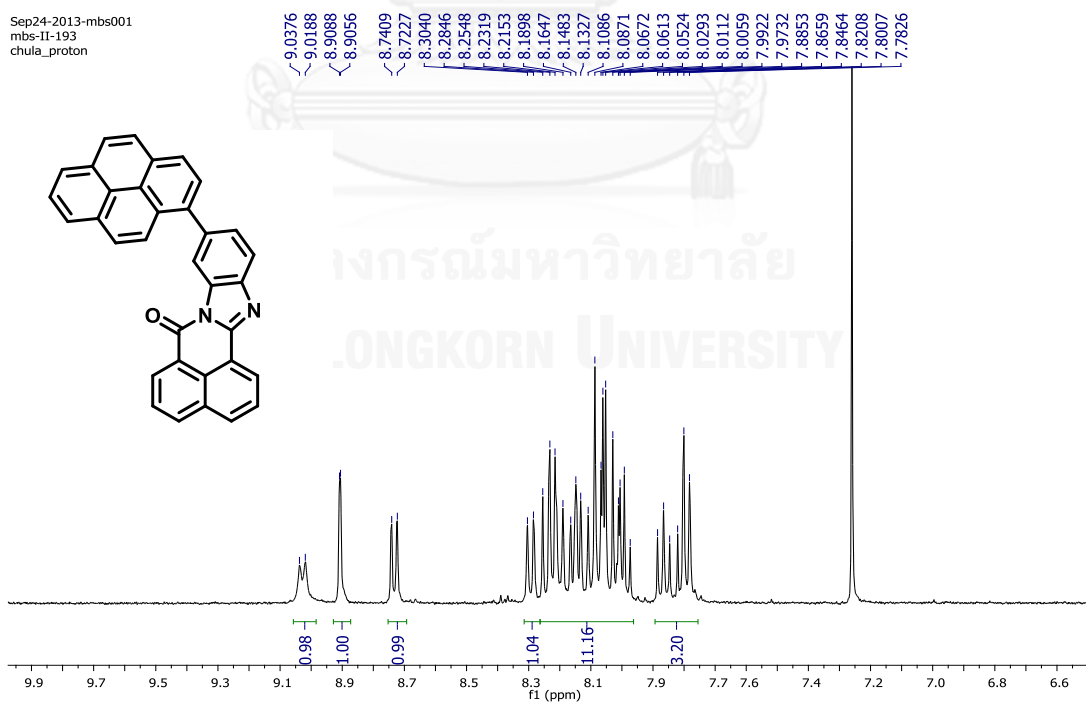


Figure A.6 The ^1H NMR of **3** in CDCl_3 .

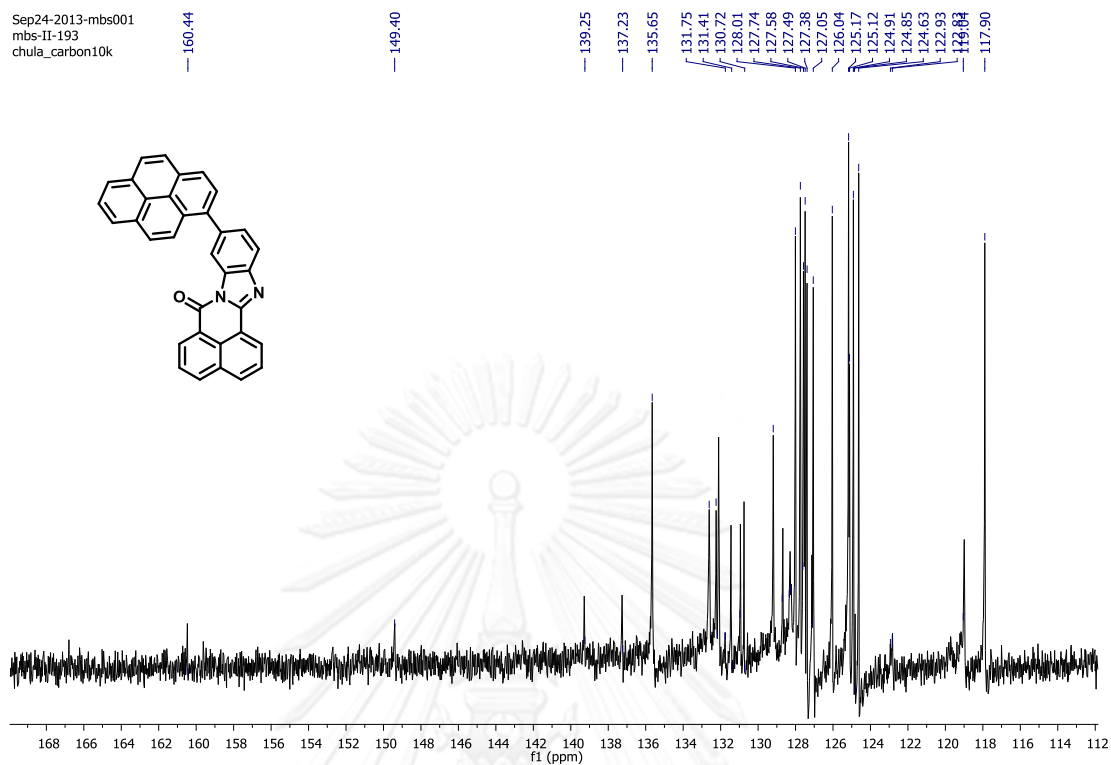


Figure A.7 The ^{13}C NMR of **3** in CDCl_3 .

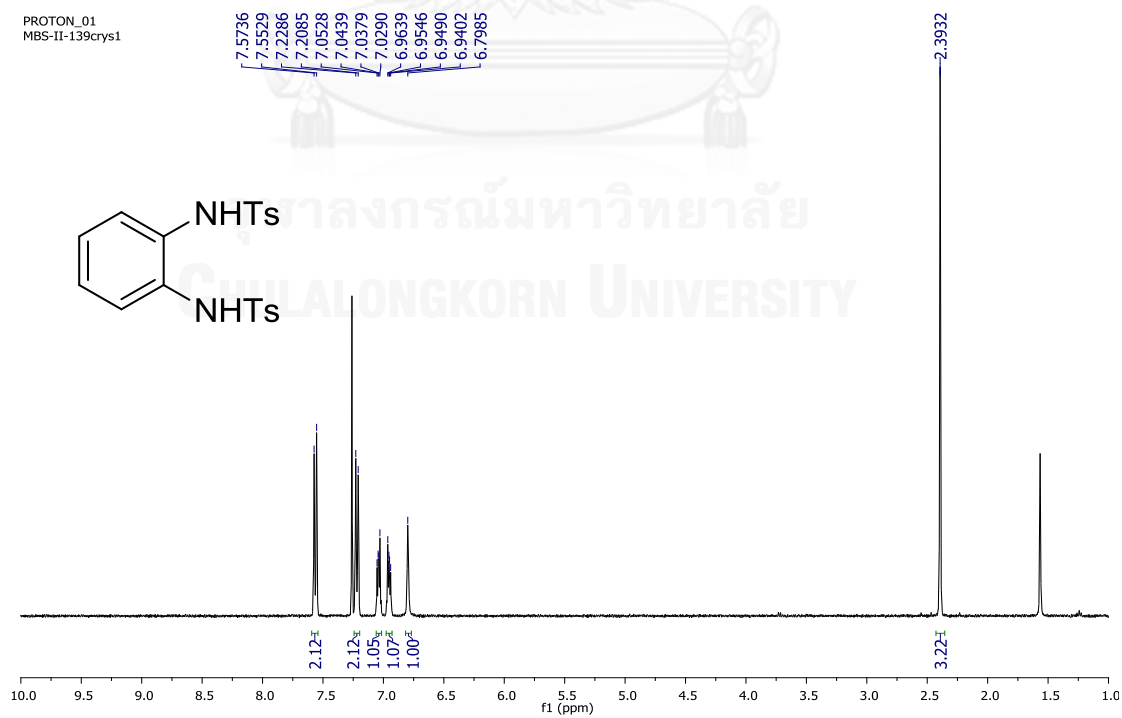


Figure A.8 The ^1H NMR of **4a** in CDCl_3 .

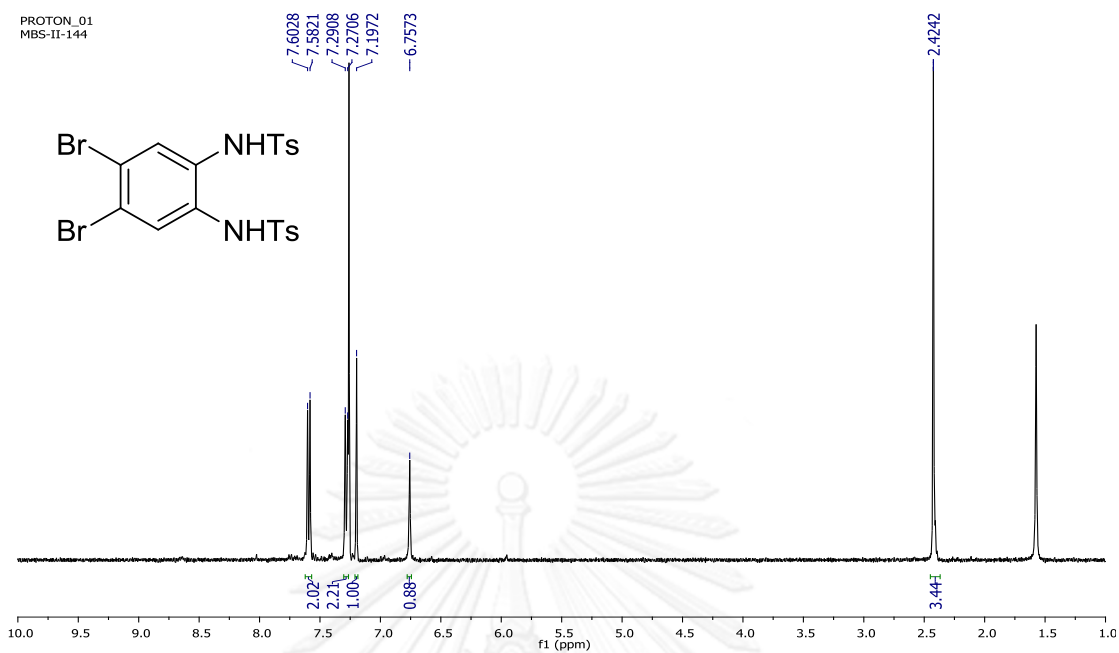


Figure A.9 The ^1H NMR of **4b** in CDCl_3 .

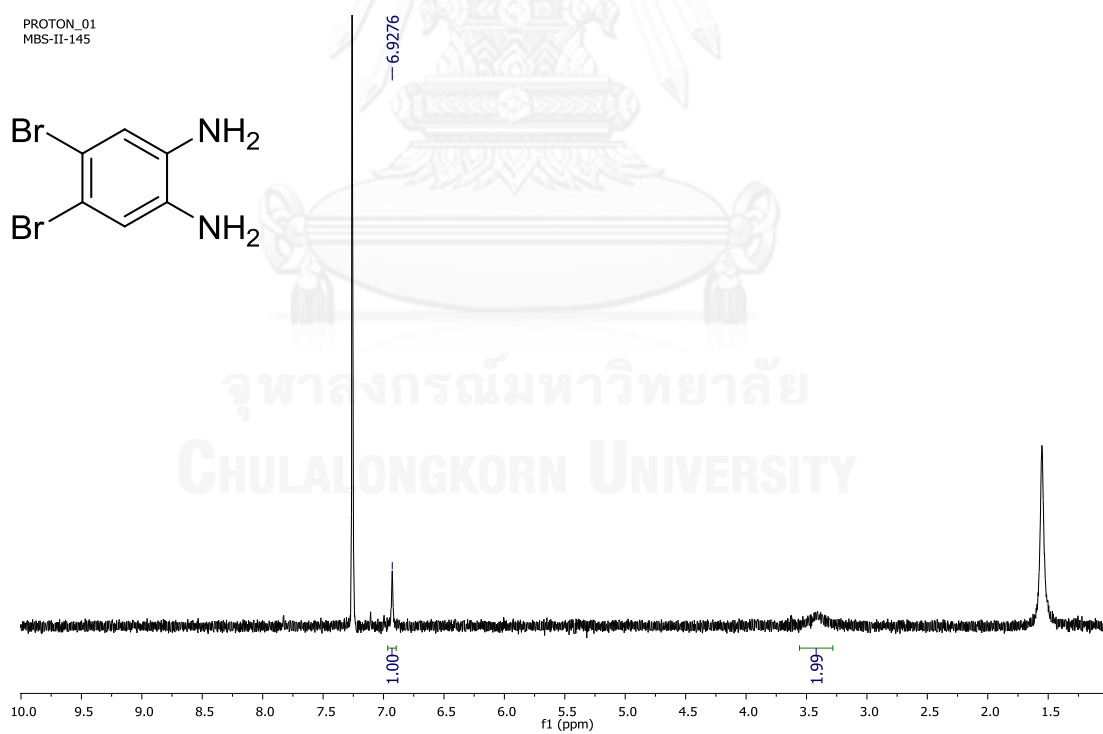


Figure A.10 The ^1H NMR of **4c** in CDCl_3 .

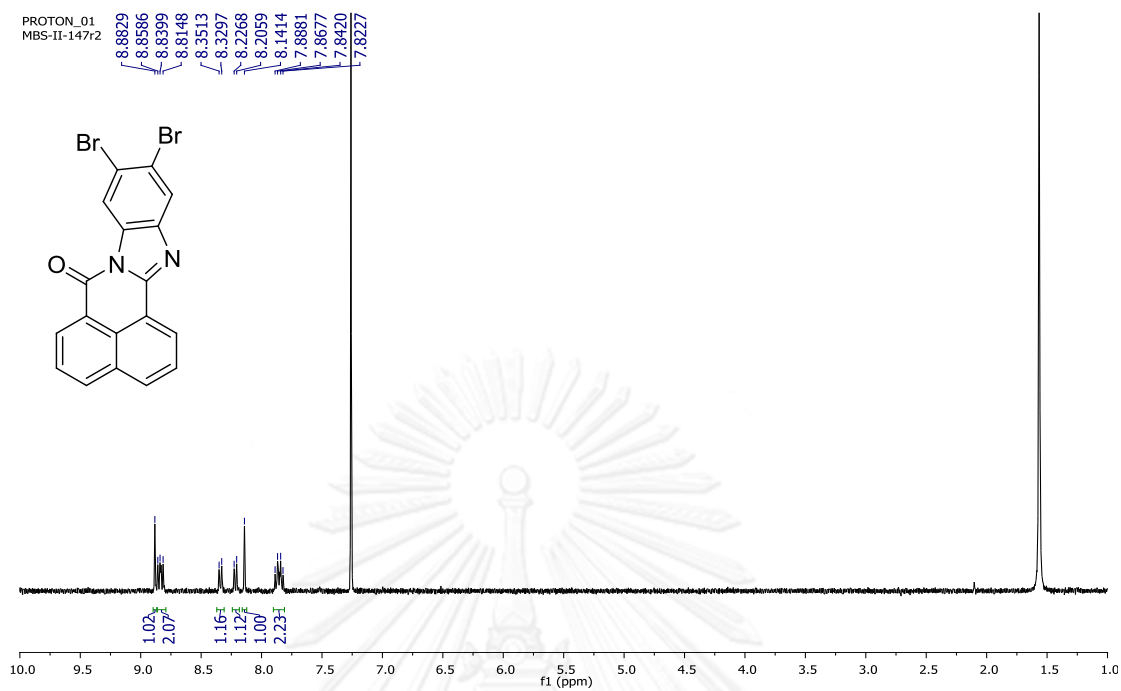


Figure A.11 The ^1H NMR of **4d** in CDCl_3 .

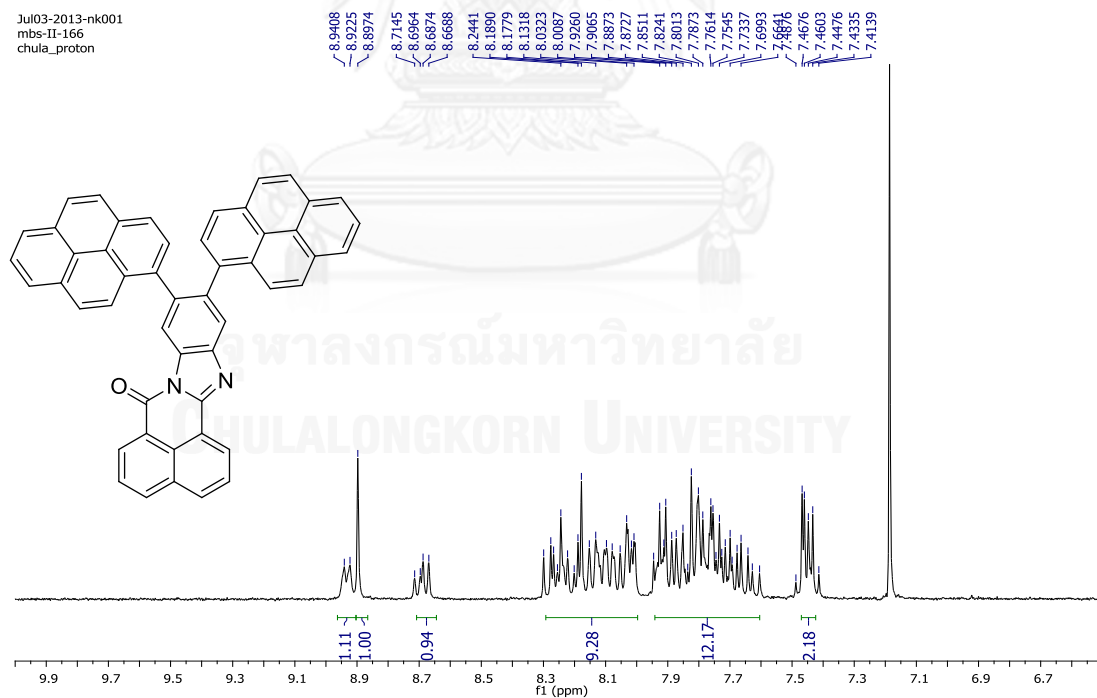


Figure A.12 The ^1H NMR of **4** in CDCl_3 .

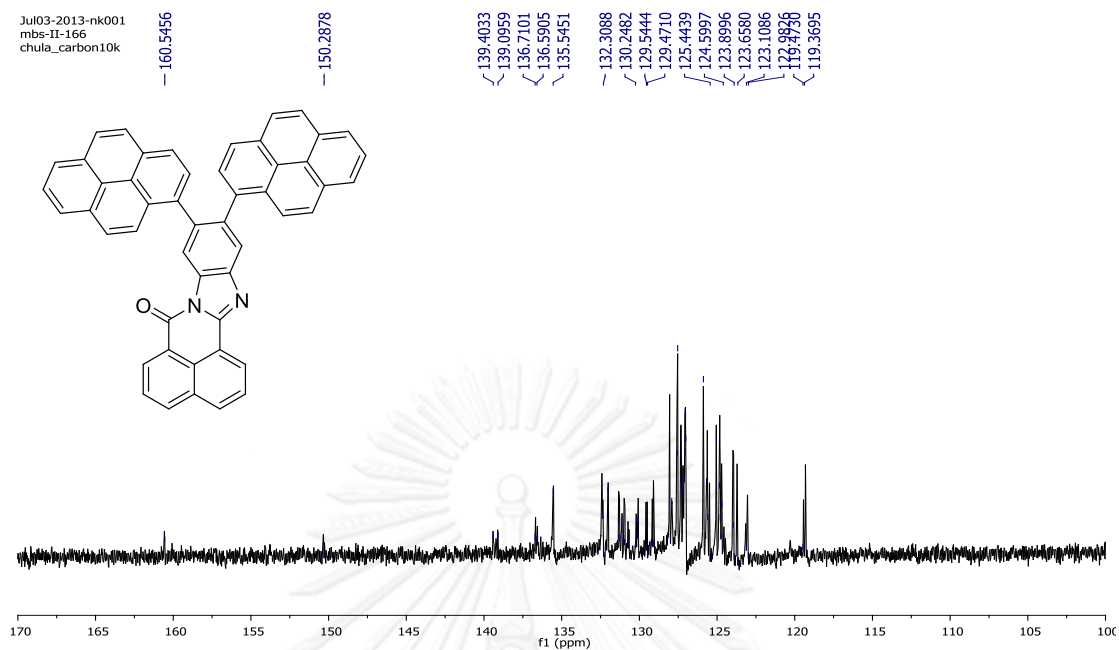


Figure A.13 The ^{13}C NMR of **4** in CDCl_3 .

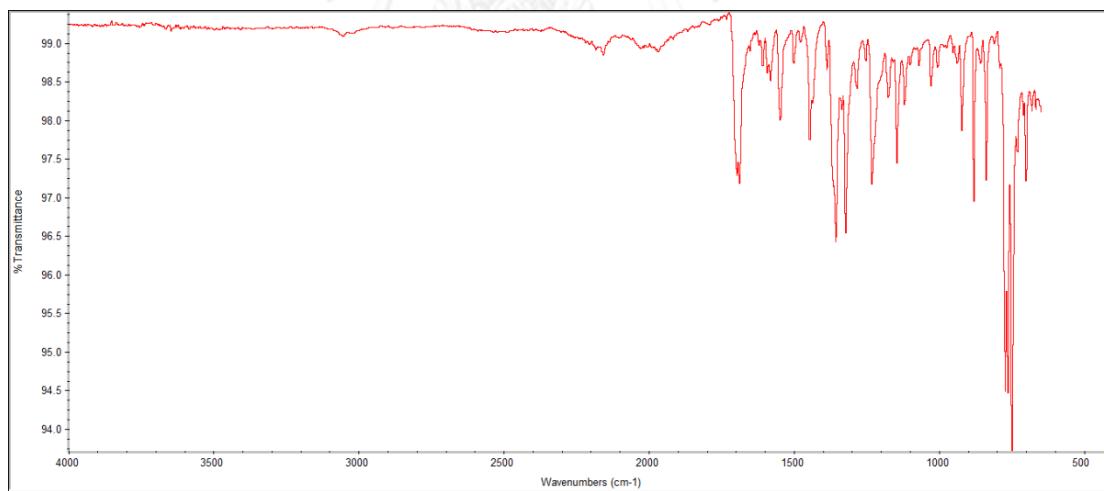


Figure A.14 The IR spectra of **1**.

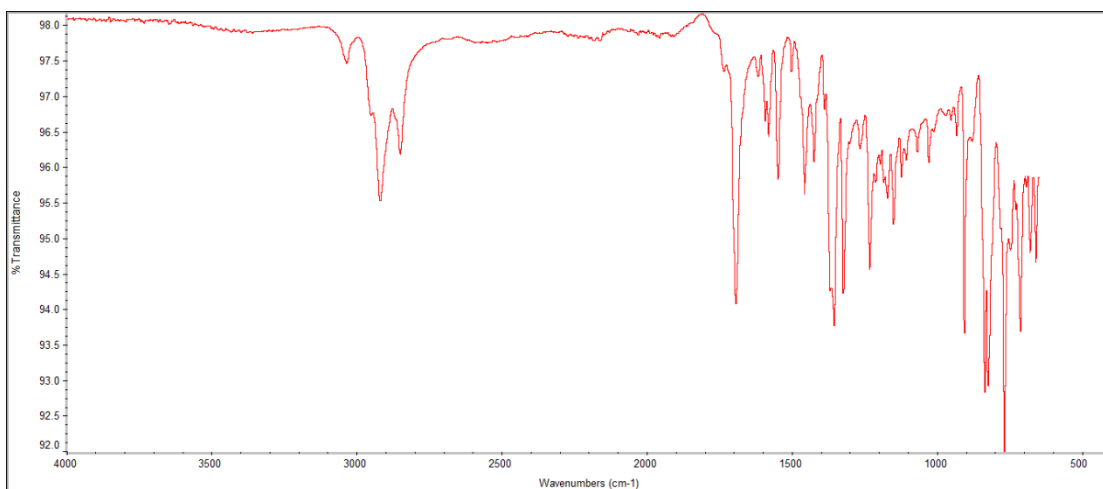


Figure A.15 The IR spectra of 2.

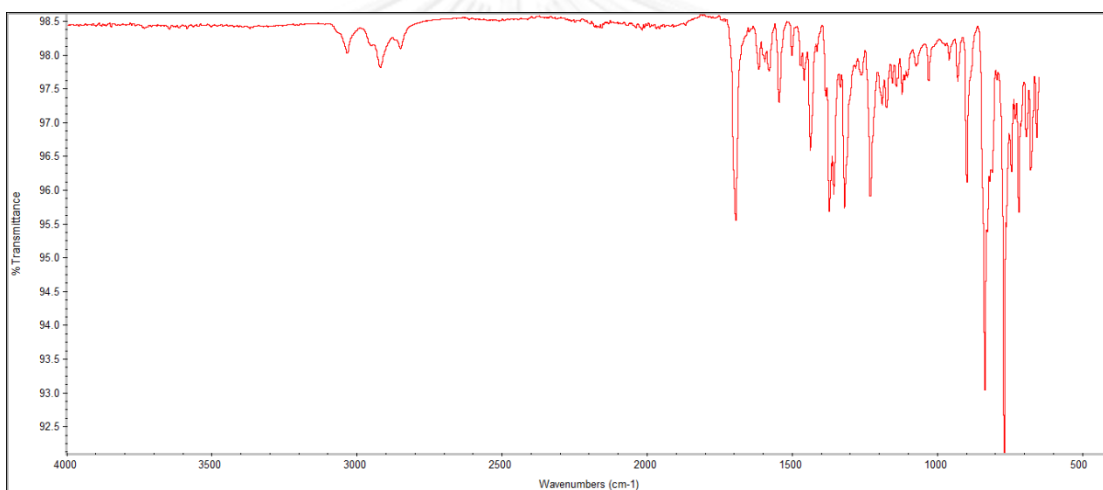


Figure A.16 The IR spectra of 3.

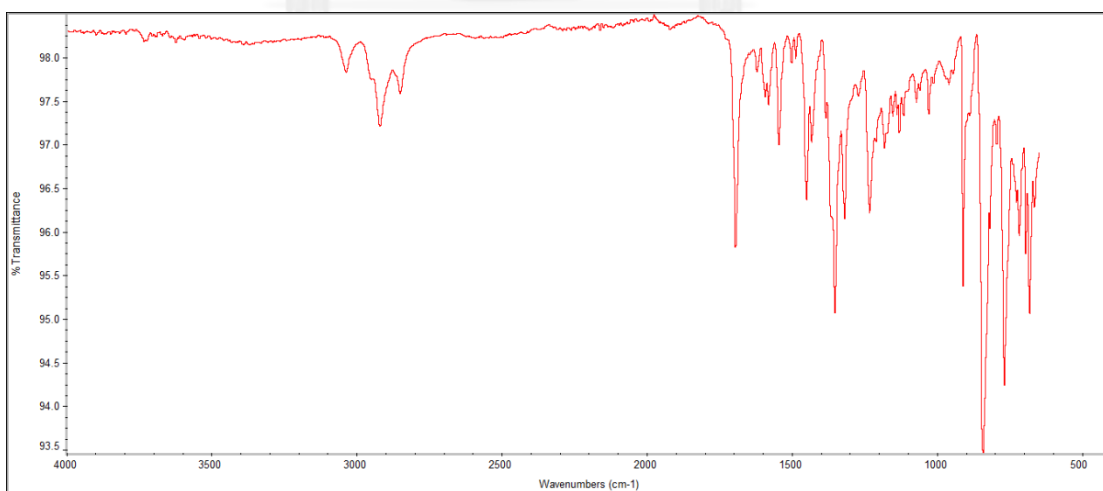


Figure A.17 The IR spectra of 4.

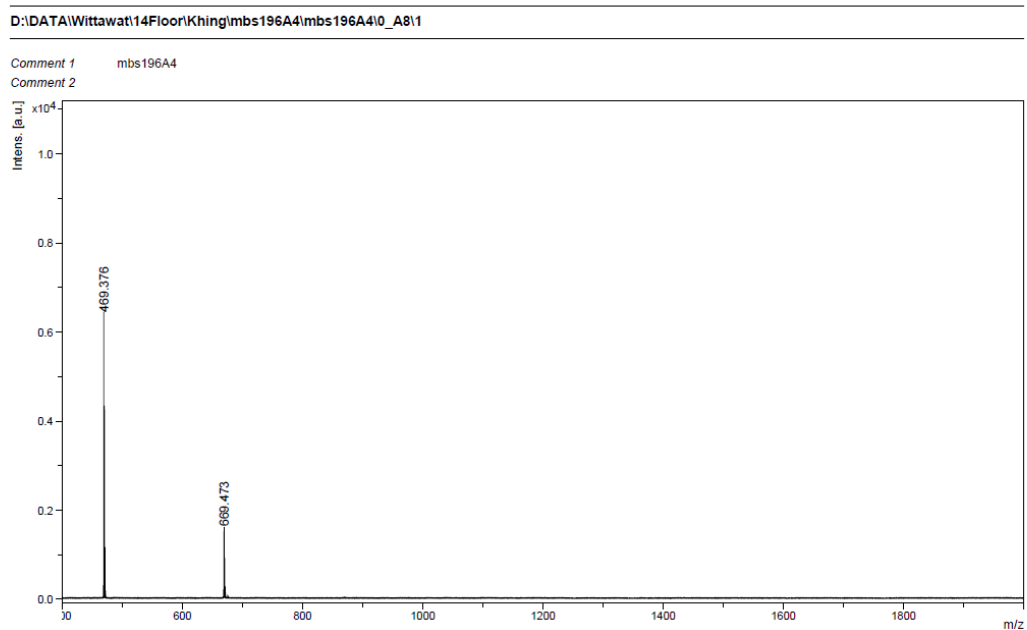


Figure A.18 MS spectra of 2.

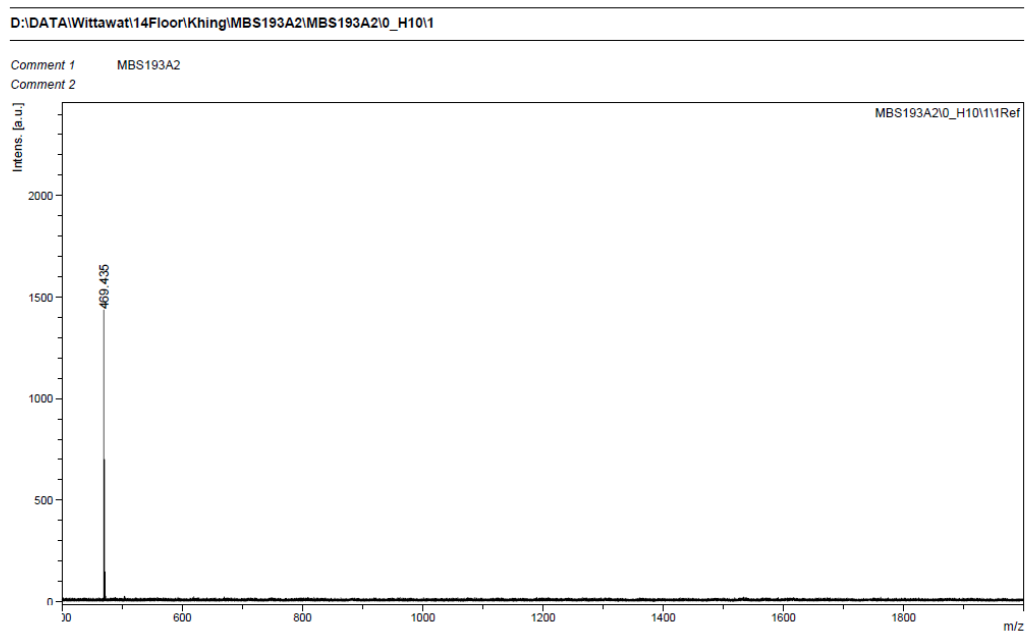


Figure A.19 MS spectra of 3.

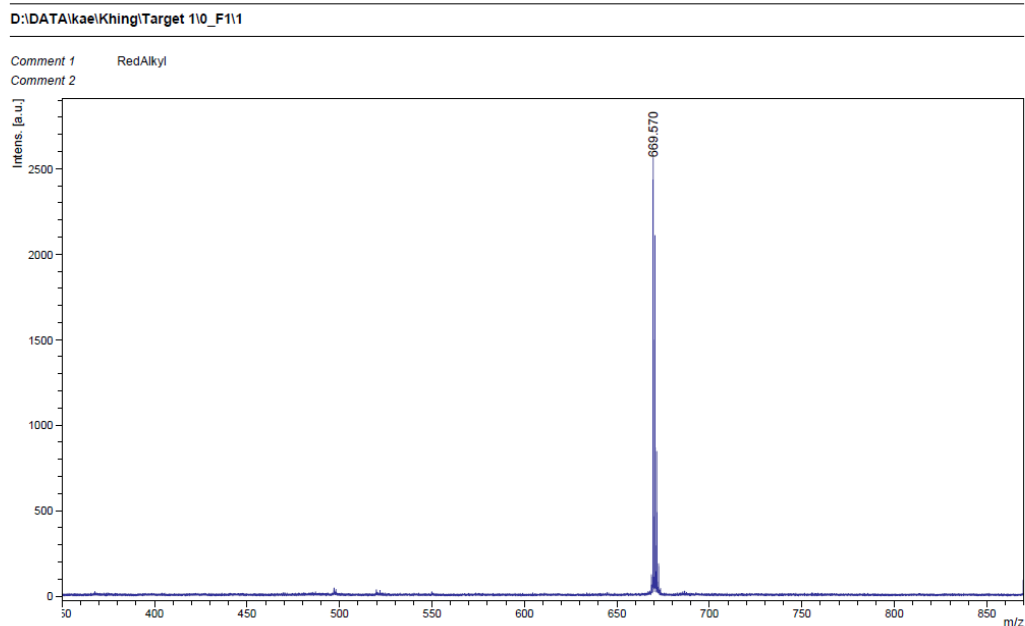


Figure A.20 MS spectra of 4.

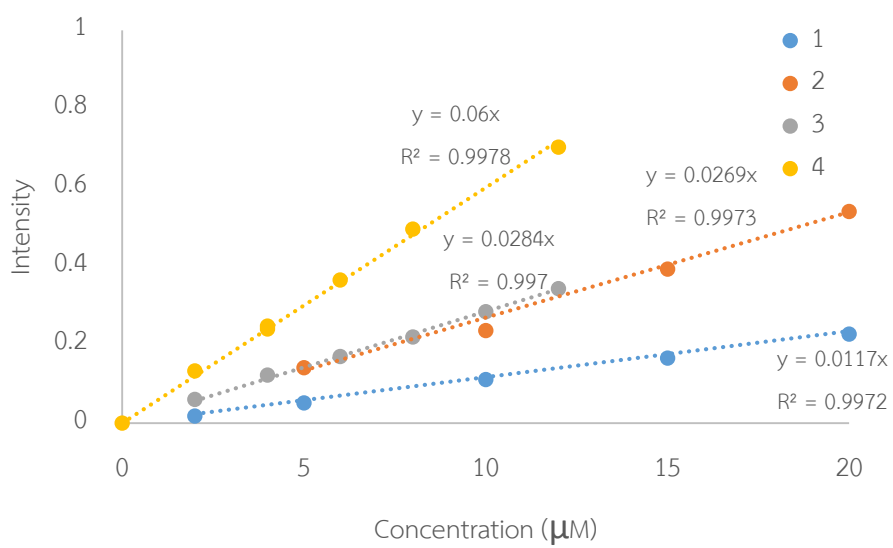


Figure A.21 Molar absorptivity of 1-4

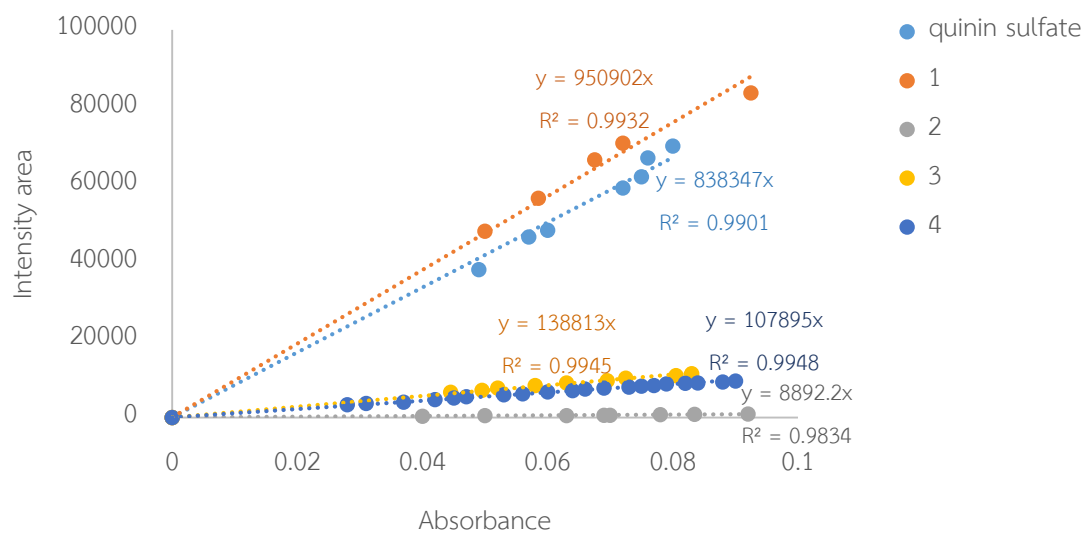


Figure A.22 Quantum yield of 1-4

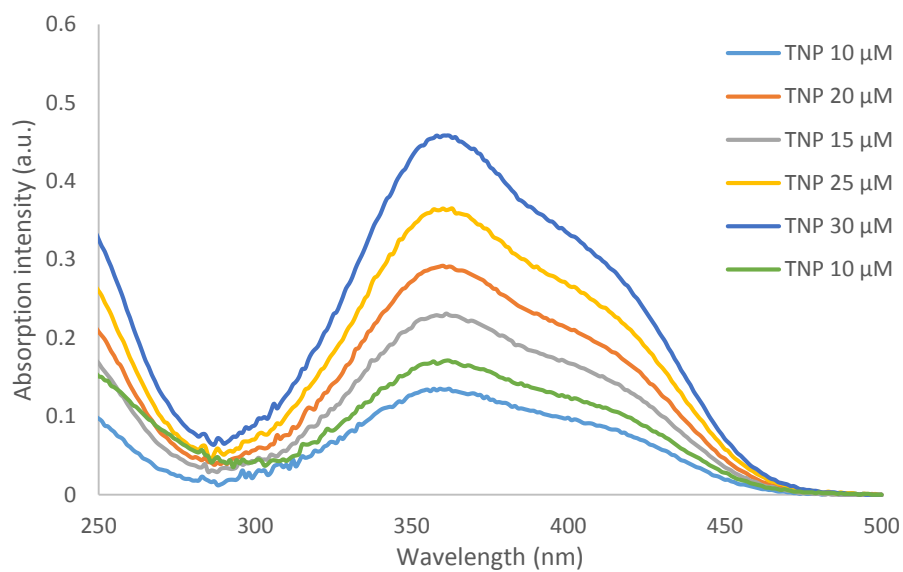


Figure A.23 Absorption spectra of TNT

VITA

Ms. Manutchanok Boonsri was born on June 26, 1984 in Patumtani, Thailand. She got a Bachelor's Degree of Science in Chemistry from Chulalongkorn University in 2011. In the same year, she started her a Master's Degree in Petrochemistry and Polymer Science program a Chulalongkorn University. During she had presented her research in The 26th International Symposium on Chemical Engineering (ISChE 2013) and SOKENDAI Asian Winter School 2013 and Pure and Applied Chemistry International Conference (PACCON 2014) by poster presentation.

Her address is 107 Moo 5, Parichart Village, 345 Road, Muang, Patumtani, 12000 Thailand.





จุฬาลงกรณ์มหาวิทยาลัย
CHULALONGKORN UNIVERSITY